

Identification of Partial-Differential-Equations-Based Models from Noisy Data via Splines

Yujie Zhao¹, Xiaoming Huo², Yajun Mei²

¹ *Biostatistics and Research Decision Sciences Department, Merck & Co., Inc*

² *H. Milton Stewart School of Industrial and Systems Engineering, Georgia Tech*

Abstract: We propose a two-stage method called *Spline Assisted Partial Differential Equation based Model Identification (SAPDEMI)* to identify partial differential equation (PDE)-based models from noisy data. In the first stage, we employ the cubic splines to estimate unobservable derivatives. The underlying PDE is based on a subset of these derivatives. This stage is computationally efficient: its computational complexity is a product of a constant with the sample size; this is the lowest possible order of computational complexity. In the second stage, we apply the Least Absolute Shrinkage and Selection Operator (Lasso) to identify the underlying PDE-based model. Statistical properties are developed, including the model identification accuracy. We validate our theory through various numerical examples and a real data case study. The case study is based on an National Aeronautics and Space Administration (NASA) data set.

Key words and phrases: partial differential equations, model identification, cubic splines, Lasso.

1. Introduction

Partial differential equations (PDE) are widely adopted to model physical processes in engineering (Wang et al., 2019), physics (Xun et al., 2013), biology (Lagergren et al., 2020), and more. There are two main technical issues: the *forward problem* and the *inverse problem*. The forward problem studies the properties of functions that PDEs determine. It has been extensively studied by mathematicians (Olver, 2014; Wang et al., 2014). Some inverse problems aim at identifying PDE-based models from the observed noisy data. The research on the inverse problem is relatively sparse. The corresponding statistical property is notably less known. In this paper, we propose a method to solve the inverse problem. The inverse problem will be called a *PDE identification problem* and will be formulated.

Given the rise of the big data, the PDE identification problem becomes indispensable. A good PDE identification approach generates at least the following two benefits. First, one can predict the future trend by utilizing the estimated PDE-driven dynamic model, conditioning such a model reflects the underlying processes. Second, an interpretable PDE model allows scientists to validate/reexamine the underlying physical/biological laws governing the process.

We propose a new method – *Spline Assisted Partial Differential Equa-*

tion based Model Identification (SAPDEMI) – for the PDE identification problem. SAPDEMI can efficiently identify the underlying PDE model from the noisy data \mathcal{D} :

$$\begin{aligned} \mathcal{D} = \{ (x_i, t_n, u_i^n) : & \ x_i \in (0, X_{\max}) \subseteq \mathbb{R}, \ \forall i = 0, \dots, M-1, \\ & t_n \in (0, T_{\max}) \subseteq \mathbb{R}, \ \forall n = 0, \dots, N-1 \} \in \Omega, \end{aligned} \quad (1.1)$$

where variable $x_i \in \mathbb{R}$ is the spatial variable with $x_i \in (0, X_{\max})$ for $i = 0, 1, \dots, M-1$, and we call M the *spatial resolution*; Variable $t_n \in \mathbb{R}$ is the temporal variable with $t_n \in (0, T_{\max})$ for $n = 0, 1, \dots, N-1$, and we call N the *temporal resolution*; We use T_{\max}, X_{\max} to denote the upper bound of the temporal variable and the spatial variable, respectively; Variable u_i^n is a representation of ground truth $u(x_i, t_n)$ contaminated by noises that follow the normal distribution with mean zero and stand deviation σ :

$$u_i^n = u(x_i, t_n) + \epsilon_i^n, \quad \epsilon_i^n \stackrel{i.i.d.}{\sim} N(0, \sigma^2), \quad (1.2)$$

where the ground truth function $u(x, t)$ is the function determined by an underlying PDE model, which is assumed to satisfy the following equation:

$$\begin{aligned} \frac{\partial}{\partial t} u(x, t) = & \beta_{00}^* + \sum_{k=0}^{q_{\max}} \sum_{i=1}^{p_{\max}} \beta_{ki}^* \left[\frac{\partial^k}{\partial^k x} u(x, t) \right]^i + \\ & \sum_{\substack{i+j \leq p_{\max} \\ i, j > 0}} \sum_{\substack{0 \leq k < l \\ l \leq q_{\max}}} \beta_{k^i, l^j}^* \left[\frac{\partial^k}{\partial^k x} u(x, t) \right]^i \left[\frac{\partial^l}{\partial^l t} u(x, t) \right]^j, \end{aligned} \quad (1.3)$$

where the left-hand side of the equation is the first-order partial derivative of the underlying function with respect to the temporal variable t ,

while the right-hand side is the p_{\max} th order polynomial of the derivatives with respect to the spatial variable x up to the q_{\max} th total order. For notational simplicity, we denote the ground truth coefficient vector, $\boldsymbol{\beta}^* = (\beta_{00}^*, \beta_{01}^*, \beta_{11}^*, \dots, \beta_{q_{\max}^{p_{\max}}}^*)$, as $\boldsymbol{\beta}^* = (\beta_1^*, \beta_2^*, \beta_3^*, \dots, \beta_K^*)^\top$, where $K = 1 + (p_{\max} + 1)q_{\max} + \frac{1}{2}q_{\max}(q_{\max} + 1)(p_{\max} - 1)!$ is the total number of coefficients on the right hand side. It is noted that, in practice, the majority of the entries in $\boldsymbol{\beta}^*$ are zero. For instance, in the transport equation $\frac{\partial}{\partial t}u(x, t) = a\frac{\partial}{\partial x}u(x, t)$ with any $a \neq 0$, we only have $\beta_3^* \neq 0$ and $\beta_i^* = 0$ for any $i \neq 3$ (see Olver, 2014, Section 2.2). Therefore, it is reasonable to assume that the coefficient $\boldsymbol{\beta}^*$ in (1.3) is sparse.

To identify the above model, one needs to overcome two technical difficulties. First, the derivatives in (1.3) are unobservable and need to be estimated from the noisy observations. Second, the underlying model, which is presumably simple (i.e., sparse), need to be identified.

We design our proposed SAPDEMI method to be a two-stage method to identify the underlying PDE models from the noisy data \mathcal{D} . The first stage is called a *functional estimation stage*, where we estimate all the derivatives from the noisy data \mathcal{D} , including $\frac{\partial}{\partial t}u(x, t)$, $\frac{\partial}{\partial x}u(x, t)$, and so on. In this stage, we first use the cubic splines (Shridhar and Balatoni, 1974) to fit the noisy data, and then we approximate the derivatives of the underlying

function via the derivatives of the estimated cubic splines. The second stage is called a *model identification stage*, where we apply the Least Absolute Shrinkage and Selection Operator (Lasso) (Tibshirani, 1996) to identify the derivatives (or their combinations) that should be included in the PDE-based models. To ensure the correctness of the identification, we develop sufficient conditions for correct identification and the asymptotic properties of the identified models. The main tool that we used in our theoretical analysis is the primal-dual witness (PDW) method (see Hastie et al., 2015, Chapter 11).

The rest of this section is organized as follows. In Section 1.1, we survey the existing methods that relates to the PDE identification problem. In Section 1.2, we summarize our contributions.

1.1 Literature Review

A pioneering work of identifying the underlying dynamic models from noisy data is Liang and Wu (2008). This method is also a two-stage method, where in the functional estimation stage, Liang and Wu (2008) use the local polynomial regression to estimate the value of the function and its derivatives. Subsequently, in the model identification stage, Liang and Wu (2008) use the least squares method. Following this pioneering work, vari-

ous extensions have been proposed.

The first class of extensions is to modify the functional estimation stage of Liang and Wu (2008), and we can divide these existing extensions into three categories: **(F1)**. In the numerical differentiation category (Wu et al., 2012; Brunton et al., 2016; Tran and Ward, 2017), the derivative $\frac{\partial}{\partial x}u(x, t)$ is simply approximated as

$$\frac{\partial}{\partial x}u(x, t) \approx \frac{u(x + \Delta x, t) - u(x - \Delta x, t)}{2\Delta x},$$

where $(x + \Delta x, t), (x - \Delta x, t)$ are two closest points of (x, t) in x -domain.

The essence of numerical differentiation is to approximate the first order derivative as the slope of a nearby secant line. Although the implementation is easy, it could be highly biased because its accuracy highly depends on Δx : if Δx is too small, the subtraction will yield large rounding errors (Ueberhuber, 2012; Butt, 2008); while if Δx is too large, the estimation of tangent slope by secants is poor. So naive numerical differentiation leads to biased estimations. **(F2)**. In the basis expansion category, researchers first approximate the unknown functions by the basis expansion methods and then approximate the derivatives of underlying function as the derivatives of the approximated functions. As for the choice of bases, there are multiple options in the existing literature. The most popular basis is the local polynomial basis, which is used by Liang and Wu (2008); Bär et al.

(1999); Schaeffer (2017); Rudy et al. (2017); Parlitz and Merkwirth (2000); Voss et al. (1999). Another popular choice of basis is the spline basis, as in Ramsay et al. (2007); Ramsay (1996); Wu et al. (2012); Xun et al. (2013); Wang et al. (2019). Our proposed method belongs to here. In this category, the major limitation of the existing approaches is the potentially high computational complexity. For instance, the local polynomial basis requires computational complexity of order $\max\{O(M^2N), O(MN^2)\}$ in the functional estimation stage. However, we will show that our proposed SAPDEMI method only requires $O(MN)$. This is the lowest possible bound in theory since it is the complexity of reading in the dataset \mathcal{D} . **(F3)**. In the machine or deep learning category, researchers first fit unknown functions by certain machine/deep learning methods and then approximate the derivatives of underlying functions as the derivatives of the approximated functions. One of the popular machine/deep learning methods is the neural network (NN) approach. For instance, Lagergren et al. (2020) and Srivastava et al. (2020) use the artificial neural network (ANN). Its limitation is the potential overfitting as well as the selection of the hyperparameters.

The second class of extension is to modify the model identification stage of Liang and Wu (2008). The existing methods fall in the framework of

the (penalized) least squares method, and we can again divide them into three categories: **(M1)**. In the least squares category, research is done in ordinary differential equation (ODE) identification (Miao et al., 2009) and PDE identification (Bär et al., 1999; Wu et al., 2012), which leads to reported overfitting issue. **(M2)**. In the ℓ_2 -penalized least squares method category, Xun et al. (2013); Azzimonti et al. (2015) and Wang et al. (2019) penalize the smoothness of the unknown function, which is assumed to be in a prescribed reproducing kernel Hilbert space (RKHS). Essentially, this method falls in the framework of the ℓ_2 -penalized least squares method. Although this method can avoid overfitting by introducing the ℓ_2 -penalty, it has limited power to do “model selection”. **(M3)**. In the ℓ_1 -penalized least squares method category, Schaeffer (2017) identifies the unknown dynamic models (i.e., functions) through the ℓ_1 -penalized least squares method, and later the author discusses the design of an efficient algorithm, which is based on the proximal mapping method. The authors do not discuss the statistical property of the identified model. Recently, Kang et al. (2019) and Lagergren et al. (2020) utilize the similar method as Schaeffer (2017) and demonstrate some empirical successes. One still needs to derive the corresponding statistical theory for these methods; and this paper fills the gap.

In addition to the ℓ_2 or ℓ_1 penalized least-squares methods, there are some other methods that have been proposed in the model selection stage. However, these methods are not as widely used as the ℓ_2/ℓ_1 penalized least-squares method. Some examples are the Akaike information criterion (AIC) in Mangan et al. (2017), smoothly clipped absolute deviation (SCAD) in Lu et al. (2011), and hard-thresholding in Rudy et al. (2017). The first two approaches may lead to NP-hard problems in the numerical implementation. The last one is ad-hoc, and may be hard to analytically analyze. This paper won't focus on these alternative approaches.

1.2 Our Contributions

We summarize the contributions of our proposed method – SAPDEMI. **(1)**. In the functional estimation stage, our proposed SAPDEMI method is computationally efficient. Specifically, we require computational complexity of order $O(MN)$, which is the lowest possible order in this stage. In comparison, the aforementioned local polynomial regression would require the computational complexity of order $\max\{O(M^2N), O(MN^2)\}$, which is higher. **(2)**. In this paper, for our proposed SAPDEMI method, a theoretical guarantee of model identification accuracy is established. We didn't find another occurrence of such a result. **(3)**. We extend to PDE-based

model identification, comparing to ODE-based model identification. The latter has more related work, while the former is not well understood in the literature.

The rest of the paper is organized as follows. In Section 2, we describe the technical details of our proposed SAPDEMI method. In Section 3, we present our main theory, including the sufficient conditions for correct identification, and the statistical properties of the identified models. In Section 4, we conduct numerical experiments to validate the theory from Section 3. In Section 5, we apply SAPDEMI to a real-world case study with data downloaded from the National Aeronautics and Space Administration (NASA). In Section 6, we summarize and discuss some future research.

2. Proposed Method: SAPDEMI

The proposed SAPDEMI can identify the underlying PDE model from noisy data \mathcal{D} . Our proposed SAPDEMI method is a two-stage method. The first stage is called a *functional estimation stage*, where we estimate the function and their derivatives from the noisy data \mathcal{D} in (1.1). These functional values and their derivatives serve as the input values in the second stage. The second stage is called a *model identification stage*, where we identify the underlying PDE-based model.

2.1 Functional Estimation Stage

For notations throughout the paper, scalars are denoted by lowercase letters (e.g., β). Vectors are denoted by lowercase bold face letters (e.g., $\boldsymbol{\beta}$), and its i th entry is denoted as β_i . Matrices are denoted by uppercase bold-face letter (e.g., \mathbf{B}), and its (i, j) th entry is denoted as B_{ij} . For the vector $\boldsymbol{\beta} \in \mathbb{R}^p$, its k th norm is defined as $\|\boldsymbol{\beta}\|_k := (\sum_{i=1}^p |\beta_i|^k)^{1/k}$. For the matrix $\mathbf{B} \in \mathbb{R}^{m \times n}$, its Frobenius norm is defined as $\|\mathbf{B}\|_F = \sqrt{\sum_{i=1}^m \sum_{j=1}^n |B_{ij}|^2}$. We write $f(n) = O(g(n))$, if there exists a $G \in \mathbb{R}^+$ and a n_0 such that $|f(n)| \leq Gg(x)$ for all $n > n_0$.

This section is organized as follows. In Section 2.1, we introduce the functional estimation stage, and in Section 2.2, we describe the model identification stage.

2.1 Functional Estimation Stage

In this subsection, we describe the functional estimation stage of our proposed SAPDEMI method, i.e., estimating the functional values and their derivatives from the noisy data \mathcal{D} in (1.1). These derivatives include the derivatives with respect to the spatial variable x and the derivatives with respect to the temporal variable t . In this section, we will take the derivatives with respect to spatial variable x as an example, and the derivatives with respect to the temporal variable t can be derived accordingly.

2.1 Functional Estimation Stage

The main tool that we use is the cubic spline. Suppose there is a cubic spline $s(x)$ over the knots $\{(x_i, u_i^n)\}_{i=0,1,\dots,M-1}$ satisfying the following properties (McKinley and Levine, 1998): **(1)**. $s(x) \in C^2[x_0, x_{M-1}]$, where $C^2[x_0, x_{M-1}]$ denotes the sets of function whose 0th, first and second derivatives are continuous in $[x_0, x_{M-1}]$; **(2)**. For any $i = 1, \dots, M - 1$, $s(x)$ is a polynomial of degree 3 in $[x_{i-1}, x_i]$; **(3)**. For the two end-points, x_0, x_{M-1} , we have $s''(x_0) = s''(x_{M-1}) = 0$, where $s''(x)$ is the second derivative of $s(x)$.

By fitting data $\{(x_i, u_i^n)\}_{i=0,1,\dots,M-1}$ (with a general fixed $n \in \{0, 1, \dots, N-1\}$) into the above cubic spline $s(x)$, one can solve $s(x)$ as the minimizer of the following optimization problem:

$$J_\alpha(s) = \alpha \sum_{i=0}^{M-1} w_i [u_i^n - s(x_i)]^2 + (1 - \alpha) \int_{x_0}^{x_{M-1}} s''(x)^2 dx, \quad (2.4)$$

where the first term $\alpha \sum_{i=0}^{M-1} w_i [u_i^n - s(x_i)]^2$ is the weighted sum of squares for residuals, and we take the weight $w_0 = w_1 = \dots = w_{M-1} = 1$ in our paper. In the second term $(1 - \alpha) \int_{x_0}^{x_{M-1}} s''(x)^2 dx$, function $s''(x)$ is the second derivative of $s(x)$, and this term is the penalty of the smoothness. In the above optimization problem, the parameter $\alpha \in (0, 1]$ controls the trade off between the goodness of fit and the smoothness of the cubic spline. By minimizing the above optimization problem, we can get the estimate of $s(x)$, together with its first derivative $s'(x)$ and its second deriva-

2.1 Functional Estimation Stage

tive $s''(x)$. If the cubic spline approximates the underlying PDE curves well, we can declare that the derivatives of the underlying dynamic system can be approximated by the derivatives of the cubic spline $s(x)$, i.e., we have $\widehat{u(x, t_n)} \approx \widehat{s(x)}$, $\widehat{\frac{\partial}{\partial x} u(x, t_n)} \approx \widehat{s'(x)}$, $\widehat{\frac{\partial^2}{\partial x^2} u(x, t_n)} \approx \widehat{s''(x)}$ (Ahlberg et al., 1967; Rubin and Graves Jr, 1975; Rashidinia and Mohammadi, 2008).

There is a closed-form solution for (2.4). First of all, the value of cubic spline $s(x)$ at the point $\{x_0, x_1, \dots, x_{M-1}\}$, i.e., $\widehat{\mathbf{s}} = \left(\widehat{s(x_0)}, \widehat{s(x_1)}, \dots, \widehat{s(x_{M-1})} \right)^\top$, can be solved as

$$\widehat{\mathbf{s}} = [\alpha \mathbf{W} + (1 - \alpha) \mathbf{A}^\top \mathbf{M} \mathbf{A}]^{-1} \alpha \mathbf{W} \mathbf{u}_\cdot^n, \quad (2.5)$$

which can be used to approximate the function that corresponds to the underlying PDE model, i.e., $\widehat{\mathbf{s}} \approx \widehat{\mathbf{f}} = \left(\widehat{u(x_0, t_n)}, \widehat{u(x_1, t_n)}, \dots, \widehat{u(x_{M-1}, t_n)} \right)^\top$.

Here, matrix $\mathbf{W} = \text{diag}(w_0, w_1, \dots, w_{M-1}) \in \mathbb{R}^{M \times M}$, vector $\mathbf{u}_\cdot^n = (u_0^n, \dots, u_{M-1}^n)^\top \in \mathbb{R}^M$, and matrix $\mathbf{A} \in \mathbb{R}^{(M-2) \times M}$, $\mathbf{M} \in \mathbb{R}^{(M-2) \times (M-2)}$ satisfy $\mathbf{A}_{ii} = 1/h_{i-1}$, $\mathbf{A}_{i,i+1} = -1/h_{i-1} - 1/h_i$, $\mathbf{A}_{i,i+2} = 1/h_i$, $\mathbf{M}_{ii} = \frac{h_{i-1} + h_i}{3}$, for $i = 1, \dots, M-2$, and $\mathbf{M}_{i,i+1} = \mathbf{M}_{i+1,i} = h_i/6$, for $i = 1, \dots, M-3$, are

$$\mathbf{A} = \begin{pmatrix} \frac{1}{h_0} & \frac{-1}{h_0} - \frac{1}{h_1} & \frac{1}{h_1} & \dots & 0 & 0 & 0 \\ 0 & \frac{1}{h_1} & \frac{-1}{h_1} - \frac{1}{h_2} & \dots & 0 & 0 & 0 \\ \vdots & \vdots & \vdots & \ddots & \vdots & \vdots & \vdots \\ 0 & 0 & 0 & \dots & \frac{1}{h_{M-3}} & \frac{-1}{h_{M-3}} - \frac{1}{h_{M-2}} & \frac{1}{h_{M-2}} \end{pmatrix}, \quad (2.6)$$

$$\mathbf{M} = \begin{pmatrix} \frac{h_0+h_1}{3} & \frac{h_1}{6} & 0 & \dots & 0 & 0 \\ \frac{h_1}{6} & \frac{h_1+h_2}{3} & \frac{h_2}{6} & \dots & 0 & 0 \\ 0 & \frac{h_2}{6} & \frac{h_2+h_3}{3} & \dots & 0 & 0 \\ \vdots & \vdots & \vdots & \ddots & \vdots & \vdots \\ 0 & 0 & 0 & \dots & \frac{h_{M-4}+h_{M-3}}{3} & \frac{h_{M-3}}{6} \\ 0 & 0 & 0 & \dots & \frac{h_{M-3}}{6} & \frac{h_{M-3}+h_{M-2}}{3} \end{pmatrix}, \quad (2.7)$$

respectively, with $h_i = x_{i+1} - x_i$ for $i = 0, 1, \dots, M-2$. For the mathematical details on how to derive (2.5) from (2.4), and the derivation of first and second order derivatives, please refer to the online supplementary material.

The advantage of the cubic spline is that, its computational complexity is only a linear polynomial of the sample size.

Proposition 2.1. Given data \mathcal{D} in (1.1), if we use the cubic spline in the functional estimation stage, i.e., estimate $\mathbf{X} \in \mathbb{R}^{MN \times K}$ via the cubic spline in (2.4) with $\alpha \in (0, 1]$ and $\nabla_t \mathbf{u} \in \mathbb{R}^{MN}$ from the cubic spline with $\bar{\alpha} \in (0, 1]$ also via (2.4), then the computation complexity in this stage is of order

$$\max\{O(p_{\max}MN), O(K^3)\},$$

where p_{\max} is the highest polynomial order in (1.3), M is the spatial resolution, N is temporal resolution and K is the number of columns of \mathbf{X} .

The proof can be found in the online supplementary material.

2.2 Model Identification Stage

As suggested by Proposition 2.1, when $p_{\max}, K \ll M, N$ (which is often the case in practice), it only requires $O(MN)$ numerical operations of the functional estimation stage. This is the lowest possible order of complexity in this stage because MN is exactly the number of the sample size and reading the data is an order $O(MN)$ task. So it can be concluded that it is very efficient to use cubic spline because its computational complexity achieves the lowest possible order of complexity.

For comparison, we discuss the computational complexity of the local polynomial regression, which is widely used in existing literature (Liang and Wu, 2008; Bär et al., 1999; Schaeffer, 2017; Rudy et al., 2017; Parlitz and Merkwirth, 2000). It turns out that its computational complexity is

$$\max\{O(M^2N), O(MN^2), O(p_{\max}MN), O(K^3)\},$$

which is much higher than ours. The proof can be found in the supplementary materials. We summarize the pros and cons of the cubic spline and the local polynomial regression in Table 1.

2.2 Model Identification Stage

In this section, we discuss the model identification stage of our proposed SAPDEMI method, where we want to identify the PDE model in (1.3).

The model in (1.3) can be regarded as a linear regression model whose

2.2 Model Identification Stage

Table 1: Pros and cons of the cubic spline and the local polynomial regression in the functional estimation stage (assume that $p_{\max}, q_{\max}, K \ll M, N$)

Method	Cubic spline	Local polynomial regression
Pros	Computational complexity is $O(MN)$	Derivatives up to any order
Cons	If higher-than-2 order is required, need extensions beyond cubic splines.	Computational complexity is $\max\{(M^2N), O(MN^2)\}$

response variable is the first order derivative with respect to the temporal variable t , i.e., $\frac{\partial u(x,t)}{\partial t}$, and the covariates are the derivative(s) with respect to the spatial variable x , including $\frac{\partial}{\partial x}u(x_i, t_n), \frac{\partial^2}{\partial x^2}u(x_i, t_n), \dots, \left(\frac{\partial^2}{\partial x^2}u(x_i, t_n)\right)^{p_{\max}}$. Because we have MN observations in the dataset \mathcal{D} in (1.1), the response vector is of length MN :

$$\nabla_t \mathbf{u} = \left(\widehat{\frac{\partial u(x_0, t_0)}{\partial t}}, \dots, \widehat{\frac{\partial u(x_{M-1}, t_0)}{\partial t}}, \dots, \widehat{\frac{\partial u(x_{M-1}, t_{N-1})}{\partial t}} \right)^\top, \quad (2.8)$$

and design matrix is of dimension $MN \times K$:

$$\mathbf{X} = \left(\widehat{\mathbf{x}}_0^0, \widehat{\mathbf{x}}_1^0, \dots, \widehat{\mathbf{x}}_{M-1}^0, \widehat{\mathbf{x}}_1^0, \dots, \widehat{\mathbf{x}}_{M-1}^{N-1} \right)^\top \in \mathbb{R}^{MN \times K}, \quad (2.9)$$

where the $(nN + i + 1)$ st, i.e., $\widehat{\mathbf{x}}_i^n \in \mathbb{R}^K$ row of the above matrix \mathbf{X} is $\widehat{\mathbf{x}}_i^n = \left(1, \widehat{u(x_i, t_n)}, \widehat{\frac{\partial}{\partial x}u(x_i, t_n)}, \widehat{\frac{\partial^2}{\partial x^2}u(x_i, t_n)}, \left(\widehat{u(x_i, t_n)}\right)^2, \dots, \left(\widehat{\frac{\partial^2}{\partial x^2}u(x_i, t_n)}\right)^{p_{\max}} \right)^\top$.

The K components of $\widehat{\mathbf{x}}_i^n$ are candidate terms in the PDE model. And all

the derivatives listed in (2.8), (2.9) are estimated from the functional estimation stage that is described in Section 2.1.

Next, we use Lasso to identify the non-zero coefficients in (1.3):

$$\hat{\boldsymbol{\beta}} = \arg \min_{\boldsymbol{\beta}} \frac{1}{2MN} \|\nabla_t \mathbf{u} - \mathbf{X}\boldsymbol{\beta}\|_2^2 + \lambda \|\boldsymbol{\beta}\|_1 \quad (2.10)$$

where $\lambda > 0$ is a turning parameter that controls the trade off of the sparsity of $\boldsymbol{\beta}$ and the goodness of fit. Given the ℓ_1 penalty in (2.10), $\hat{\boldsymbol{\beta}}$ will be sparse, i.e., only a few of its entries will likely be non-zero. Accordingly, we can identify the underlying PDE model as

$$\frac{\partial}{\partial t} u(x, t) = \mathbf{x}^\top \hat{\boldsymbol{\beta}}. \quad (2.11)$$

where $\mathbf{x} = \left(1, u(x, t), \frac{\partial}{\partial x} u(x, t), \frac{\partial^2}{\partial x^2} u(x, t), (u(x, t))^2, \dots, \left(\frac{\partial^2}{\partial x^2} u(x, t)\right)^{p_{\max}}\right)^\top \in \mathbb{R}^K$. To solve equation (2.10), one can use the coordinate descent method (Beck and Tetrushvili, 2013; Tseng, 2001) and we articulate its details in the online supplementary material.

3. Theory on Statistical Properties

The theoretical evaluation is done from two aspects. First, we check if our identified PDE model contains derivatives that are included in the ‘true’ underlying PDE model. This is called *support set recovery* property. Mathematically, it is to check if $\text{supp}(\hat{\boldsymbol{\beta}}) \subseteq \text{supp}(\boldsymbol{\beta}^*)$, where $\hat{\boldsymbol{\beta}}$ is the minimizer of

3.1 Conditions in the Theorems

(2.10), $\boldsymbol{\beta}^*$ is the ground truth, and $\text{supp}(\boldsymbol{\beta}) = \{i : \beta_i \neq 0, \forall i, 1 \leq i \leq K\}$ for a general vector $\boldsymbol{\beta} \in \mathbb{R}^K$. However, the support recovery depends on the choice of the penalty parameter λ . A large λ leads to $\text{supp}(\hat{\boldsymbol{\beta}}) = \emptyset$ (empty set), while a small λ results in a non-sparse $\hat{\boldsymbol{\beta}}$. A proper way to select λ hopefully leads to correct recovery of the support set recovery, i.e., we have $\text{supp}(\hat{\boldsymbol{\beta}}) \subseteq \text{supp}(\boldsymbol{\beta}^*)$. We will discuss the selection of λ to achieve the above goal in Theorem 3.1. Second, we are interested in an upper bound of the estimation error of our estimator, i.e., we consider $\|\hat{\boldsymbol{\beta}}_{\mathcal{S}} - \boldsymbol{\beta}_{\mathcal{S}}^*\|_{\infty}$, where $\mathcal{S} = \text{supp}(\boldsymbol{\beta}^*)$, vector $\hat{\boldsymbol{\beta}}_{\mathcal{S}}$ and $\boldsymbol{\beta}_{\mathcal{S}}^*$ are subvectors of $\hat{\boldsymbol{\beta}}$ and $\boldsymbol{\beta}^*$ and only contain elements whose indices are in \mathcal{S} . An upper bound of the above estimation error will be discussed in Theorem 3.2.

This section is organized as follows. In Section 3.1, we present conditions for theorems. In Section 3.2, we state two theorems.

3.1 Conditions in the Theorems

In this section, we introduce conditions that are used in our paper. We begin with three frequently used conditions in ℓ_1 -regularized regression models; these conditions provide sufficient conditions for exact sparse recovery (see Hastie et al., 2015, Chapter 11). Subsequently, we introduce three conditions that are widely used in cubic splines-based functional estimation (see

Silverman, 1984, (2.5)-(2.8)).

Condition 3.1 (Invertibility Condition). Suppose for the design matrix \mathbf{X} defined in (2.9), we have that matrix $\mathbf{X}_S^\top \mathbf{X}_S$ is invertible almost surely, where \mathbf{X}_S is the columns of \mathbf{X} whose indices are in \mathcal{S} .

Condition 3.2 (Mutual Incoherence Condition). For some *incoherence parameter* $\mu \in (0, 1]$ and $P_\mu \in [0, 1]$, we have $\mathbb{P}(\|\mathbf{X}_{S^c}^\top \mathbf{X}_S (\mathbf{X}_S^\top \mathbf{X}_S)^{-1}\|_\infty \leq 1 - \mu) \geq P_\mu$, where matrix \mathbf{X}_{S^c} is the complement of \mathbf{X}_S .

Condition 3.3 (Minimal Eigenvalue Condition). There exists some constant $C_{\min} > 0$ such that $\Lambda_{\min}(\frac{1}{NM} \mathbf{X}_S^\top \mathbf{X}_S) \geq C_{\min}$, almost surely. Here $\Lambda_{\min}(\mathbf{A})$ denotes the minimal eigenvalue of a square matrix $\mathbf{A} \in \mathbb{R}^{n \times n}$.

Condition 3.4 (Knots c.d.f. Convergence Condition). Suppose for the sequence of the empirical distribution function over the design points $x_0 < x_1 < \dots < x_{M-1}$ with different sample size M is denoted as $F_M(x)$, i.e., we have $F_M(x) = \frac{1}{M} \sum_{i=0}^{M-1} \mathbb{1}\{x_i \leq x\}$, there exists an absolutely continuous distribution function F on $[x_0, x_{M-1}]$ such that $F_M \rightarrow F$ uniformly as $M \rightarrow +\infty$. Here $\mathbb{1}\{A\}$ is the indicator of event A . A similar condition also holds for the temporal variable.

Condition 3.5 (Knots p.d.f. Convergence Condition). Suppose the first derivative of the function F, G (defined in Condition 3.4) is denoted as f, g ,

respectively, then we have

$$0 < \inf_{[x_0, x_{M-1}]} f \leq \sup_{[x_0, x_{M-1}]} f < +\infty \text{ and } 0 < \inf_{[t_0, t_{N-1}]} g \leq \sup_{[t_0, t_{N-1}]} g < +\infty,$$

and f, g also have bounded first derivatives on $[x_0, x_{M-1}]$, $[t_0, t_{N-1}]$.

Condition 3.6 (Gentle Decrease of Smoothing Parameter Condition). Suppose that $\zeta(M) = \sup_{[x_0, x_{M-1}]} |F_M - F|$, The smoothing parameter α in (2.4) depends on M in such a way that $\alpha \rightarrow 0$ and $\alpha^{-1/4} \zeta(M) \rightarrow 0$ as $M \rightarrow +\infty$. A similar condition also hold for the temporal variable.

3.2 Main Theory

In the first theorem, we develop the lower bound of λ to realize the correct recovery of the support set, i.e., $\mathcal{S}(\hat{\beta}) \subseteq \mathcal{S}(\beta^*)$.

Theorem 3.1. Provided with the data in (1.1) and suppose the conditions in Lemma D.1 and Corollary D.1 (see details in the online supplementary material) hold and Condition 3.1 - 3.6 also hold, if we take $M = O(N)$, then there exists a constant $\mathcal{C}_{(\sigma, \|u\|_{L^\infty(\Omega)})} > 0$, which is independent of spatial resolution M and temporal resolution N , such that if we set the cubic spline smoothing parameter with the spatial variable x in (2.4) as $\alpha = O\left((1 + M^{-4/7})^{-1}\right)$, set the cubic spline smoothing parameter with

temporal variable t as $\bar{\alpha} = O\left((1 + N^{-4/7})^{-1}\right)$, and set turning parameter

$$\lambda \geq \mathcal{C}(\sigma, \|u\|_{L^\infty(\Omega)}) \frac{\sqrt{K} \log(N)}{\mu N^{3/7-r}}, \quad (3.12)$$

to identify the PDE model in (2.10) for some $r \in (0, \frac{3}{7})$ with sufficient large N , then with probability greater than $P_\mu - \underbrace{O(Ne^{-Nr})}_{P'}$, we can have $\mathcal{S}(\hat{\beta}) \subseteq \mathcal{S}(\beta^*)$. Here K is the number of columns of the design matrix \mathbf{X} in (2.10), and μ, P_μ are defined in Condition 3.2.

The proof of the above theorem can be found in the online supplementary material. For the interest of page limitation, we put some lemmas in supplementary material, whose conditions is standardized in cubic splines.

The above theorem provides the lower bound of λ to realize the correct recovery of the support set. The lower bound in (3.12) is affected by several factors. First, it is affected by the temporal resolution N : as N increases, there is more flexibility in tuning this penalty parameter λ . Second, the lower bound in (3.12) is affected by the incoherence parameter μ : if μ is small, then the lower bound increases. This is because small μ means that the group of feature variable candidates are similar to each other. It should be noted that μ is decided by the dataset \mathcal{D} itself (see Condition 3.2). Third, this lower bound in (3.12) is affected by the number of columns of the matrix \mathbf{X} . If its number of columns is very large, then it requires larger

λ to identify significant feature variables among potential feature variables.

We also want to point out that, the probability $P_\mu - P'$ converges to P_μ as $N \rightarrow +\infty$. This limiting probability P_μ is determined by the data \mathcal{D} (see Condition (3.2)). So we know that when N is very large, our proposed SAPDEMI method can realize $\mathcal{S}(\hat{\beta}) \subseteq \mathcal{S}(\beta^*)$.

In the second theorem, we develop upper bound of estimating error.

Theorem 3.2. Suppose the conditions in Theorem 3.1 hold, then with probability greater than $1 - O(Ne^{-N^r}) \rightarrow 1$, there exist a $\dot{N} > 0$, such that when $N > \dot{N}$, we have

$$\left\| \hat{\beta}_{\mathcal{S}} - \beta_{\mathcal{S}}^* \right\|_{\infty} \leq \sqrt{K} C_{\min} \left(\sqrt{K} \mathcal{C}_{(\sigma, \|u\|_{L^\infty(\Omega)})} \frac{\log(N)}{N^{3/7-r}} + \lambda \right),$$

where K is the number of columns of the matrix \mathbf{X} , $\mathcal{S} := \{i : \beta_i^* \neq 0, \forall i = 1, \dots, K\}$ and vectors $\hat{\beta}_{\mathcal{S}}$ and $\beta_{\mathcal{S}}^*$ are the subvectors of $\hat{\beta}$ and β^* that only contain elements whose indices are in \mathcal{S} . Viewing from this theorem, we can see that when $N \rightarrow +\infty$, the error bound will convergence to 0.

The proof can be found in the online supplementary material.

From the above theorem, we can see that, the estimation error bound for the ℓ_∞ -norm of the coefficient error in (3.13) consists of two components. The first component is affected by the temporal resolution N , and the number of feature variable candidates K . As $N \rightarrow +\infty$, this first component

convergence to 0 without explicit dependence on the choice of feature variable selected from (2.10). The second component is $\sqrt{K}C_{\min}\lambda$. When N increases to $+\infty$, this second component will also converge to 0. This is because, as stated in Theorem 3.1, we find that when $N \rightarrow +\infty$, the lower bound of λ —which realizes correct support recovery—converges to 0. So the accuracy of the coefficient estimation will improve if we increase N .

By combining Theorems 3.1 and 3.2, we find that when the minimum absolute value of the nonzero entries of β^* is large enough, with the adequate choice of λ , the exact recovery can be guaranteed. Mathematically speaking, when $\min_{i \in \mathcal{S}} |(\beta_S^*)_i| > \sqrt{K}C_{\min} \left(\sqrt{K}\mathcal{C}_{(\sigma, \|u\|_{L^\infty(\Omega)})} \frac{\log(N)}{N^{3/7-r}} + \lambda \right)$, the vector $\hat{\beta}$ will have a correct signed-support, where $(\beta_S^*)_i$ refers to the i th element in vector β_S^* . This helps for the selection of the penalty parameters λ . Besides, the solution paths plot also helps with the selection of the penalty parameters λ , and we will discuss it in Section 4 with concrete examples.

4. Numerical Examples

We conduct numerical experiments to verify the computational efficiency and the statistical accuracy of our proposed SAPDEMI method.

Our examples are based on (1) the transport equation, (2) the inviscid Burgers' equation, and (3) the viscous Burgers' equation. We select

4.1 Example 1: Transport Equation

these three PDE models as representatives because all these PDE models play fundamental roles in modeling physical phenomenon and demonstrate characteristic behaviors shared by a more complex system, such as dissipation and shock-formation (Haberman, 1983). The difficulty to identify the above PDE models increases from the first example—the transport equation—to the last example—the viscous Burgers’ equation. We set $p_{\max} = 2$ for all the three numerical examples. For the computational efficiency, the results of these three examples are the same, so we only present the result for the first example.

We also verify Condition 3.1 - 3.6 of the above three examples. The details of the verification can be found in the online supplementary material.

4.1 Example 1: Transport Equation

The PDE problem we used in this subsection is the transport equation (see Olver, 2014, Section 2.2):

$$\begin{cases} \frac{\partial}{\partial t}u(x, t) = a \frac{\partial}{\partial x}u(x, t), & \forall 0 \leq x \leq X_{\max}, 0 \leq t \leq T_{\max}; \\ u(x, 0) = f(x); \end{cases} \quad (4.13)$$

where we set $f(x) = 2 \sin(4x)$, $a = -2$, $X_{\max} = 1$, $T_{\max} = 0.1$. Given this settings, there is a closed-form solution, which is $u(x, t) = 2 \sin(4x - 8t)$.

The dynamic pattern of the above transport equation is visualized in

4.1 Example 1: Transport Equation

Fig. 1, where subfigures (a), (b), and (c) are the ground truth, and noisy observations under $\sigma = 0.05$ and $\sigma = 0.1$, respectively. From this figure, we can see that the larger the noise, the more un-smoothed the shape of the transport equation would be, which potentially leads to more difficulties in the PDE model identification.

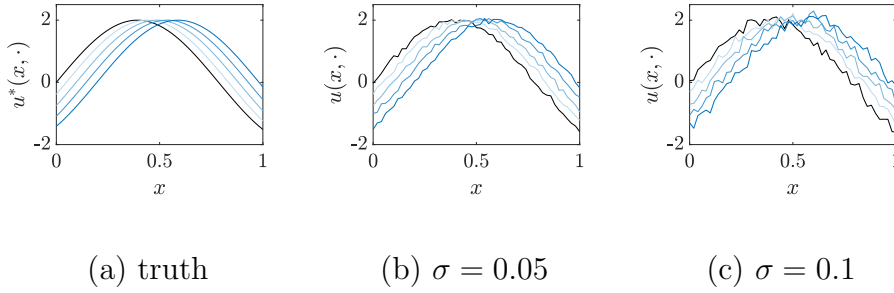


Figure 1: The noisy curves that are generated based on the transport equation ($M = N = 100$)

First of all, let us take a look at the computational complexity of the functional estimation stage. We select the local polynomial regression as a benchmark and visualize the number of numerical operations of the above two methods in Fig. 2, where the x-axis is $\log(M)$ or $\log(N)$, and the y-axis is the logarithm of the number of numerical operations. In Fig. 2, two scenarios are discussed: (1) M is fixed as 20; (2) N is fixed as 20. We find that the cubic splines method needs fewer numerical operations, compared with the local polynomial regression. Furthermore, if we conduct a simple

4.1 Example 1: Transport Equation

linear regression of the four lines in Fig. 2, we find that in (a), the slope of the cubic spline is 0.9998, and as N goes to infinity, the slope will get closer to 1. This validates that the computational complexity of the cubic splines-based method is of order $O(N)$ when M is fixed. A similar story happens to (b), so we numerically verify the computational complexity of cubic spline is of order $O(MN)$. Similarly, for local polynomial, we can also numerically validate its computational complexity, which is $\max\{O(M^2N), O(MN^2)\}$.

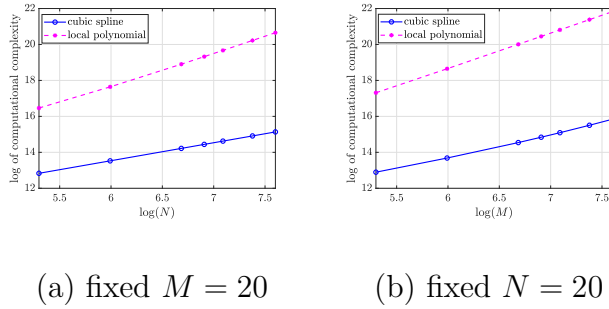


Figure 2: Computational complexity of cubic spline & local polynomial regression with fixed $M = 20$ or fixed $N = 20$.

We now numerically verify that with high probability, our SAPDEMI can correctly identify the underlying PDE models. From the formula of the transport equation in equation (4.13), we know that the correct feature variable is only $\frac{\partial}{\partial x}u(x, t)$. While other feature variables should not be identified. We discuss the identification accuracy under different sample sizes and magnitudes of noises. We find that the accuracy stays at 100%.

4.2 Example 2: Inviscid Burgers' Equation

To explain the high accuracy, we plot the solution paths in Fig. 3 under different σ , i.e., $\sigma = 0.01, 0.1, 1$. From Fig. 3, we find one can increase λ to overcome this difficulty, and thus achieve correct PDE identification.

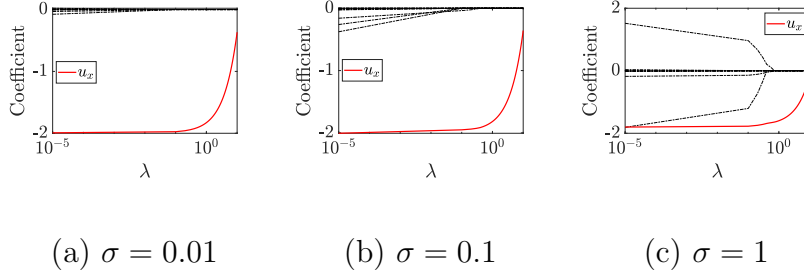


Figure 3: Solution paths in the transport equation case under different σ 's and $M = N = 100$. Notation u_x is the simplification of $\frac{\partial}{\partial x}u(x, t)$.

4.2 Example 2: Inviscid Burgers' Equation

In this section, we investigate the inviscid Burgers' equation (see Olver, 2014, Section 8.4):

$$\begin{cases} \frac{\partial}{\partial t}u(x, t) = -\frac{1}{2}u(x, t)\frac{\partial}{\partial x}u(x, t) \\ u(x, 0) = f(x) & 0 \leq x \leq X_{\max} \\ u(0, t) = u(1, t) = 0 & 0 \leq t \leq T_{\max} \end{cases}, \quad (4.14)$$

where we set $f(x) = \sin(2\pi x)$, $X_{\max} = 1$, $T_{\max} = 0.1$. Fig. 4(a), (b), and (c) show the ground truth, noisy observations under $\sigma = 0.05$, $\sigma = 0.1$, respectively.

4.2 Example 2: Inviscid Burgers' Equation

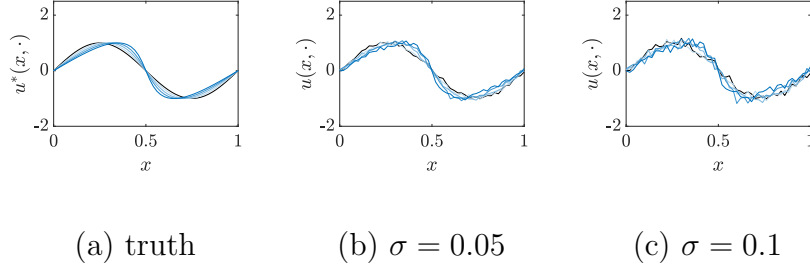


Figure 4: The curves from the inviscid Burgers' equation ($M = 50, N = 50$)

In this example, SAPDEMI can correctly identify, with accuracy above 99% (see Fig. 8(a)). The effect of σ also reflects in Fig. 5, where the length of λ -interval for correct identification decreases as σ increases.

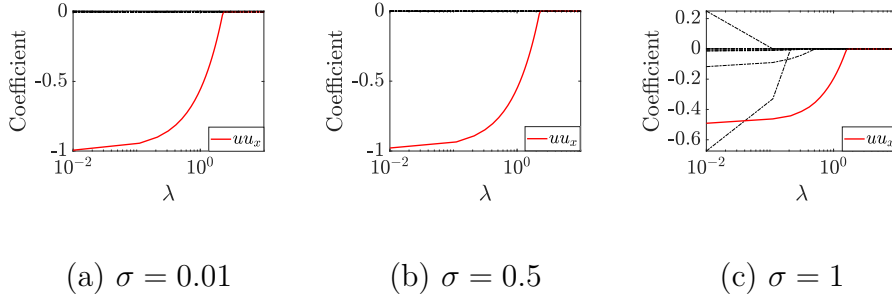


Figure 5: Solution paths in inviscid Burger's equation under different σ 's and $M = N = 100$. u and u_x are simplifications of $u(x, t)$ and $\frac{\partial}{\partial x}u(x, t)$.

4.3 Example 3: Viscous Burgers' Equation

In this section, we investigate more challenging viscous Burgers' equation (see Olver, 2014, Section 8.4):

$$\begin{cases} \frac{\partial u(x,t)}{\partial t} = -\frac{1}{2}u(x,t)\frac{\partial u(x,t)}{\partial x} + \nu\frac{\partial^2 u(x,t)}{\partial x^2} \\ u(x,0) = f(x) \\ u(0,t) = u(1,t) = 0 \end{cases} \quad \begin{matrix} 0 \leq x \leq X_{\max} \\ 0 \leq t \leq T_{\max} \end{matrix}, \quad (4.15)$$

where we set $f(x) = \sin^2(4\pi x) + \sin^3(2\pi x)$, $X_{\max} = 1$, $T_{\max} = 0.1$, $\nu = 0.1$.

Fig. 6 shows the corresponding curves, where (a), (b), and (c) are the ground truth, noisy observations under $\sigma = 0.05$ and $\sigma = 0.1$, respectively.

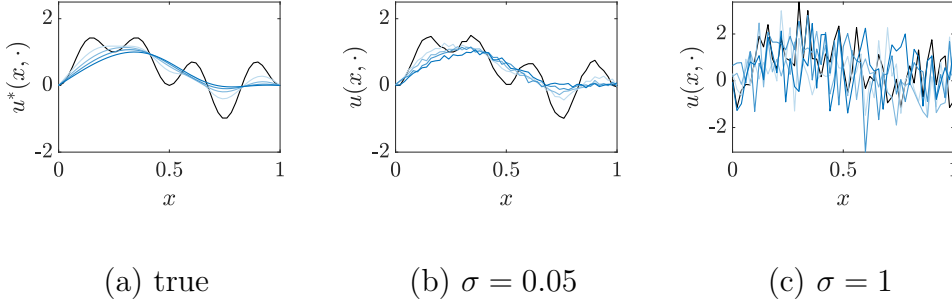


Figure 6: The curves of the viscous Burgers' equation ($M = 50, N = 50$).

Based on Fig. 8(b), we conclude that with high probability, our proposed SAPDEMI can correctly identify the underlying viscous Burgers' equation, with the reasons as follows. When $M = N = 200$ or 150 , the accuracy stays above 90% for all levels of $\sigma \in [0.01, 1]$. When $M = N = 100$, the accuracy are above 70% when $\sigma \in [0.01, 0.5]$, and reduces to 50% when

4.3 Example 3: Viscous Burgers' Equation

$\sigma = 1$, which makes sense because as reselected by Fig. 7, when σ increase from 0.01 to 1, the length of λ -interval for correct identification decreases, which make it difficult to realize correct identification. So if we encounter a heavily noised dataset \mathcal{D} , a larger sample size is preferred.

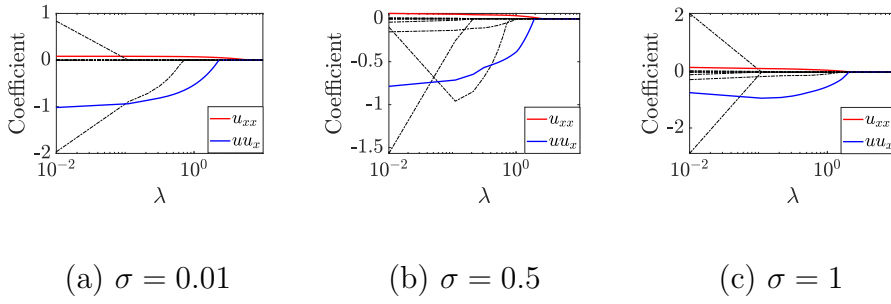


Figure 7: Solution paths in the viscous Burger's equation under different σ and $M = N = 100$. u_{xx}, uu_x are the simplification of $u(x, t) \frac{\partial}{\partial x} u(x, t), \frac{\partial^2}{\partial x^2} u(x, t)$, respectively.

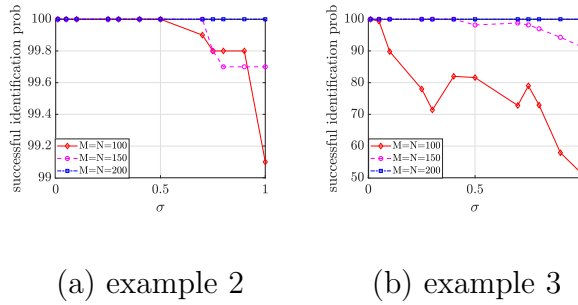
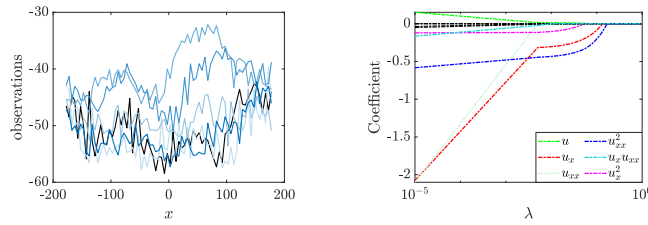


Figure 8: The successful identification probability curves under different magnitude of σ and sample size M, N .

5. Case Study

In this section, we apply SAPDEMI to a real-world dataset, which is a subset of the Cloud-Aerosol Lidar and Infrared Pathfinder Satellite Observations (CALIPSO) dataset downloaded from the NASA. The CALIPSO reports the monthly mean of temperature in 2017 at 34°N and 110.9418 meters above earth surface over a uniform spatial grid from 180°W to 180°E with equally spaced 5° interval.



(a) observed temperature (b) solution path

Figure 9: (a) is observed curves (black curve is January 2017, and the lighter color presents the later month); (b) is solution path plot.

The identified PDE model ($N = 12, M = 72$), reasonably speaking, is

$$\frac{\partial}{\partial t}u(x, t) = a \frac{\partial}{\partial x}u(x, t) + b \left(\frac{\partial^2}{\partial x^2}u(x, t) \right)^2, \quad (5.16)$$

where the values of a, b can be estimated by a simple linear regression only on the selected derivatives, i.e., $\frac{\partial}{\partial x}u(x, t)$ and $\left(\frac{\partial^2}{\partial x^2}u(x, t) \right)^2$. The linear regression suggests reasonable values of $a = -0.2505, b = 1.7648$. It should

be noticed that our paper mainly focuses on the identification, i.e., identify $\frac{\partial}{\partial x}u(x, t)$ and $\left(\frac{\partial^2}{\partial x^2}u(x, t)\right)^2$ from many derivatives candidates, instead of coefficients estimation, so we use $a = -0.2505$ and $b = 1.7648$ as reference.

Because the CALIPSP is a real-world dataset, we do not know the ground truth of the underlying PDE model. But here we provide some justifications. First, from the solution path in Fig. 9(b), we found the coefficients of $\frac{\partial}{\partial x}u(x, t)$ and $\left(\frac{\partial^2}{\partial x^2}u(x, t)\right)^2$ remain non-zeros under $\lambda = 0.05$, while other coefficients are all zero. Second, the identified PDE model in (5.16) fits well to the training data, i.e., temperature in 2017 (see Fig. 10 (a.1)-(a.3)). The value to plot Fig. 10(a.2) is calculated as follows. First, we use the identified PDE model in (5.16) to predict the value of $\frac{\partial}{\partial t}u(x, t)$ in January 2017. Then, we use the explicit Euler method (Butcher and Goodwin, 2008; Nørsett and Wanner, 1993) to predict the future value from February 2017 to December 2017, i.e., we have $u(x, t + \Delta t) = u(x, t) + \frac{\partial}{\partial t}u(x, t)\Delta t$. The three-dimension surface plot of the residual between the observed temperature and the fitted temperature can be found in Fig. 10(a.3). Seeing from Fig. 10(a.1)-(a.3), we find the fitted temperature captures the dynamic trend of the raw data well. Although the magnitude of the residual is not small, it is still satisfying. Third, the identified PDE model in (5.16) predicts well in the testing data, i.e., the temperatures in 2018 (see Fig 10

(b.1)-(b.3)). Seeing Fig. 10(b.1)-(b.3), we find the predicted temperature captures the trend of the test data in 2018 well. As for the residual plot in Fig. 10(b.3), its magnitude is not small given the inaccuracy of the explicit Euler method and the different dynamic patterns of the temperature in 2017 and 2018. This difference can potentially lead to a different PDE model in 2017 and 2018. If we persist to use the PDE model identified by the temperature in 2017 to predict the temperature in 2018, then we fail to capture difference patterns in 2018. Considering the above reasons, we think our proposed SAPDEMI method performs well in the CALIPSO dataset since it adequately predicts the feature values in 2018.

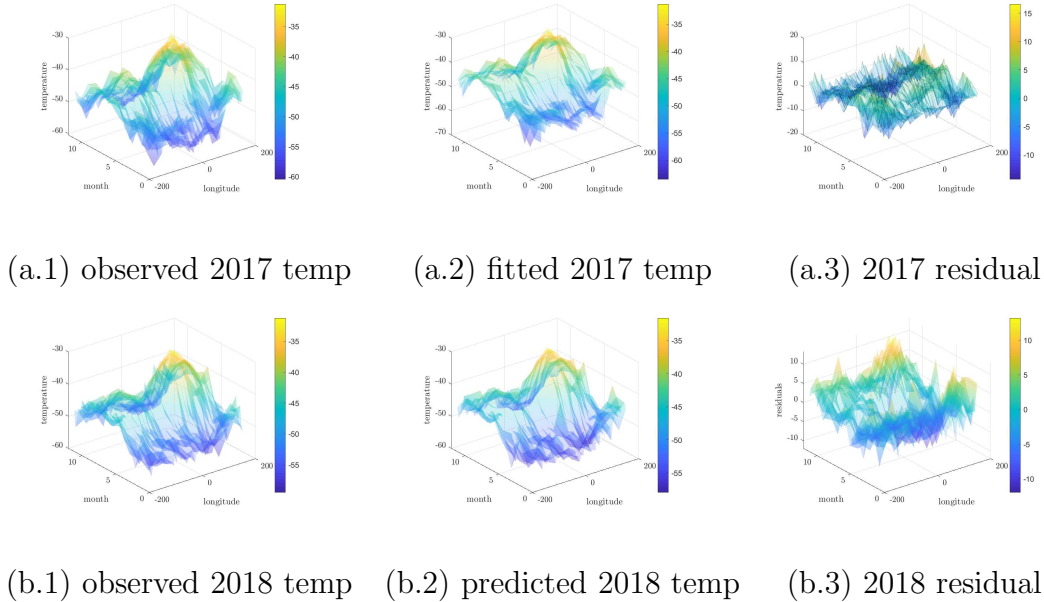


Figure 10: 3D surface plots of the temperatures in 2017/2018.

6. Conclusion

In this paper, we propose the SAPDEMI method to identify underlying PDE models from noisy data. The proposed method is computationally efficient, and we can derive a statistical guarantee on its performance. We realize there are lots of promising future research directions, including but not limited to multivariate spatial variable ($\mathbf{x} \in \mathbb{R}^d$ with $d \geq 2$), interactions between spatial variables and temporal variables. In our paper, we aim at showing the methodology to solve the PDE identification, so we do not discuss the above future research in detail and our paper should provide a good starting point for these further research.

Acknowledgements

The authors gratefully acknowledge NSF grant DMS-2015405, DMS-2015363, and the TRIAD (a part of the TRIPODS program at NSF and locates at Georgia Tech, enabled by the NSF grant CCF-1740776).

References

- Ahlberg, J., J. Walsh, R. Bellman, and E. N. Nilson (1967). *The theory of splines and their applications*. Academic press.
- Azzimonti, L., L. M. Sangalli, P. Secchi, M. Domanin, and F. Nobile (2015). Blood flow velocity

REFERENCES

- field estimation via spatial regression with PDE penalization. *Journal of the American Statistical Association* 110(511), 1057–1071.
- Bär, M., R. Hegger, and H. Kantz (1999). Fitting partial differential equations to space-time dynamics. *Physical Review E* 59(1), 337.
- Beck, A. and L. Tetruashvili (2013). On the convergence of block coordinate descent type methods. *SIAM journal on Optimization* 23(4), 2037–2060.
- Brunton, S. L., J. L. Proctor, and J. N. Kutz (2016). Discovering governing equations from data by sparse identification of nonlinear dynamical systems. *Proceedings of the national academy of sciences* 113(15), 3932–3937.
- Butcher, J. C. and N. Goodwin (2008). *Numerical methods for ordinary differential equations*, Volume 2. Wiley Online Library.
- Butt, R. (2008). *Introduction to numerical analysis using MATLAB*. Laxmi Publications, Ltd.
- Craven, P. and G. Wahba (1978). Smoothing noisy data with spline functions. *Numerische mathematik* 31(4), 377–403.
- Fan, J., T. Gasser, I. Gijbels, M. Brockmann, and J. Engel (1997). Local polynomial regression: optimal kernels and asymptotic minimax efficiency. *Annals of the Institute of Statistical Mathematics* 49(1), 79–99.
- Friedman, J., T. Hastie, and R. Tibshirani (2010). Regularization paths for generalized linear models via coordinate descent. *Journal of statistical software* 33(1), 1.

REFERENCES

- Haberman, R. (1983). *Elementary applied partial differential equations*, Volume 987. Prentice Hall Englewood Cliffs, NJ.
- Hastie, T., R. Tibshirani, and M. Wainwright (2015). *Statistical learning with sparsity: the lasso and generalizations*. CRC press.
- Kang, S. H., W. Liao, and Y. Liu (2019). IDENT: Identifying differential equations with numerical time evolution. *arXiv preprint arXiv:1904.03538*.
- Lagergren, J. H., J. T. Nardini, G. Michael Lavigne, E. M. Rutter, and K. B. Flores (2020). Learning partial differential equations for biological transport models from noisy spatio-temporal data. *Proceedings of the Royal Society A* 476(2234), 20190800.
- Lambert, J. D. et al. (1991). *Numerical methods for ordinary differential systems*, Volume 146. Wiley New York.
- Liang, H. and H. Wu (2008). Parameter estimation for differential equation models using a framework of measurement error in regression models. *Journal of the American Statistical Association* 103(484), 1570–1583.
- Lu, T., H. Liang, H. Li, and H. Wu (2011). High-dimensional ODEs coupled with mixed-effects modeling techniques for dynamic gene regulatory network identification. *Journal of the American Statistical Association* 106(496), 1242–1258.
- Mack, Y.-p. and B. W. Silverman (1982). Weak and strong uniform consistency of kernel regression estimates. *Zeitschrift für Wahrscheinlichkeitstheorie und verwandte Gebiete* 61(3), 405–415.

REFERENCES

- Mangan, N. M., J. N. Kutz, S. L. Brunton, and J. L. Proctor (2017). Model selection for dynamical systems via sparse regression and information criteria. *Proceedings of the Royal Society A: Mathematical, Physical and Engineering Sciences* 473(2204), 20170009.
- McKinley, S. and M. Levine (1998). Cubic spline interpolation. *College of the Redwoods* 45(1), 1049–1060.
- Messer, K. (1991). A comparison of a spline estimate to its equivalent kernel estimate. *The Annals of Statistics* 19(2), 817–829.
- Miao, H., C. Dykes, L. M. Demeter, and H. Wu (2009). Differential equation modeling of HIV viral fitness experiments: model identification, model selection, and multimodel inference. *Biometrics* 65(1), 292–300.
- Nørsett, S. P. and G. Wanner (1993). *Solving ordinary differential equations: Stiff and differential-algebraic problems*. Springer-Verlag.
- Olver, P. J. (2014). *Introduction to partial differential equations*. Springer.
- Parlitz, U. and C. Merkwirth (2000). Prediction of spatiotemporal time series based on reconstructed local states. *Physical review letters* 84(9), 1890.
- Ramsay, J. O. (1996). Principal differential analysis: Data reduction by differential operators. *Journal of the Royal Statistical Society: Series B (Methodological)* 58(3), 495–508.
- Ramsay, J. O., G. Hooker, D. Campbell, and J. Cao (2007). Parameter estimation for differential equations: a generalized smoothing approach. *Journal of the Royal Statistical Society:*

REFERENCES

- Series B (Statistical Methodology)* 69(5), 741–796.
- Rashidinia, J. and R. Mohammadi (2008). Non-polynomial cubic spline methods for the solution of parabolic equations. *International Journal of Computer Mathematics* 85(5), 843–850.
- Rice, J. and M. Rosenblatt (1983). Smoothing splines: regression, derivatives and deconvolution. *The annals of Statistics*, 141–156.
- Rosenblatt, M. (1952). Remarks on a multivariate transformation. *The annals of mathematical statistics* 23(3), 470–472.
- Rubin, S. G. and R. A. Graves Jr (1975). A cubic spline approximation for problems in fluid mechanics. *NASA STI/Recon Technical Report N 75*, 33345.
- Rudy, S. H., S. L. Brunton, J. L. Proctor, and J. N. Kutz (2017). Data-driven discovery of partial differential equations. *Science Advances* 3(4), e1602614.
- Schaeffer, H. (2017). Learning partial differential equations via data discovery and sparse optimization. *Proceedings of the Royal Society A: Mathematical, Physical and Engineering Sciences* 473(2197), 20160446.
- Shridhar, M. and N. Balatoni (1974). A generalized cubic spline technique for identification of multivariable systems. *Journal of Mathematical Analysis and Applications* 47(1), 78–90.
- Silverman, B. W. (1978). Weak and strong uniform consistency of the kernel estimate of a density and its derivatives. *The Annals of Statistics*, 177–184.
- Silverman, B. W. (1984). Spline smoothing: the equivalent variable kernel method. *The Annals*

REFERENCES

- of Statistics*, 898–916.
- Srivastava, K., M. Ahlawat, J. Singh, and V. Kumar (2020). Learning partial differential equations from noisy data using neural networks. In *Journal of Physics: Conference Series*, Volume 1655, pp. 012075. IOP Publishing.
- Tibshirani, R. (1996). Regression shrinkage and selection via the lasso. *Journal of the Royal Statistical Society: Series B (Methodological)* 58(1), 267–288.
- Tran, G. and R. Ward (2017). Exact recovery of chaotic systems from highly corrupted data. *Multiscale Modeling & Simulation* 15(3), 1108–1129.
- Tseng, P. (2001). Convergence of a block coordinate descent method for nondifferentiable minimization. *Journal of optimization theory and applications* 109(3), 475–494.
- Tusnády, G. (1977). A remark on the approximation of the sample DF in the multidimensional case. *Periodica Mathematica Hungarica* 8(1), 53–55.
- Ueberhuber, C. W. (2012). *Numerical computation 1: methods, software, and analysis*. Springer Science & Business Media.
- Voss, H. U., P. Kolodner, M. Abel, and J. Kurths (1999). Amplitude equations from spatiotemporal binary-fluid convection data. *Physical review letters* 83(17), 3422.
- Wang, D., K. Liu, and X. Zhang (2019). Spatiotemporal thermal field modeling using partial differential equations with time-varying parameters. *IEEE Transactions on Automation Science and Engineering*.

REFERENCES

- Wang, H., D. Yang, and S. Zhu (2014). Inhomogeneous Dirichlet boundary-value problems of space-fractional diffusion equations and their finite element approximations. *SIAM Journal on Numerical Analysis* 52(3), 1292–1310.
- Winkelbauer, A. (2012). Moments and absolute moments of the normal distribution. *arXiv preprint arXiv:1209.4340*.
- Wu, H., H. Xue, and A. Kumar (2012). Numerical discretization-based estimation methods for ordinary differential equation models via penalized spline smoothing with applications in biomedical research. *Biometrics* 68(2), 344–352.
- Xun, X., J. Cao, B. Mallick, A. Maity, and R. J. Carroll (2013). Parameter estimation of partial differential equation models. *Journal of the American Statistical Association* 108(503), 1009–1020.

Biostatistics and Research Decision Sciences Department, Merck & Co., Inc

E-mail: (yujie.zhao@merck.com)

H. Milton Stewart School of Industrial and Systems Engineering, Georgia Tech

E-mail: (huo@gatech.edu)

H. Milton Stewart School of Industrial and Systems Engineering, Georgia Tech

E-mail: (ymei@isye.gatech.edu)

Appendix

A. Derivation of the 0-th, First, Second Derivative of the Cubic Spline in Section 2.1.

In this section, we focus on solving the derivatives of $u(x, t_n)$ with respect to x , i.e.,

$$\left\{ u(x_i, t_n), \frac{\partial}{\partial x} u(x_i, t_n), \frac{\partial^2}{\partial x^2} u(x_i, t_n) \right\}_{i=0,1,\dots,M-1}$$

for any $n = 0, 1, \dots, N-1$. To realize this objective, we first fix t as t_n for a general $n \in$

$\{0, 1, \dots, N-1\}$. Then we use cubic spline to fit data $\{(x_i, u_n^i)\}_{i=0,1,\dots,M-1}$.

Suppose the cubic polynomial spline over the knots $\{(x_i, u_n^i)\}_{i=0,1,\dots,M-1}$ is $s(x)$. So under good approximation, we can regard $s(x), s'(x), s''(x)$ as the estimators of $u(x_i, t_n), \frac{\partial}{\partial x} u(x, t_n), \frac{\partial^2}{\partial x^2} u(x, t_n)$, where $s'(x), s''(x)$ is the first and second derivatives of $s(x)$, respectively.

Let first take a look at the zero-order derivatives of $s(x)$. By introducing matrix algebra, the objective function in equation (2.4) can be rewritten as

$$J_\alpha(s) = \alpha(\mathbf{u}_\cdot^n - \mathbf{f})^\top \mathbf{W}(\mathbf{u}_\cdot^n - \mathbf{f}) + (1 - \alpha)\mathbf{f}^\top \mathbf{A}^\top \mathbf{M}^{-1} \mathbf{A} \mathbf{f} \quad (\text{A.17})$$

where vector

$$\mathbf{f} = \begin{pmatrix} s(x_0) \\ s(x_1) \\ \vdots \\ s(x_{M-1}) \end{pmatrix} \triangleq \begin{pmatrix} f_0 \\ f_1 \\ \vdots \\ f_{M-1} \end{pmatrix}, \mathbf{u}_\cdot^n = \begin{pmatrix} u_0^n \\ u_1^n \\ \vdots \\ u_{M-1}^n \end{pmatrix}$$

and matrix $\mathbf{W} = \text{diag}(w_0, w_1, \dots, w_{M-1})$ and matrix \mathbf{A} is defined in (2.6). By taking the derivative of (A.17) with respect to \mathbf{f} and set it as zero, we have

$$\widehat{\mathbf{f}} = [\alpha \mathbf{W} + (1 - \alpha) \mathbf{A}^\top \mathbf{M} \mathbf{A}]^{-1} \alpha \mathbf{W} \mathbf{u}^n. \quad (\text{A.18})$$

Then we solve the second-order derivative with respect to x . Let us first suppose that the cubic spline $s(x)$ in $[x_i, x_{i+1}]$ is denoted $s_i(x)$, and we denote $s_i''(x_i) = \sigma_i, s_i''(x_{i+1}) = \sigma_{i+1}$.

Then we have $\forall x \in [x_i, x_{i+1}]$ ($0 \leq i \leq M - 2$),

$$s_i''(x) = \sigma_i \frac{x_{i+1} - x}{h_i} + \sigma_{i+1} \frac{x - x_i}{h_i},$$

where matrix \mathbf{M} is defined in (2.7). This is because $s_i''(x)$ with $x \in [x_i, x_{i+1}]$ is a linear function.

By taking a double integral of the above equation, we have

$$s_i(x) = \frac{\sigma_i}{6h_i} (x_{i+1} - x)^3 + \frac{\sigma_{i+1}}{6h_i} (x - x_i)^3 + c_1(x - x_i) + c_2(x_{i+1} - x), \quad (\text{A.19})$$

where c_1, c_2 is the unknown parameters to be estimated. Because $s_i(x)$ interpolates two end-points (x_i, f_i) and (x_{i+1}, f_{i+1}) , if we plug x_i, x_{i+1} into the above $s_i(x)$, we have

$$\begin{cases} f_i &= s_i(x_i) = \frac{\sigma_i}{6} h_i^2 + c_2 h_i \\ f_{i+1} &= s_i(x_{i+1}) = \frac{\sigma_{i+1}}{6} h_i^2 + c_1 h_i, \end{cases}$$

where we can solve c_1, c_2 as

$$\begin{cases} c_1 &= (f_{i+1} - \frac{\sigma_{i+1}}{6} h_i^2) / h_i \\ c_2 &= (f_i - \frac{\sigma_i}{6} h_i^2) / h_i. \end{cases}$$

By plugging in the value of c_1, c_2 into equation (A.19), we have ($0 \leq i \leq M-2$)

$$s_i(x) = \frac{\sigma_i}{6h_i}(x_{i+1} - x)^3 + \frac{\sigma_{i+1}}{6h_i}(x - x_i)^3 + \left(\frac{f_{i+1}}{h_i} - \frac{\sigma_{i+1}h_i}{6} \right) (x - x_i) + \left(\frac{f_i}{h_i} - \frac{\sigma_i h_i}{6} \right) (x_{i+1} - x)$$

with its first derivative as

$$s'_i(x) = -\frac{\sigma_i}{2h_i}(x_{i+1} - x)^2 + \frac{\sigma_{i+1}}{2h_i}(x - x_i)^2 + \frac{f_{i+1} - f_i}{h_i} - \frac{h_i}{6}(\sigma_{i+1} - \sigma_i). \quad (\text{A.20})$$

Because $s'_{i-1}(x_i) = s'_i(x_i)$, we have ($1 \leq i \leq M-2$)

$$\frac{1}{6}h_{i-1}\sigma_{i-1} + \frac{1}{3}(h_{i-1} + h_i)\sigma_i + \frac{1}{6}h_i\sigma_{i+1} = \frac{f_{i+1} - f_i}{h_i} - \frac{f_i - f_{i-1}}{h_{i-1}}. \quad (\text{A.21})$$

Equation (A.21) gives $M-2$ equations. Recall $\sigma_0 = \sigma_{M-1} = 0$, so totally we get M equations,

which is enough to solve M parameters, i.e., $\sigma_0, \sigma_1, \dots, \sigma_{M-1}$. We write out the above system

of linear equations, where we hope to identify a fast numerical approach to solve it. The system

of linear equations is:

$$\left\{ \begin{array}{llllll} & \frac{1}{3}(h_0 + h_1)\sigma_1 & + & \frac{1}{6}h_1\sigma_2 & = & \frac{u_2^n - u_1^n}{h_1} - \frac{f_1 - u_0}{h_0} \\ \frac{1}{6}h_1\sigma_1 & + & \frac{1}{3}(h_1 + h_2)\sigma_2 & + & \frac{1}{6}h_2\sigma_3 & = & \frac{f_3 - f_2}{h_1} - \frac{f_2 - f_1}{h_0} \\ & & & \vdots & & \\ \frac{1}{6}h_{M-4}\sigma_{M-4} & + & \frac{1}{3}(h_{M-4} + h_{M-3})\sigma_{M-3} & + & \frac{1}{6}h_{M-3}\sigma_{M-2} & = & \frac{f_{M-2} - f_{M-3}}{h_{M-3}} - \frac{f_{M-3} - f_{M-4}}{h_{M-4}} \\ \frac{1}{6}h_{M-3}\sigma_{M-3} & + & \frac{1}{3}(h_{M-3} + h_{M-2})\sigma_{M-2} & & & = & \frac{f_{M-1} - f_{M-2}}{h_{M-2}} - \frac{f_{M-2} - f_{M-3}}{h_{M-3}} \end{array} \right. .$$

From the above system of equation, we can see that the second derivative of cubic spline $s(x)$

can be solved by the above system of linear equation, i.e.,

$$\hat{\sigma} = \mathbf{M}^{-1} \mathbf{A} \hat{\mathbf{f}} \quad (\text{A.22})$$

where vector $\widehat{\mathbf{f}}$ is defined in (A.18), matrix $\mathbf{A} \in \mathbb{R}^{(M-2) \times M}$ is defined in (2.6), and matrix $\mathbf{M} \in \mathbb{R}^{(M-2) \times (M-2)}$ is defined as (2.7).

Finally, we focus on solving the first derivative of cubic spline $s(x)$. Let $\theta_i = s'(x_i)$ for $i = 0, 1, \dots, M-1$, then we have

$$\begin{aligned}
s_i(x) &= \theta_i \frac{(x_{i+1}-x)^2(x-x_i)}{h_i^2} - \theta_{i+1} \frac{(x-x_i)^2(x_{i+1}-x)}{h_i^2} + f_i \frac{(x_{i+1}-x)^2[2(x-x_i)+h_i]}{h_i^3} + \\
&\quad f_{i+1} \frac{(x-x_i)^2[2(x_{i+1}-x)+h_i]}{h_i^3} \\
s'_i(x) &= \theta_i \frac{(x_{i+1}-x)(2x_i+x_{i+1}-3x)}{h_i^2} - \theta_{i+1} \frac{(x-x_i)(2x_{i+1}+x_i-3x)}{h_i^2} + 6 \frac{u_{i+1}^n - u_i^n}{h_i^3} (x_{i+1} - x)(x - x_i) \\
s''_i(x) &= -2\theta_i \frac{2x_{i+1}+x_i-3x}{h_i^2} - 2\theta_{i+1} \frac{2x_i+x_{i+1}-3x}{h_i^2} + 6 \frac{u_{i+1}^n - u_i^n}{h_i^3} (x_{i+1} + x_i - 2x)
\end{aligned}$$

By plugging x_i into $s''_i(x)$ and $s''_{i-1}(x)$, we have

$$\begin{cases}
s''_i(x) &= -2\theta_i \frac{2x_{i+1}+x_i-3x}{h_i^2} - 2\theta_{i+1} \frac{2x_i+x_{i+1}-3x}{h_i^2} + 6 \frac{f_{i+1}-f_i}{h_i^3} (x_{i+1} + x_i - 2x) \\
s''_{i-1}(x) &= -2\theta_{i-1} \frac{2x_i+x_{i-1}-3x}{h_{i-1}^2} - 2\theta_i \frac{2x_{i-1}+x_i-3x}{h_{i-1}^2} + 6 \frac{f_i-f_{i-1}}{h_{i-1}^3} (x_i + x_{i-1} - 2x)
\end{cases}$$

which gives

$$\begin{cases}
s''_i(x) &= \frac{-4}{h_i} \theta_i + \frac{-2}{h_i} \theta_{i+1} + 6 \frac{f_{i+1}-f_i}{h_i^2} \\
s''_{i-1}(x) &= \frac{2}{h_{i-1}} \theta_{i-1} + \frac{4}{h_{i-1}} \theta_i - 6 \frac{f_i-f_{i-1}}{h_{i-1}^2}.
\end{cases}$$

Because $s''_i(x_i) = s''_{i-1}(x_i)$, we have ($\forall i = 1, 2, \dots, M-2$)

$$\begin{aligned}
\frac{-4}{h_i} \theta_i + \frac{-2}{h_i} \theta_{i+1} + 6 \frac{f_{i+1}-f_i}{h_i^2} &= \frac{2}{h_{i-1}} \theta_{i-1} + \frac{4}{h_{i-1}} \theta_i - 6 \frac{f_i-f_{i-1}}{h_{i-1}^2} \\
\Leftrightarrow \frac{2}{h_{i-1}} \theta_{i-1} + (\frac{4}{h_{i-1}} + \frac{4}{h_i}) \theta_i + \frac{2}{h_i} \theta_{i+1} &= 6 \frac{f_{i+1}-f_i}{h_i^2} + 6 \frac{f_i-f_{i-1}}{h_{i-1}^2} \\
\Leftrightarrow \frac{1}{h_{i-1}} \theta_{i-1} + (\frac{2}{h_{i-1}} + \frac{2}{h_i}) \theta_i + \frac{1}{h_i} \theta_{i+1} &= 3 \frac{f_{i+1}-f_i}{h_i^2} + 3 \frac{f_i-f_{i-1}}{h_{i-1}^2}.
\end{aligned}$$

By organizing the above system of equation into matrix algebra, we have

$$\begin{aligned}
& \begin{pmatrix} \frac{1}{h_0} & \frac{2}{h_0} + \frac{2}{h_1} & \frac{1}{h_1} & 0 & \dots & 0 & 0 & 0 \\ 0 & \frac{1}{h_1} & \frac{2}{h_1} + \frac{2}{h_2} & 0 & \dots & 0 & 0 & 0 \\ \vdots & \vdots & \vdots & \vdots & \ddots & \vdots & \vdots & \vdots \\ 0 & 0 & 0 & 0 & \dots & \frac{1}{h_{M-3}} & \frac{2}{h_{M-3}} + \frac{2}{h_{M-2}} & \frac{1}{h_{M-2}} \end{pmatrix} \begin{pmatrix} \theta_0 \\ \theta_1 \\ \theta_2 \\ \vdots \\ \theta_{M-1} \end{pmatrix} \\
&= \begin{pmatrix} 3 \frac{f_2 - f_1}{h_1^2} + 3 \frac{f_1 - f_0}{h_0^2} \\ 3 \frac{f_3 - f_2^n}{h_2^2} + 3 \frac{f_2 - f_1}{h_1^2} \\ \vdots \\ 3 \frac{f_{M-1} - f_{M-2}}{h_{M-2}^2} + 3 \frac{f_{M-2}^n - f_{M-3}}{h_{M-3}^2} \end{pmatrix}.
\end{aligned}$$

For the endpoint θ_0 , because $s_0''(x_0) = 0$, we have

$$s_0''(x) = -2\theta_0 \frac{2x_1 + x_0 - 3x}{h_0^2} - 2\theta_1 \frac{2x_0 + x_1 - 3x}{h_0^2} + 6 \frac{f_1 - f_0}{h_0^3} (x_1 + x_0 - 2x).$$

When we take the value of x as x_0 , we have

$$\begin{aligned}
s_0''(x_0) &= -2\theta_0 \frac{2x_1 + x_0 - 3x_0}{h_0^2} - 2\theta_1 \frac{2x_0 + x_1 - 3x_0}{h_0^2} + 6 \frac{f_1 - f_0}{h_0^3} (x_1 + x_0 - 2x_0) \\
&= \frac{-4}{h_0} \theta_0 + \frac{-2}{h_0} \theta_1 + 6 \frac{f_1 - f_0}{h_0^2} \\
&= 0
\end{aligned}$$

For the two endpoint θ_{M-1} , because $s_{M-2}''(x_{M-1}) = 0$, we have

$$\begin{aligned}
s_{M-2}''(x) &= -2\theta_{M-2} \frac{2x_{M-1} + x_{M-2} - 3x}{h_{M-2}^2} - 2\theta_{M-1} \frac{2x_{M-2} + x_{M-1} - 3x}{h_{M-2}^2} + \\
&\quad 6 \frac{f_{M-1} - f_{M-2}}{h_{M-2}^3} (x_{M-1} + x_{M-2} - 2x)
\end{aligned}$$

When we take the value of x as x_{M-1} , we have

$$\begin{aligned}
s''_{M-2}(x_{M-1}) &= -2\theta_{M-2} \frac{2x_{M-1}+x_{M-2}-3x_{M-1}}{h_{M-2}^2} - 2\theta_{M-1} \frac{2x_{M-2}+x_{M-1}-3x_{M-1}}{h_{M-2}^2} + \\
&\quad 6 \frac{f_{M-1}-f_{M-2}}{h_{M-2}^3} (x_{M-1} + x_{M-2} - 2x_{M-1}) \\
&= \frac{2}{h_{M-2}} \theta_{M-2} + \frac{4}{h_{M-2}} \theta_{M-1} - 6 \frac{f_{M-1}-f_{M-2}}{h_{M-2}^2} \\
&= 0.
\end{aligned}$$

So the first order derivative $\boldsymbol{\theta} = (\theta_0, \theta_1, \dots, \theta_{M-1})^\top$ can be solved by

$$\begin{aligned}
&\underbrace{\begin{pmatrix} \frac{2}{h_0} & \frac{1}{h_0} & 0 & 0 & \dots & 0 & 0 & 0 \\ \frac{1}{h_0} & \frac{2}{h_0} + \frac{2}{h_1} & \frac{1}{h_1} & 0 & \dots & 0 & 0 & 0 \\ 0 & \frac{1}{h_1} & \frac{2}{h_1} + \frac{2}{h_2} & 0 & \dots & 0 & 0 & 0 \\ \vdots & \vdots & \vdots & \vdots & \ddots & \vdots & \vdots & \vdots \\ 0 & 0 & 0 & 0 & \dots & \frac{1}{h_{M-3}} & \frac{2}{h_{M-3}} + \frac{2}{h_{M-2}} & \frac{1}{h_{M-2}} \\ 0 & 0 & 0 & 0 & \dots & 0 & \frac{1}{h_{M-2}} & \frac{2}{h_{M-2}} \end{pmatrix}}_{\mathbf{Q} \in \mathbb{R}^{M \times M}} \underbrace{\begin{pmatrix} \theta_0 \\ \theta_1 \\ \theta_2 \\ \theta_3 \\ \theta_4 \\ \vdots \\ \theta_{M-1} \end{pmatrix}}_{\boldsymbol{\theta}} \\
&= \underbrace{\begin{pmatrix} 3 \frac{f_1-f_0}{h_0^2} \\ 3 \frac{f_2-f_1}{h_1^2} + 3 \frac{f_1-f_0}{h_0^2} \\ 3 \frac{f_3-f_2}{h_2^2} + 3 \frac{f_2-f_1}{h_1^2} \\ \vdots \\ 3 \frac{f_{M-1}-f_{M-2}}{h_{M-2}^2} + 3 \frac{f_{M-2}-f_{M-3}}{h_{M-3}^2} \\ 3 \frac{f_{M-1}-f_{M-2}}{h_{M-2}^2} \end{pmatrix}}_{\mathbf{q}}
\end{aligned}$$

In matrix algebra, the first order derivative $\boldsymbol{\theta} = (\theta_0, \theta_1, \dots, \theta_{M-1})^\top$ can be solved by

$$\hat{\boldsymbol{\theta}} = \mathbf{Q}^{-1}\hat{\mathbf{q}} = \mathbf{Q}^{-1}\mathbf{B}\hat{\mathbf{f}}, \quad (\text{A.23})$$

where $\hat{\mathbf{f}}$ is defined in (A.18), and matrix $\mathbf{B} \in \mathbb{R}^{M \times M}$ is defined as

$$\mathbf{B} = \begin{pmatrix} \frac{-3}{h_0^2} & \frac{3}{h_0^2} & 0 & 0 & \dots & 0 & 0 & 0 \\ \frac{-3}{h_0^2} & \frac{3}{h_0^2} - \frac{3}{h_1^2} & \frac{3}{h_1^2} & 0 & \dots & 0 & 0 & 0 \\ 0 & \frac{-3}{h_1^2} & \frac{3}{h_1^2} - \frac{3}{h_2^2} & \frac{3}{h_2^2} & \dots & 0 & 0 & 0 \\ \vdots & \vdots & \vdots & \vdots & \ddots & \vdots & \vdots & \vdots \\ & 0 & 0 & 0 & 0 & \frac{-3}{h_{M-3}^2} & \frac{3}{h_{M-3}^2} - \frac{3}{h_{M-2}^2} & \frac{3}{h_{M-2}^2} \\ & 0 & 0 & 0 & 0 & 0 & \frac{-3}{h_{M-2}^2} & \frac{3}{h_{M-2}^2} \end{pmatrix}.$$

B. Computational Complexity of Local Polynomial Regression Method

In the functional estimation stage, the computational complexity of the local polynomial regression method is stated in the following proportion.

Proposition B.1. Given data \mathcal{D} in (1.1), if we use the local polynomial regression in the functional estimation stage, i.e., estimate $\mathbf{X} \in \mathbb{R}^{MN \times K}$, $\nabla_t \mathbf{u} \in \mathbb{R}^{MN}$ via the local polynomial regression described as in online supplementary material, then the computation complexity of this stage is of order

$$\max\{O(q_{\max}^2 M^2 N), O(MN^2), O(q_{\max}^3 MN), O(p_{\max} MN), O(K^3)\},$$

where p_{\max} is the highest polynomial order in (1.3), q_{\max} is the highest order of derivatives in (1.3), M is the spatial resolution, N is the temporal resolution, and K is the number of columns of \mathbf{X} .

If we set $q_{\max} = 2$ to match the derivative order of the local polynomial regression to the cubic spline, then the computation complexity is of order

$$\max\{O(M^2N), O(MN^2), O(p_{\max}MN), O(K^3)\}.$$

As suggested by Proposition B.1, the computational complexity of local polynomial regression is much higher than that in the cubic spline. But the advantage of local polynomial regression is that it can derive any order of derivatives, i.e., $q_{\max} \geq 0$ in (1.3), while for the cubic spline, $q_{\max} = 2$. In applications, $q_{\max} = 2$ should be sufficient because most of the PDE models are governed by derivatives up to the second derivative, for instance, heat equation, wave equation, Laplace's equation, Helmholtz equation, Poisson's equation, and so on. In our paper, we mainly use cubic spline as an illustration example due to its simplification and computational efficiency. Readers can extend our proposed SAPDEMI method to the higher-order spline with $q_{\max} > 2$ if they are interested in higher-order derivatives.

C. Coordinate Gradient Descent to Solve the Optimization problem in Section 2.2.

In this section, we briefly review the implement of the coordinate descent algorithm in Friedman et al. (2010) to solve (2.10). The main idea of the coordinate descent is to update the estimator in

a coordinate-wise fashion, which is the main difference between the coordinate descent and regular gradient descent. For instance, in the k -th iteration, the coordinate descent updates the iterative estimator $\boldsymbol{\beta}^{(k)}$ by using partial of the gradient information, instead of the whole gradient information. Mathematically speaking, in the k -th iteration, the coordinate descent optimizes $F(\boldsymbol{\beta}) = \frac{1}{2MN} \|\nabla_t \mathbf{u} - \mathbf{X}\boldsymbol{\beta}\|_2^2 + \lambda \|\boldsymbol{\beta}\|_1$ with respect to $\boldsymbol{\beta}$ by

$$\beta_j^{(k+1)} = \arg \min_{\beta_j} F((\beta_1^{(k)}, \beta_2^{(k)}, \dots, \beta_{j-1}^{(k)}, \beta_j, \beta_{j+1}^{(k)}, \dots, \beta_K^{(k)}))$$

for all $j = 1, 2, \dots, K$. To minimize the above optimization problem, we can derive the first derivative and set it as 0:

$$\frac{\partial}{\partial \beta_j} F(\boldsymbol{\beta}^{(k)}) = \frac{1}{MN} \left(\mathbf{e}_j^\top \mathbf{X}^\top \mathbf{X} \boldsymbol{\beta}^{(k)} - \nabla_t \mathbf{u}^\top \mathbf{X} \mathbf{e}_j \right) + \lambda \text{sign}(\beta_j) = 0,$$

where \mathbf{e}_j is a vector of length K whose entries are all zero except the j -th entry is 1. By solving the above equation, we can solve $\beta_j^{(k+1)}$ by

$$\beta_j^{(k+1)} = S \left(\nabla_t \mathbf{u}^\top \mathbf{X} \mathbf{e}_j - \sum_{l \neq j} (\mathbf{X}^\top \mathbf{X})_{jl} \beta_l^{(k)}, MN\lambda \right) / (\mathbf{X}^\top \mathbf{X})_{jj},$$

where $S(\cdot)$ is the soft-thresholding function defined as

$$S(x, \alpha) = \begin{cases} x - \alpha & \text{if } x \geq \alpha \\ x + \alpha & \text{if } x \leq -\alpha \\ 0 & \text{otherwise} \end{cases}.$$

The detailed procedure of this algorithm is summarized in Algorithm 1.

Algorithm 1: Algorithm for the coordinate descent to minimize

$F(\boldsymbol{\beta})$

Input: response vector $\nabla_t \mathbf{u}$, design matrix \mathbf{X} , and number of
iterations M

Output: coefficient estimation $\hat{\boldsymbol{\beta}}$

1 **Initialize** $\boldsymbol{\beta}^{(0)}$

2 **for** $\ell = 1, \dots, \mathcal{L}$ **do**

3 **for** $j = 1, \dots, K$ **do**
4 $\left[\begin{array}{l} \boldsymbol{\beta}_j^{(\ell)} = \\ S \left(\nabla_t \mathbf{u}^\top \mathbf{X} \mathbf{e}_j - \sum_{l \neq j} (\mathbf{X}^\top \mathbf{X})_{jl} \boldsymbol{\beta}_l^{(\ell-1)}, MN\lambda \right) / (\mathbf{X}^\top \mathbf{X})_{jj} \end{array} \right]$

5 $\hat{\boldsymbol{\beta}} = \boldsymbol{\beta}^{(\mathcal{L})}$

D. Some Important Lemmas

In this section, we present some important preliminaries, which are important blocks for the proofs of the main theories. To begin with, we first give the upper bound of $\widehat{u(x, t_n)} - u(x, t_n)$ for $x \in \{x_0, x_1, \dots, x_{M-1}\}$, which is distance between the ground truth $u(x, t_n)$ and the estimated zero-order derivatives by cubic spline $\widehat{u(x, t_n)}$.

Lemma D.1. Assume that

1. for any fixed $n = 0, 1, \dots, N-1$, we have the spatial variable x is sorted in nondecreasing order, i.e., $x_0 < x_1 < \dots < x_{M-1}$;
2. for any fixed $n = 0, 1, \dots, N-1$, we have the ground truth function $f^*(x) := u(x, t_n) \in C^4$, where C^4 refers to the set of functions that is forth-time differentiable;
3. for any fixed $n = 0, 1, \dots, N-1$, we have $\frac{\partial^2}{\partial x^2} u(x_0, t_n) = \frac{\partial^2}{\partial x^2} u(x_{M-1}, t_n) = 0$, and $\frac{\partial^3}{\partial x^3} u(x_0, t_n) \neq 0, \frac{\partial^3}{\partial x^3} u(x_{M-1}, t_n) = 0$;
4. for any fixed $n = 0, 1, \dots, N-1$, the value of third order derivative of function $f^*(x) := u(x, t_n)$ at point $x = 0$ is bounded, i.e., $\frac{d^3}{dx^3} f^*(0) < +\infty$;
5. for any U_i^n generated by the underlying PDE system $U_i^n = u(x_i, t_n) + w_i^n$ with $w_i^n \stackrel{i.i.d}{\sim} N(0, \sigma^2)$, we have $\eta^2 := \max_{i=0, \dots, M-1, n=0, \dots, N-1} E(U_i^n)^2$ is bounded;
6. for function $K(x) = \frac{1}{2}e^{-|x|/\sqrt{2}} [\sin(|x|\sqrt{2}) + \pi/4]$, we assume that it is uniformly continuous with modulus of continuity w_K and of bounded variation $V(K)$ and we also

assume that $\int |K(x)|dx$, $\int |x|^{1/2}|dK(x)|$, $\int |x \log |x||^{1/2}|dK(x)|$ are bounded and denote

$$K_{\max} := \max_{x \in \max_{x \in [0, X_{\max}]} \cup [0, T_{\max}]} K(x);$$

7. the smoothing parameter in (2.4) is set as $\alpha = \left(1 + M^{-4/7}\right)^{-1}$;

8. the Condition 3.4 - Condition 3.5 hold.

Then there exist finite positive constant $\mathcal{C}_{(\sigma, \|u\|_{L^\infty(\Omega)})} > 0$, $C_{(\sigma, \|u\|_{L^\infty(\Omega)})} > 0$, $\tilde{C}_{(\sigma, \|u\|_{L^\infty(\Omega)})} > 0$, $Q_{(\sigma, \|u\|_{L^\infty(\Omega)})} > 0$, $\gamma_{(M)} > 0$, $\omega_{(M)} > 1$, such that for any ϵ satisfying

$$\begin{aligned} \epsilon &> \mathcal{C}_{(\sigma, \|u\|_{L^\infty(\Omega)})} \max \left\{ 4K_{\max} M^{-3/7}, 4AM^{-3/7}, 4\sqrt{2} \frac{d^3}{dx^3} f^*(0) M^{-3/7}, \right. \\ &\quad \frac{16 \left[C_{(\sigma, \|u\|_{L^\infty(\Omega)})} \log(M) + \gamma_{(M)} \right] \log(M)}{M^{3/7}}, \\ &\quad \left. 16\sqrt{\frac{\omega_{(M)}}{7}} \tilde{C}_{(\sigma, \|u\|_{L^\infty(\Omega)})} \frac{\sqrt{\log(M)}}{M^{3/7}} \right\}, \end{aligned}$$

there exist a $\dot{M} > 0$, such that when $M > \dot{M}$, we have

$$\begin{aligned} &P \left[\sup_{x \in [0, X_{\max}]} \left| \frac{\partial^k}{\partial x^k} \widehat{u(x, t_n)} - \frac{\partial^k}{\partial x^k} u(x, t_n) \right| > \epsilon \right] \\ &< 2Me^{-\frac{(M^{3/7} - \|u\|_{L^\infty(\Omega)})^2}{2\sigma^2}} + Q_{(\sigma, \|u\|_{L^\infty(\Omega)})} e^{-L\gamma_{(M)}} + 4\sqrt{2}\eta^4 M^{-\omega_{(M)}/7} \end{aligned}$$

for $k = 0, 1, 2$. Here $A = \sup_{\alpha} \int |u|^s f_M(\alpha, u) du \times \int_{x \in [0, X_{\max}]} |K(x)| dx$.

Proof. See online supplementary material. □

In the above lemma, we add $(\sigma, \|u\|_{L^\infty(\Omega)})$ as the subscript of constants $\mathcal{C}, C, \tilde{C}, Q$ to emphasize that these constant are independent of the temporal resolution N and spatial resolution M , and only depends on the noisy data \mathcal{D} in (1.1) itself. We add M as the subscript of constants

γ, ω to emphasize that γ, ω are function of the spatial resolution M , and we will discuss the value of γ, ω in Lemma D.2.

The above lemma show the closeness between $\frac{\partial^k}{\partial x^k} \widehat{u(x, t_n)}$ and $\frac{\partial^k}{\partial x^k} u(x, t_n)$ for $k = 0, 1, 2$.

This results can be easily extend of the closeness between $\frac{\partial}{\partial t} \widehat{u(x_i, t)}$ and $\frac{\partial}{\partial t} u(x_i, t)$, which is shown in the following corollary.

Corollary D.1. Assume that

1. for any fixed $i = 0, 1, \dots, M-1$, we have the spatial variable t is sorted in nondecreasing order, i.e., $t_0 < t_1 \dots < t_{N-1}$;

2. for any fixed $i = 0, 1, \dots, M-1$, we have the ground truth function $f^*(t) := u(x_i, t) \in C^4$, where C^4 refers to the set of functions that is forth-time differentiable;

3. for any fixed $i = 0, 1, \dots, M-1$, we have $\frac{\partial^2}{\partial t^2} u(x_i, t_0) = \frac{\partial^2}{\partial t^2} u(x_i, t_{N-1}) = 0$, and $\frac{\partial^3}{\partial t^3} u(x_i, t_0) \neq 0, \frac{\partial^3}{\partial t^3} u(x_i, t_{N-1}) = 0$;

4. for any fixed $i = 0, 1, \dots, M-1$, the value of third order derivative of function $\bar{f}^*(x) := u(x_i, t)$ at point $t = 0$ is bounded, i.e., $\frac{d^3}{dt^3} \bar{f}^*(0) < +\infty$;

5. for any U_i^n generated by the underlying PDE system $U_i^n = u(x_i, t_n) + w_i^n$ with $w_i^n \stackrel{i.i.d}{\sim} N(0, \sigma^2)$, we have $\max_{i=0, \dots, M-1, n=0, \dots, N-1} E(U_i^n)^2$ is bounded;

6. for function $K(x) = \frac{1}{2} e^{-|x|/\sqrt{2}} [\sin(|x|\sqrt{2}) + \pi/4]$, we have $K(x)$ is uniformly continuous with modulus of continuity w_K and of bounded variation $V(K)$, and we also assume

that $\int_{x \in [0, X_{\max}]} |K(x)| dx, \int |x|^{1/2} |dK(x)|, \int |x \log |x||^{1/2} |dK(x)|$ are bounded and denote

$$K_{\max} := \max_{x \in [0, X_{\max}] \cup [0, T_{\max}]} K(x);$$

7. the smoothing parameter in (2.4) is set as $\bar{\alpha} = O\left(\left(1 + N^{-4/7}\right)^{-1}\right)$;

8. the Condition 3.4 - Condition 3.5 hold.

then there exist finite positive constant $\mathcal{C}_{(\sigma, \|u\|_{L^\infty(\Omega)})} > 0, C_{(\sigma, \|u\|_{L^\infty(\Omega)})} > 0, \tilde{C}_{(\sigma, \|u\|_{L^\infty(\Omega)})} >$

$0, Q_{(\sigma, \|u\|_{L^\infty(\Omega)})} > 0, \gamma_{(N)} > 0, \omega_{(N)} > 1$, such that for any ϵ satisfying

$$\begin{aligned} \epsilon &> \mathcal{C}_{(\sigma, \|u\|_{L^\infty(\Omega)})} \max \left\{ 4K_{\max} N^{-3/7}, 4\bar{A} N^{-3/7}, 4\sqrt{2} \frac{d^3}{dx^3} f^*(0) N^{-3/7}, \right. \\ &\quad \frac{16 \left[C_{(\sigma, \|u\|_{L^\infty(\Omega)})} \log(N) + \gamma_{(N)} \right] \log(N)}{N^{3/7}}, \\ &\quad \left. 16\sqrt{\frac{\omega_{(N)}}{7}} \tilde{C}_{(\sigma, \|u\|_{L^\infty(\Omega)})} \frac{\sqrt{\log(N)}}{N^{3/7}} \right\}, \end{aligned}$$

there exist a $\dot{N} > 0$, such that when $N > \dot{N}$, we have

$$\begin{aligned} P \left[\sup_{t \in [0, T_{\max}]} \left| \frac{\partial}{\partial t} \widehat{u(x_i, t)} - \frac{\partial}{\partial t} u(x_i, t) \right| > \epsilon \right] &< 2Ne^{-\frac{(N^{3/7} - \|u\|_{L^\infty(\Omega)})^2}{2\sigma^2}} + \\ &Q_{(\sigma, \|u\|_{L^\infty(\Omega)})} e^{-L\gamma_{(N)}} + 4\sqrt{2}\eta^4 N^{-\omega_{(N)}/7}. \end{aligned}$$

Here $\bar{A} = \sup_{\alpha} \int |u|^s \bar{f}_N(\alpha, u) du \times \int_{t \in [0, T_{\max}]} |K(x)| dx$.

After bounding the error of all the derivatives, we then aim to bound $\|\nabla_t \mathbf{u} - \mathbf{X}\beta^*\|_\infty$. It

is important to bound $\|\nabla_t \mathbf{u} - \mathbf{X}\beta^*\|_\infty$, with the reason described as follows in Lemma D.2.

Lemma D.2. Suppose the conditions in Lemma D.1 and Corollary D.1 hold and we set $M =$

$O(N)$, then there exist finite positive constant $\mathcal{C}_{(\sigma, \|u\|_{L^\infty(\Omega)})} > 0$ such that for any ϵ satisfying

$$\epsilon > \mathcal{C}_{(\sigma, \|u\|_{L^\infty(\Omega)})} \frac{\log(N)}{N^{3/7-r}},$$

and any $r \in (0, \frac{3}{7})$, there exist $\dot{N} > 0$, such that when $N > \dot{N}$, we have

$$P(\|\nabla_t \mathbf{u} - \mathbf{X}\boldsymbol{\beta}^*\|_\infty > \epsilon) < Ne^{-N^r},$$

where $\mathcal{C}_{(\sigma, \|u\|_{L^\infty(\Omega)})}$ is a constant which do not depend on the temporal resolution M and spatial resolution N .

Proof. See online supplementary material. □

E. Tables to draw the curve in Fig. 2 and Fig. 8

In this section, we present the table to draw the curves in Fig. 2,8 in Table 2, 3, respectively.

Table 2: Computational complexity of the functional estimation by cubic spline and local polynomial regression in transport equation

	M = 20						
	N=200	N=400	N=800	N=1000	N=1200	N=1600	N=2000
cubic spline	374,389	748,589	1,496,989	1,871,189	2,245,389	2,993,789	3,742,189
local poly	14,136,936	45,854,336	162,089,136	246,606,536	348,723,936	605,758,736	933,193,536
	N = 20						
	M=200	M=400	M=800	M=1000	M=1200	M=1600	M=2000
cubic spline	398,573	875,773	207,0173	2,787,373	3,584,573	5,418,973	7,573,373
local poly	33,046,336	125,596,136	489,255,736	760,365,536	1,090,995,336	1,930,814,936	3,008,714,536

F. The reasons why the RK4 is not feasible.

In this section, we discuss the reasons why the RK4 is not feasible. Generally speaking, RK4

is used to approximate solutions of ordinary differential equations. In our content, it aims at

Table 3: Correct identification probability of transport equation, inviscid Burgers equation and viscous Burgers's equation

	σ											
	0.01	0.05	0.1	0.25	0.3	0.4	0.5	0.7	0.75	0.8	0.9	1
	transport equation											
$M = N = 100$	100%	100%	100%	100%	100%	100%	100%	100%	100%	100%	100%	100%
$M = N = 150$	100%	100%	100%	100%	100%	100%	100%	100%	100%	100%	100%	100%
$M = N = 200$	100%	100%	100%	100%	100%	100%	100%	100%	100%	100%	100%	100%
	inviscid Burgers equation											
$M = N = 100$	100%	100%	100%	100%	100%	100%	100%	99.9%	99.8%	99.8%	99.8%	99.1%
$M = N = 150$	100%	100%	100%	100%	100%	100%	100%	100%	99.8%	99.7%	99.7%	99.7%
$M = N = 200$	100%	100%	100%	100%	100%	100%	100%	100%	100%	100%	100%	100%
	viscous Burgers equation											
$M = N = 100$	100%	99.4%	89.8%	78.0%	71.4%	82.0%	91.6%	72.8%	79.0%	72.9%	57.9%	51.3%
$M = N = 150$	100%	100%	100%	97.3%	96.5%	96.2%	97.6%	95.6%	93.3%	86.6%	79.9%	73.6%
$M = N = 200$	100%	100%	100%	100%	99.6%	99.6%	98.2%	98.8%	98.2%	97.0%	94.3%	91.3%

¹ The simulation results are based on 1000 times of simulations.

solveing the solution of the following differential equation with fixed $i \in \{0, \dots, M-1\}$:

$$\begin{cases} \frac{\partial}{\partial t} u(x_i, t) = p(u, t) \\ u(x_i, t_0) = u_i^0 \end{cases}, \quad (\text{F.24})$$

where $p(u, t)$ is the function interpolated through data set

$$\left\{ t_n, u_i^n, \frac{u(x_i, t_n + \Delta t) - u(x_i, t_n)}{\Delta t} \right\}_{n=0, \dots, N-2}.$$

Then as shown by Chapter 5 in Lambert et al. (1991), the solution can be approximate by

$$u(x_i, t_{n+1}) = u(x_i, t_n) + \frac{\Delta t}{6}(k_1 + k_2 + k_3 + k_4),$$

where $\Delta t = t_{n+1} - t_n$ and k_1, k_2, k_3, k_4 are defined as

$$\begin{cases} k_1 = p(t_n, u_i^n) \\ k_2 = p(t_n + \Delta t/2, u_i^n + k_1 \Delta t/2) \\ k_3 = p(t_n + \Delta t/2, u_i^n + k_2 \Delta t/2) \\ k_4 = p(t_n + \Delta t, u_i^n + k_3 \Delta t). \end{cases} \quad (\text{F.25})$$

Given the above implementation of RK4, we find it is infeasible to be used in our case study due to the following two reasons. First, it is infeasible to obtain $p(u, t)$ in (F.24), even though the interpolation methods. Second, it is infeasible to get the value of k_3 in (F.25). Because the calculation of k_3 depends on the value of k_2 and k_2 needs to be obtained (at least) by interpolation, it is complicated to calculate k_1, k_2, k_3, k_4 through one-time operation. Given the complicated implementation of RK4, we use the explicit Euler method in our case study.

G. Proofs

G.1 Proof of Proposition 2.1

Proof. The computational complexity in the functional estimation stage lies in calculating all elements in matrix \mathbf{X} and vector $\nabla_t \mathbf{u}$, including

$$\left\{ \widehat{u(x_i, t_n)}, \widehat{\frac{\partial}{\partial x} u(x_i, t_n)}, \widehat{\frac{\partial^2}{\partial x^2} u(x_i, t_n)}, \widehat{\frac{\partial}{\partial t} u(x_i, t_n)} \right\}_{i=0, \dots, M-1, n=0, \dots, N-1}.$$

by cubic spline in (2.4).

We divide our proof into two scenarios: (1) $\alpha = 1$ and (2) $\alpha \in (0, 1)$.

- First of all, we discuss a very simple case, i.e., $\alpha = 1$. When $\alpha = 1$, we call the cubic spline as *interpolating cubic spline* since there is no penalty on the smoothness.

For the zero-order derivative, i.e., $\left\{ \widehat{u(x_i, t_n)} \right\}_{i=0, \dots, M-1, n=0, \dots, N-1}$, it can be estimated as $\widehat{u(x_i, t_n)} = u_i^n$ for $i = 0, 1, \dots, M-1, n = 0, 1, \dots, N-1$. So there is no computational complexity involved.

For the second order derivatives, i.e., $\left\{ \widehat{\frac{\partial^2}{\partial x^2} u(x_i, t_n)} \right\}_{i=0, \dots, M-1}$, with $n \in \{0, \dots, N-1\}$ fixed, it can be solved in a closed-form, i.e.,

$$\hat{\boldsymbol{\sigma}} = \mathbf{M}^{-1} \mathbf{A} \mathbf{u}^n$$

where $\hat{\boldsymbol{\sigma}} = \left(\widehat{\frac{\partial^2}{\partial x^2} u(x_0, t_n)}, \widehat{\frac{\partial^2}{\partial x^2} u(x_1, t_n)}, \dots, \widehat{\frac{\partial^2}{\partial x^2} u(x_{M-1}, t_n)} \right)^\top$. So the main computational load lies in the calculation of \mathbf{M}^{-1} . Recall $\mathbf{M} \in \mathbb{R}^{(M-2) \times (M-2)}$ is a tri-diagonal

G.1 Proof of Proposition 2.1

matrix:

$$\mathbf{M} = \begin{pmatrix} \frac{h_0+h_1}{3} & \frac{h_1}{6} & 0 & \dots & 0 & 0 \\ \frac{h_1}{6} & \frac{h_1+h_2}{3} & \frac{h_2}{6} & \dots & 0 & 0 \\ 0 & \frac{h_2}{6} & \frac{h_2+h_3}{3} & \ddots & 0 & 0 \\ \vdots & \vdots & \ddots & \ddots & \ddots & \vdots \\ 0 & 0 & 0 & \ddots & \frac{h_{M-4}+h_{M-3}}{3} & \frac{h_{M-3}}{6} \\ 0 & 0 & 0 & \dots & \frac{h_{M-3}}{6} & \frac{h_{M-3}+h_{M-2}}{3} \end{pmatrix}.$$

For this type of tri-diagonal matrix, there exist a fast algorithm to calculate its inverse.

The main idea of this fast algorithm is to decompose \mathbf{M} through Cholesky decomposition

as

$$\mathbf{M} = \mathbf{L}\mathbf{D}\mathbf{L}^\top,$$

where $\mathbf{L} \in \mathbb{R}^{(M-2) \times (M-2)}$, $\mathbf{D} \in \mathbb{R}^{(M-2) \times (M-2)}$ has the form of

$$\mathbf{L} = \begin{pmatrix} 1 & 0 & 0 & \dots & 0 \\ l_1 & 1 & 0 & \dots & 0 \\ 0 & l_2 & 1 & \dots & 0 \\ \vdots & \vdots & \ddots & \ddots & \vdots \\ 0 & 0 & 0 & l_{M-3} & 1 \end{pmatrix}, \mathbf{D} = \begin{pmatrix} d_1 & 0 & \dots & 0 \\ 0 & d_2 & \dots & 0 \\ \vdots & \vdots & \ddots & \vdots \\ 0 & 0 & \dots & d_{M-2} \end{pmatrix}.$$

After decomposing matrix \mathbf{M} into $\mathbf{L}\mathbf{D}\mathbf{L}^\top$, the second derivatives $\hat{\boldsymbol{\sigma}}$ can be solved as

$$\hat{\boldsymbol{\sigma}} = (\mathbf{L}^\top)^{-1} \mathbf{D}^{-1} \underbrace{\mathbf{L}^{-1} \mathbf{A} \mathbf{u}^n}_{\boldsymbol{\xi}}.$$

In the remaining of the proof in this scenario, we will verify the following two issues:

G.1 Proof of Proposition 2.1

1. the computational complexity to decompose \mathbf{M} into \mathbf{LDL}^\top is $O(M)$ with $n \in \{0, \dots, N-1\}$ fixed;
2. the computational complexity to compute $\hat{\boldsymbol{\sigma}} = (\mathbf{L}^\top)^{-1} \mathbf{D}^{-1} \mathbf{L}^{-1} \boldsymbol{\xi}$ is $O(M)$ with $n \in \{0, \dots, N-1\}$ fixed and \mathbf{L}, \mathbf{D} available.

For the decomposition of $\mathbf{M} = \mathbf{LDL}^\top$, its essence is to derive l_1, \dots, l_{M-3} in matrix \mathbf{L} and d_1, \dots, d_{M-2} in matrix \mathbf{D} . By utilizing the method of undetermined coefficients to inequality $\mathbf{M} = \mathbf{LDL}^\top$, we have:

$$= \begin{bmatrix} d_1 & d_1 l_1 & 0 & \dots & 0 & 0 \\ d_1 l_1 & d_2 & d_2 l_2 & \dots & 0 & 0 \\ 0 & d_2 l_2 & d_3 & \dots & 0 & 0 \\ \vdots & \vdots & \vdots & \ddots & \vdots & \vdots \\ 0 & 0 & 0 & \dots & d_{M-3} l_{M-3} & d_{M-3} l_{M-3}^2 + d_{M-2} \end{bmatrix} \\ = \begin{bmatrix} M_{11} & M_{12} & \dots & 0 \\ M_{21} & M_{22} & \dots & 0 \\ 0 & M_{32} & \dots & 0 \\ \vdots & \vdots & \ddots & \vdots \\ 0 & 0 & \dots & M_{M-2, M-2} \end{bmatrix},$$

where $M_{i,j}$ is the (i,j) th entry in matrix \mathbf{M} . Through the above method of undetermined coefficients, we can solve the exact value of the entries in matrix \mathbf{L}, \mathbf{D} , which is summarized in Algorithm 2. It can be seen from Algorithm 2 that, the computational

G.1 Proof of Proposition 2.1

complexity of solve \mathbf{L}, \mathbf{D} is of order $O(M)$.

For the calculation of $\hat{\sigma} = (\mathbf{L}^\top)^{-1} \mathbf{D}^{-1} \mathbf{L}^{-1} \boldsymbol{\xi}$ with matrix \mathbf{L}, \mathbf{D} available, we will first verify that the computational complexity to solve $\bar{\boldsymbol{\xi}} = \mathbf{L}^{-1} \boldsymbol{\xi}$ is $O(M)$. Then, we will verify that the computational complexity to solve $\bar{\bar{\boldsymbol{\xi}}} = \mathbf{D}^{-1} \bar{\boldsymbol{\xi}}$ is $O(M)$. Finally, we will verify that the computational complexity to solve $\bar{\bar{\bar{\boldsymbol{\xi}}}} = (\mathbf{L}^\top)^{-1} \bar{\bar{\boldsymbol{\xi}}}$ is $O(M)$. First, the computational complexity of calculating $\bar{\boldsymbol{\xi}} = \mathbf{L}^{-1} \boldsymbol{\xi}$ is $O(M)$, this is because by $\mathbf{L} \bar{\boldsymbol{\xi}} = \boldsymbol{\xi}$, we have the following system of equations:

$$\left\{ \begin{array}{l} \xi_1 = \bar{\xi}_1 \\ \xi_2 = \bar{\xi}_2 + l_1 \bar{\xi}_1 \\ \vdots \\ \xi_{M-2} = \bar{\xi}_{M-2} + l_{M-3} \bar{\xi}_{M-3} \end{array} \right.$$

where $\xi_i, \bar{\xi}_i$ is the i -th entry in $\boldsymbol{\xi}, \bar{\boldsymbol{\xi}}$, respectively. Through the above system of equations, we can solve the values of all entries in $\bar{\boldsymbol{\xi}}$, which is summarized in Algorithm 3. From Algorithm 3, we know that the computational complexity of solving $\mathbf{L}^{-1} \boldsymbol{\xi}$ is $O(M)$. Next, it is obvious that the computational complexity of $\bar{\bar{\boldsymbol{\xi}}} = \mathbf{D}^{-1} \bar{\boldsymbol{\xi}}$ is $O(M)$, because \mathbf{D} is a diagonal matrix. Finally, with the similar logic flow, we can verify that the computational complexity of $\bar{\bar{\bar{\boldsymbol{\xi}}}} = (\mathbf{L}^\top)^{-1} \bar{\bar{\boldsymbol{\xi}}}$ is still $O(M)$. So, the computational complexity is to calculate $\hat{\sigma} = (\mathbf{L}^\top)^{-1} \mathbf{D}^{-1} \mathbf{L}^{-1} \boldsymbol{\xi}$, with known \mathbf{L}, \mathbf{D} is $O(M)$.

As a summary, the computational complexity is to calculate $\left\{ \widehat{\frac{\partial^2}{\partial x^2} u(x_i, t_n)} \right\}_{i=0, \dots, M-1}$

with a fixed $n \in \{0, 1, \dots, N-1\}$ is $O(M)$. Accordingly, the computational complexity

G.1 Proof of Proposition 2.1

to solve $\left\{ \widehat{\frac{\partial^2}{\partial x^2} u(x_i, t_n)} \right\}_{i=0, \dots, M-1, n=0, \dots, N-1}$ is $O(MN)$.

For the first order derivatives, i.e., $\left\{ \frac{\partial}{\partial x} u(x_i, t_n), \frac{\partial}{\partial x} u(x_i, t_n) \right\}_{i=0, \dots, M-1, n=0, \dots, N-1}$, we

can verify the computational complexity to solve them is also $O(MN)$ with the similar

logic as that in the second order derivatives.

Algorithm 2: Pseudo code to solve \mathbf{L}, \mathbf{D}

Input: matrix \mathbf{M}

Output: matrix \mathbf{L}, \mathbf{D}

```

1 Initialize  $d_1 = M_{1,1}$ 

2 for  $i = 1, 2, \dots, M-3$  do
3    $l_i = M_{i,i+1}/d_i$ 
4    $d_{i+1} = M_{i+1,i+1} - d_i l_i^2$ 

```

Algorithm 3: Pseudo code to solve $\mathbf{L}^{-1} \boldsymbol{\xi}$

Input: matrix $\mathbf{L}, \boldsymbol{\xi}$

Output: matrix $\bar{\boldsymbol{\xi}}$

```

1 Initialize  $\bar{\xi}_1 = \xi_1$ 

2 for  $i = 2, \dots, M-2$  do
3    $\bar{\xi}_i = \xi_i - l_{i-1} \bar{\xi}_{i-1}$ 

```

- Next, we discuss the scenario when $\alpha \in (0, 1)$.

Since all the derivatives has similar closed-form formulation as shown in (2.5), (A.23),

(A.22), we take the zero-order derivative $\{u(x_i, t_n)\}_{i=0, \dots, M-1, n=0, \dots, N-1}$ as an illustra-

G.1 Proof of Proposition 2.1

tion example, and other derivatives can be derived similarly.

Recall that in Section 2.1, the zero-order derivative $\{u(x_i, t_n)\}_{i=0, \dots, M-1}$ with $n \in \{0, 1, \dots, N-1\}$ fixed can be estimated through cubic spline as in equation (2.5):

$$\hat{\mathbf{f}} = \underbrace{[\alpha \mathbf{W} + (1 - \alpha) \mathbf{A}^\top \mathbf{M} \mathbf{A}]}_{\mathbf{Z}}^{-1} \underbrace{\alpha \mathbf{W} \mathbf{u}^n}_{\mathbf{y}},$$

where $\alpha \in (0, 1)$ trades off the fitness of the cubic spline and the smoothness of the cubic

spline, vector $\hat{\mathbf{f}} = \left(\widehat{u(x_0, t_n)}, \widehat{u(x_1, t_n)}, \dots, \widehat{u(x_{M-1}, t_n)} \right)^\top$, vector $\mathbf{u}^n = (u_0^n, \dots, u_{M-1}^n)^\top$,

matrix $\mathbf{W} = \text{diag}(w_0, w_1, \dots, w_{M-1})$, matrix $\mathbf{A} \in \mathbb{R}^{(M-2) \times M}$, $\mathbf{M} \in \mathbb{R}^{(M-2) \times (M-2)}$ are

defined as

$$\mathbf{A} = \begin{pmatrix} \frac{1}{h_0} & -\frac{1}{h_0} - \frac{1}{h_1} & \frac{1}{h_1} & 0 & \dots & 0 & 0 & 0 \\ 0 & \frac{1}{h_1} & -\frac{1}{h_1} - \frac{1}{h_2} & \frac{1}{h_2} & \dots & 0 & 0 & 0 \\ \vdots & \vdots & \vdots & \vdots & \ddots & \vdots & \vdots & \vdots \\ 0 & 0 & 0 & 0 & \dots & \frac{1}{h_{M-3}} & -\frac{1}{h_{M-3}} - \frac{1}{h_{M-2}} & \frac{1}{h_{M-2}} \end{pmatrix},$$

$$\mathbf{M} = \begin{pmatrix} \frac{h_0+h_1}{3} & \frac{h_1}{6} & 0 & \dots & 0 & 0 \\ \frac{h_1}{6} & \frac{h_1+h_2}{3} & \frac{h_2}{6} & \dots & 0 & 0 \\ 0 & \frac{h_2}{6} & \frac{h_2+h_3}{3} & \dots & 0 & 0 \\ \vdots & \vdots & \vdots & \ddots & \vdots & \vdots \\ 0 & 0 & 0 & \dots & \frac{h_{M-4}+h_{M-3}}{3} & \frac{h_{M-3}}{6} \\ 0 & 0 & 0 & \dots & \frac{h_{M-3}}{6} & \frac{h_{M-3}+h_{M-2}}{3} \end{pmatrix}$$

with $h_i = x_{i+1} - x_i$ for $i = 0, 1, \dots, M-2$.

G.1 Proof of Proposition 2.1

By simple calculation, we know that matrix $\mathbf{Z} = \alpha \mathbf{W} + (1 - \alpha) \mathbf{A}^\top \mathbf{M} \mathbf{A} \in \mathbb{R}^{M \times M}$ is a symmetric seventh-diagonal matrix:

$$\mathbf{Z} = \begin{pmatrix} z_{11} & z_{12} & z_{13} & z_{14} & 0 & \dots \\ z_{21} & z_{22} & z_{23} & z_{24} & z_{25} & \dots \\ z_{31} & z_{32} & z_{33} & z_{34} & z_{35} & \ddots \\ z_{41} & z_{42} & z_{43} & z_{44} & z_{45} & \ddots \\ 0 & z_{52} & z_{53} & z_{54} & z_{55} & \ddots \\ \vdots & \vdots & \ddots & \ddots & \ddots & \ddots \end{pmatrix}$$

By applying Cholesky decomposition to matrix \mathbf{Z} as $\mathbf{Z} = \mathbf{P} \mathbf{\Sigma} \mathbf{P}^\top$, we can calculate $\hat{\mathbf{f}}$ as

$$\hat{\mathbf{f}} = \mathbf{Z}^{-1} \mathbf{y} = (\mathbf{P}^\top)^{-1} \mathbf{\Sigma}^{-1} \mathbf{P}^{-1} \mathbf{y},$$

where $\mathbf{P} \in \mathbb{R}^{M \times M}$, $\mathbf{\Sigma} \in \mathbb{R}^{M \times M}$ has the form of

$$\mathbf{P} = \begin{pmatrix} 1 & 0 & 0 & 0 & \dots & 0 & 0 \\ \ell_1 & 1 & 0 & 0 & \dots & 0 & 0 \\ \gamma_1 & \ell_2 & 1 & 0 & \dots & 0 & 0 \\ \eta_1 & \gamma_2 & \ell_3 & 1 & \dots & 0 & 0 \\ 0 & \eta_2 & \gamma_3 & \ell_4 & \ddots & 0 & 0 \\ \vdots & \vdots & \ddots & \ddots & \ddots & 1 & 0 \\ 0 & 0 & \dots & \eta_{M-3} & \gamma_{M-2} & \ell_{M-1} & 1 \end{pmatrix}, \mathbf{\Sigma} = \begin{pmatrix} s_1 & 0 & 0 & \dots & 0 \\ 0 & s_2 & 0 & \dots & 0 \\ 0 & 0 & s_3 & \dots & 0 \\ \vdots & \vdots & \vdots & \ddots & 0 \\ 0 & 0 & 0 & \dots & s_M \end{pmatrix}.$$

In the remaining of the proof in this scenario, we will verify the following two issues:

G.1 Proof of Proposition 2.1

1. the computational complexity to decompose \mathbf{Z} into $\mathbf{P}\mathbf{\Sigma}\mathbf{P}^\top$ is $O(M)$ with $n \in$

$\{0, \dots, N-1\}$ fixed;

2. the computational complexity to compute $(\mathbf{P}^\top)^{-1}\mathbf{\Sigma}^{-1}\mathbf{P}^{-1}\mathbf{y}$ is $O(M)$ with $n \in$

$\{0, \dots, N-1\}$ fixed.

First of all, we verify that the computational complexity to decompose \mathbf{Z} into $\mathbf{P}\mathbf{\Sigma}\mathbf{P}^\top$ is

$O(M)$ when $n \in \{0, \dots, N-1\}$ fixed By applying method of undetermined coefficients

to equality $\mathbf{Z} = \mathbf{P}\mathbf{\Sigma}\mathbf{P}^\top$, we have

$$\begin{bmatrix} s_1 & s_1\ell_1 & s_1\gamma_1 & \dots & 0 \\ s_1\ell_1 & s_1\ell_1^2 + s_2 & s_1\ell_1\gamma_1 + s_2\ell_2 & \dots & 0 \\ s_1\gamma_1 & s_1\ell_1\gamma_1 + s_2\ell_2 & s_1\gamma_1^2 + s_2\ell_2^2 + s_3 & \dots & 0 \\ s_1\eta_1 & s_1\eta_1\ell_1 + s_2\gamma_2 & s_1\eta_1\gamma_1 + s_2\gamma_2\ell_2 + s_3\ell_3 & \dots & 0 \\ 0 & s_2\eta_2 & s_2\eta_2\ell_2 + s_3\gamma_3 & \dots & 0 \\ 0 & 0 & s_3\eta_3 & \dots & 0 \\ \vdots & \vdots & \vdots & \ddots & \vdots \\ 0 & 0 & 0 & \dots & s_{M-3}\eta_{M-3}^2 + s_{M-2}\gamma_{M-2}^2 \\ & & & & + s_{M-1}\gamma_{M-1}\ell_{M-1}^2 + s_M \end{bmatrix} = [z_{i,j}],$$

where $[z_{i,j}]$ denotes matrix \mathbf{Z} with its (i, j) th entry as $z_{i,j}$. Through the above method of

undetermined coefficients, we can solve the explicit value of all entries in matrix \mathbf{P} , $\mathbf{\Sigma}$, i.e.,

$\ell_1, \dots, \ell_{M-1}, \gamma_1, \dots, \gamma_{M-2}, \eta_1, \dots, \eta_{M-3}$ in matrix \mathbf{P} and s_1, \dots, s_M in matrix $\mathbf{\Sigma}$, which

is summarized in Algorithm 4. From Algorithm 4, we can see that the computational

G.1 Proof of Proposition 2.1

complexity to decompose \mathbf{Z} into $\mathbf{P}\mathbf{\Sigma}\mathbf{P}^\top$ is $O(M)$ with $n \in \{0, \dots, N-1\}$ fixed.

Second, we verify the computational complexity to compute $(\mathbf{P}^\top)^{-1}\mathbf{\Sigma}^{-1}\mathbf{P}^{-1}\mathbf{y}$ is $O(M)$

with $n \in \{0, \dots, N-1\}$ fixed and matrix $\mathbf{P}, \mathbf{\Sigma}$ available. To realize this objective, we will

first verify that the computational complexity to calculate $\bar{\mathbf{y}} = \mathbf{P}^{-1}\mathbf{y}$ is $O(M)$. Then,

we will first verify that the computational complexity to calculate $\bar{\bar{\mathbf{y}}} = \mathbf{\Sigma}^{-1}\bar{\mathbf{y}}$ is $O(M)$.

Finally, we will first verify that the computational complexity to calculate $\bar{\bar{\bar{\mathbf{y}}}} = (\mathbf{P}^\top)^{-1}\bar{\bar{\mathbf{y}}}$

is $O(M)$. First of all, let us verify the computational complexity to compute $\bar{\mathbf{y}} = \mathbf{P}^{-1}\mathbf{y}$

is $O(M)$ with $n \in \{0, \dots, N-1\}$ fixed. Because we have a system of equations derived

from $\mathbf{P}\bar{\mathbf{y}} = \mathbf{y}$:

$$\left\{ \begin{array}{lcl} \bar{y}_1 & = & y_1 \\ \bar{y}_2 & = & y_2 - \ell_1 \bar{y}_1 \\ \bar{y}_3 & = & y_3 - \gamma_1 \bar{y}_1 - \ell_2 \bar{y}_2 \\ \bar{y}_4 & = & y_4 - \eta_1 \bar{y}_1 - \gamma_2 \bar{y}_2 - \ell_3 \bar{y}_3 \\ \bar{y}_5 & = & y_5 - \eta_2 \bar{y}_3 - \gamma_3 \bar{y}_3 - \ell_4 \bar{y}_4 \\ \vdots & & \\ \bar{y}_M & = & y_M - \eta_{M-3} \bar{y}_{M-3} - \gamma_{M-2} \bar{y}_{M-2} - \ell_{M-1} \bar{y}_{M-1} \end{array} \right. ,$$

we can solve vector $\bar{\mathbf{y}} = (\bar{y}_1, \bar{y}_2, \dots, \bar{y}_M)^\top$ explicitly through Algorithm 5, which only

requires $O(M)$ computational complexity. After deriving $\bar{\mathbf{y}} = \mathbf{P}^{-1}\mathbf{y}$, we can easily verify

that the computational complexity to derive $\bar{\bar{\mathbf{y}}} = \mathbf{\Sigma}^{-1}\bar{\mathbf{y}}$ is still $O(M)$ because $\boldsymbol{\sigma}$ is a

diagonal matrix. Finally, after deriving $\bar{\bar{\bar{\mathbf{y}}}} = \mathbf{\Sigma}^{-1}\bar{\bar{\mathbf{y}}}$, we can verify that the computational

G.1 Proof of Proposition 2.1

complexity to derive $\bar{\bar{\mathbf{y}}} = (\mathbf{P}^\top)^{-1}\bar{\bar{\mathbf{y}}}$ is still $O(M)$ with the similar logic as that in $\bar{\mathbf{y}} = \mathbf{P}^{-1}\mathbf{y}$.

From the above discussion, we know that the computational complexity to calculate

$\widehat{\mathbf{f}} = (\widehat{u(x_0, t_n)}, \widehat{u(x_1, t_n)}, \dots, \widehat{u(x_{M-1}, t_n)})^\top$, is $O(M)$ with $n \in \{0, 1, \dots, N-1\}$ fixed.

In other words, the computational complexity to derive $\left\{ \widehat{u(x_i, t_n)} \right\}_{i=0, \dots, M-1}$ is $O(M)$.

According, the computational complexity to derive $\left\{ \widehat{u(x_i, t_n)} \right\}_{i=0, \dots, M-1, n=0, \dots, N-1}$ is

$O(MN)$.

Algorithm 4: Pseudo code to solve \mathbf{P}, Σ

Input: matrix \mathbf{Z}

Output: matrix \mathbf{P}, Σ

```

1 Initialize  $s_j = \eta_j = \gamma_j = \ell_j = 0 \forall j \leq 0$ 

2 for  $i = 1, 2, \dots, M$  do
3    $s_i = z_{ii} - s_{i-3}\eta_{i-3}^2 - s_{i-2}\gamma_{i-2}^2 - s_{i-1}\ell_{i-1}^2$ 
4    $\ell_i = (z_{i,i+1} - s_{i-2}\gamma_{i-2}\eta_{i-2} - s_{i-1}\gamma_{i-1}\ell_{i-1})/s_i$ 
5    $\eta_i = a_{i,i+3}/s_i$ 

```

Algorithm 5: Pseudo code to solve $\mathbf{P}^{-1}\mathbf{y}$

Input: matrix \mathbf{P}, \mathbf{y}

Output: vector $\bar{\mathbf{y}}$

```

1 Initialize  $\eta_i = \gamma_i = \ell_i = 0 \forall i \leq 0$ 

2 for  $i = 1, \dots, M$  do
3    $\bar{y}_i = y_i - \eta_{i-3}\bar{y}_{i-3} - \gamma_{i-2}\bar{y}_{i-2} - \ell_{i-1}\bar{y}_{i-1}$ 

```

□

G.2 Proof of Proposition B.1

Proof. We have discussed how to use cubic spline to derive derivatives of $u(x, t)$. In this section, we discuss how to use local polynomial regression to derive derivatives, as a benchmark method.

Recall that the derivatives can be estimated by local polynomial regression includes

G.2 Proof of Proposition B.1

$u(x_i, t_n), \frac{\partial}{\partial x}u(x_i, t_n), \frac{\partial^2}{\partial x^2}u(x_i, t_n), \dots$. And here we take the derivation $\frac{\partial^l}{\partial x^l}u(x, t_n)$ as an example ($l = 0, 1, 2, \dots$), and the other derivatives can be derived with the same logic flow. To derive the estimation of $\frac{\partial^l}{\partial x^l}u(x, t_n)$, we fix the temporal variable t_n for a general $n \in \{0, 1, \dots, N-1\}$.

Then we locally fit a degree \tilde{p} polynomial over the data $\{(x_i, u_i^n)\}_{i=0, \dots, M-1}$, i.e.,

$$\left\{ \begin{array}{lcl} u(x_0, t_n) & = & u(x, t_n) + \frac{\partial}{\partial x}u(x, t_n)(x_0 - x) + \dots + \frac{\partial^{\tilde{p}}}{\partial x^{\tilde{p}}}u(x, t_n)(x_0 - x)^{\tilde{p}} \\ u(x_1, t_n) & = & u(x, t_n) + \frac{\partial}{\partial x}u(x, t_n)(x_1 - x) + \dots + \frac{\partial^{\tilde{p}}}{\partial x^{\tilde{p}}}u(x, t_n)(x_1 - x)^{\tilde{p}} \\ \vdots & & \vdots \\ u(x_{M-1}, t_n) & = & u(x, t_n) + \frac{\partial}{\partial x}u(x, t_n)(x_{M-1} - x) + \dots + \frac{\partial^{\tilde{p}}}{\partial x^{\tilde{p}}}u(x, t_n)(x_{M-1} - x)^{\tilde{p}} \end{array} \right. .$$

For the choice of \tilde{p} , we choose $\tilde{p} = l + 3$ to realize minmax efficiency (Fan et al., 1997). If we denote $\mathbf{b}(x) = \left(u(x, t_n), \frac{\partial}{\partial x}u(x, t_n), \dots, \frac{\partial^{\tilde{p}}}{\partial x^{\tilde{p}}}u(x, t_n) \right)^\top$, then $\frac{\partial^l}{\partial x^l}u(x, t_n)$ can be obtained as the $(l+1)$ -th entry of the vector $\widehat{\mathbf{b}(x)}$, and $\widehat{\mathbf{b}(x)}$ is obtained by the following optimization problem:

$$\widehat{\mathbf{b}(x)} = \arg \min_{\mathbf{b}(x)} \sum_{i=0}^{M-1} \left[u_i^n - \sum_{j=0}^{\tilde{p}} \frac{\partial^j}{\partial x^j}u(x, t_n)(x_i - x)^j \right]^2 \mathcal{K}\left(\frac{x_i - x}{h}\right), \quad (\text{G.26})$$

where h is the bandwidth parameter, and \mathcal{K} is a kernel function, and in our paper, we use the Epanechnikov kernel $\mathcal{K}(x) = \frac{3}{4} \max\{0, 1 - x^2\}$ for $x \in \mathbb{R}$. Essentially, the optimization problem in equation (G.26) is a weighted least squares model, where $\mathbf{b}(x)$ can be solved in a close form:

$$\mathbf{b}(x) = \left(\mathbf{X}_{\text{spa}}^\top \mathbf{W}_{\text{spa}} \mathbf{X}_{\text{spa}} \right)^{-1} \mathbf{X}_{\text{spa}}^\top \mathbf{W}_{\text{spa}} \mathbf{u}_i^n, \quad (\text{G.27})$$

G.2 Proof of Proposition B.1

where

$$\mathbf{X}_{\text{spa}} = \begin{bmatrix} 1 & (x_0 - x) & \dots & (x_0 - x)^{\bar{p}} \\ 1 & (x_1 - x) & \dots & (x_1 - x)^{\bar{p}} \\ \vdots & \vdots & \ddots & \vdots \\ 1 & (x_{M-1} - x) & \dots & (x_{M-1} - x)^{\bar{p}} \end{bmatrix}, \mathbf{u}^n = \begin{bmatrix} u_0^n \\ u_1^n \\ \vdots \\ u_{M-1}^n \end{bmatrix}$$

and $\mathbf{W}_{\text{spa}} = \text{diag} \left(\mathcal{K} \left(\frac{x_0 - x}{h} \right), \dots, \mathcal{K} \left(\frac{x_{M-1} - x}{h} \right) \right)$.

By implementing the local polynomial in this way, the computational complexity is much higher than our method, and we summarize its computational complexity in the following proposition.

Following please find the proof.

Similar to the proof of the computational complexity in cubic spline, the proof of the computational complexity of local polynomial regression in the functional estimation stage lies in calculating all elements in matrix \mathbf{X} and vector $\nabla_t \mathbf{u}$, including

$$\left\{ \widehat{u(x_i, t_n)}, \widehat{\frac{\partial}{\partial x} u(x_i, t_n)}, \widehat{\frac{\partial^2}{\partial x^2} u(x_i, t_n)}, \widehat{\frac{\partial}{\partial t} u(x_i, t_n)} \right\}_{i=0, \dots, M-1, n=0, \dots, N-1}.$$

We will take the estimation of $\widehat{\frac{\partial^p}{\partial x^p} u(x_i, t_n)}$ with a general $p \in \mathbb{N}$ as an example. To solve $\left\{ \widehat{\frac{\partial^p}{\partial x^p} u(x_i, t_n)} \right\}_{i=0, \dots, M-1, n=0, \dots, N-1}$, we first focus on $\left\{ \widehat{\frac{\partial^p}{\partial x^p} u(x_i, t_n)} \right\}_{i=0, \dots, M-1}$, with $n \in \{0, \dots, N-1\}$ fixed. To solve it, the main idea of local polynomial regression is to do Taylor

G.2 Proof of Proposition B.1

expansion:

$$\left\{ \begin{array}{lcl} u(x_0, t_n) & = & u(x, t_n) + \frac{\partial}{\partial x} u(x, t_n)(x_0 - x) + \dots + \frac{\partial^{\tilde{p}}}{\partial x^{\tilde{p}}} u(x, t_n)(x_0 - x)^{\tilde{p}} \\ u(x_1, t_n) & = & u(x, t_n) + \frac{\partial}{\partial x} u(x, t_n)(x_1 - x) + \dots + \frac{\partial^{\tilde{p}}}{\partial x^{\tilde{p}}} u(x, t_n)(x_1 - x)^{\tilde{p}} \\ \vdots & & \vdots \\ u(x_{M-1}, t_n) & = & u(x, t_n) + \frac{\partial}{\partial x} u(x, t_n)(x_{M-1} - x) + \dots + \frac{\partial^{\tilde{p}}}{\partial x^{\tilde{p}}} u(x, t_n)(x_{M-1} - x)^{\tilde{p}} \end{array} \right. ,$$

where \tilde{p} is usually set as $\tilde{p} = p + 3$ to obtain asymptotic minimax efficiency (Fan et al., 1997).

In the above system of equations, if we denote

$$\mathbf{b}(x) = \left(u(x, t_n), \frac{\partial}{\partial x} u(x, t_n), \dots, \frac{\partial^{\tilde{p}}}{\partial x^{\tilde{p}}} u(x, t_n) \right)^\top ,$$

then we can solve $\mathbf{b}(x)$ through the optimization problem in (G.26) with a closed-form solution

shown in (G.27):

$$\mathbf{b}(x) = \left(\mathbf{X}_{\text{spa}}^\top \mathbf{W}_{\text{spa}} \mathbf{X}_{\text{spa}} \right)^{-1} \mathbf{X}_{\text{spa}}^\top \mathbf{W}_{\text{spa}} \mathbf{u}_\cdot^n, \quad (\text{G.28})$$

where

$$\mathbf{X}_{\text{spa}} = \begin{bmatrix} 1 & (x_0 - x) & \dots & (x_0 - x)^{\tilde{p}} \\ 1 & (x_1 - x) & \dots & (x_1 - x)^{\tilde{p}} \\ \vdots & \vdots & \ddots & \vdots \\ 1 & (x_{M-1} - x) & \dots & (x_{M-1} - x)^{\tilde{p}} \end{bmatrix}, \quad \mathbf{u}_\cdot^n = \begin{bmatrix} u_0^n \\ u_1^n \\ \vdots \\ u_{M-1}^n \end{bmatrix}$$

and $\mathbf{W}_{\text{spa}} = \text{diag} \left(\mathcal{K} \left(\frac{x_0 - x}{h} \right), \dots, \mathcal{K} \left(\frac{x_{M-1} - x}{h} \right) \right)$.

The main computational complexity to derive $\mathbf{b}(x)$ lies in the computation of inverse of

G.2 Proof of Proposition B.1

matrix $\mathbf{X}_{\text{spa}}^\top \mathbf{W}_{\text{spa}} \mathbf{X}_{\text{spa}} \in \mathbb{R}^{(\check{p}+1) \times (\check{p}+1)}$, where

$$\mathbf{X}_{\text{spa}}^\top \mathbf{W}_{\text{spa}} \mathbf{X}_{\text{spa}} = \begin{bmatrix} \sum_{i=0}^{M-1} w_i & \sum_{i=0}^{M-1} w_i(x_i - x) & \sum_{i=0}^{M-1} w_i(x_i - x)^2 & \dots & \sum_{i=0}^{M-1} w_i(x_i - x)^{\check{p}} \\ \sum_{i=0}^{M-1} w_i(x_i - x) & \sum_{i=0}^{M-1} w_i(x_i - x)^2 & \sum_{i=0}^{M-1} w_i(x_i - x)^3 & \dots & \sum_{i=0}^{M-1} w_i(x_i - x)^{\check{p}+1} \\ \sum_{i=0}^{M-1} w_i(x_i - x)^2 & \sum_{i=0}^{M-1} w_i(x_i - x)^3 & \sum_{i=0}^{M-1} w_i(x_i - x)^4 & \dots & \sum_{i=0}^{M-1} w_i(x_i - x)^{\check{p}+2} \\ \vdots & \vdots & \vdots & \ddots & \vdots \\ \sum_{i=0}^{M-1} w_i(x_i - x)^{\check{p}} & \sum_{i=0}^{M-1} w_i(x_i - x)^{\check{p}+1} & \sum_{i=0}^{M-1} w_i(x_i - x)^{\check{p}+2} & \dots & \sum_{i=0}^{M-1} w_i(x_i - x)^{2\check{p}} \end{bmatrix}$$

and

$$\mathbf{X}_{\text{spa}}^\top \mathbf{W}_{\text{spa}} \mathbf{u}^n = \begin{pmatrix} \sum_{i=0}^{M-1} w_i u_i^n \\ \sum_{i=0}^{M-1} w_i(x_i - x) u_i^n \\ \sum_{i=0}^{M-1} w_i(x_i - x)^2 u_i^n \\ \sum_{i=0}^{M-1} w_i(x_i - x)^3 u_i^n \\ \sum_{i=0}^{M-1} w_i(x_i - x)^4 u_i^n \end{pmatrix},$$

we know that for a fixed $n \in \{0, \dots, N-1\}$ and $x \in \{x_0, \dots, x_{M-1}\}$, the computational

complexity of computing $\mathbf{X}_{\text{spa}}^\top \mathbf{W}_{\text{spa}} \mathbf{X}_{\text{spa}}$ and $\mathbf{X}_{\text{spa}}^\top \mathbf{W}_{\text{spa}} \mathbf{u}^n$ is $O(\check{p}^2 M)$. Besides, the compu-

tational complexity to derive $(\mathbf{X}_{\text{spa}}^\top \mathbf{W}_{\text{spa}} \mathbf{X}_{\text{spa}})^{-1}$ is $O(\check{p}^3)$. So we know that for a fixed $n \in$

$\{0, \dots, N-1\}$ and $x \in \{x_0, \dots, x_{M-1}\}$, the computational complexity of computing $\frac{\partial^p}{\partial x^p} u(x_i, t_n)$

is $\max\{O(\check{p}^2 M), O(\check{p}^3)\}$ with \check{p} usually set as $\check{p} = p + 3$. Accordingly, the computational

complexity of computing $\left\{ \frac{\partial^p}{\partial x^p} u(x_i, t_n) \right\}_{i=0, \dots, M-1, n=0, \dots, N-1}$ is $\max\{O(\check{p}^2 M^2 N), O(\check{p}^3 MN)\}$.

Because $p \leq q_{\max}$, we know that the computational complexity of computing all derivatives

with respect to x with highest order as q_{\max} is $\max\{O(q_{\max}^2 M^2 N), O(q_{\max}^3 MN)\}$. Similarly,

G.3 Proof of Lemma D.1

the computational complexity of computing the first order derivatives with respect to t is $\max\{O(MN^2), O(MN)\}$. In conclusion, the computational complexity to derive all elements in matrix \mathbf{X} and vector $\nabla_t \mathbf{u}$, including

$$\left\{ \widehat{u(x_i, t_n)}, \widehat{\frac{\partial}{\partial x} u(x_i, t_n)}, \widehat{\frac{\partial^2}{\partial x^2} u(x_i, t_n)}, \widehat{\frac{\partial}{\partial t} u(x_i, t_n)} \right\}_{i=0, \dots, M-1, n=0, \dots, N-1}.$$

by local polynomial regression in (2.4) is $\max\{O(q_{\max}^2 M^2 N), O(MN^2), O(q_{\max}^3 MN)\}$, where q_{\max} is the highest order of derivatives desired in (1.3). \square

G.3 Proof of Lemma D.1

Proof. In this proof, we take $k = 0$ as an illustration example, i.e., prove that when

$$\epsilon > \mathcal{C}(\sigma, \|u\|_{L^\infty(\Omega)}) \max \left\{ \frac{4K_{\max}}{M^{3/7}}, 4AM^{-3/7}, 4\sqrt{2} \frac{d^3}{dx^3} f^*(0) M^{-3/7}, \frac{16(C \log M + \gamma) \log(M)}{M^{3/7}}, \right. \\ \left. 16\sqrt{\frac{\omega}{7}} \tilde{C}(\sigma, \|u\|_{L^\infty(\Omega)}) \frac{\sqrt{\log(M)}}{M^{3/7}} \right\},$$

we have

$$P \left[\sup_{x \in [0, X_{\max}]} \left| \widehat{u(x, t_n)} - u(x, t_n) \right| > \epsilon \right] < 2Me^{-\frac{M^{2/7}}{2\sigma^2}} + Qe^{-L\gamma} + 4\sqrt{2}\eta^4 M^{-\frac{2}{7}\omega}$$

for a fixed t_n with $n \in \{0, 1, \dots, N-1\}$. For $k = 1, 2$, it can be derived with the same logic flow.

Recall in Section 2.1, the fitted value of the smoothing cubic spline $s(x)$ is the minimizer of the optimization problem in (2.4). From Theorem A in Silverman (1984) (also mentioned by Messer (1991) in the Section 1, and equation (2.2) in Craven and Wahba (1978)) that when Condition 3.4 - Condition 3.5 hold and for large M and small $\tilde{\lambda} = \frac{1-\alpha}{\alpha}$, we have

$$\hat{f}_i = \frac{1}{M\tilde{\lambda}^{1/4}} \sum_{j=0}^{M-1} K \left(\frac{x_i - x_j}{\tilde{\lambda}^{1/4}} \right) u_j^n,$$

where $\widehat{f}_i = u(\widehat{x_i, t_n})$, $\widetilde{\lambda}$ trades off the goodness-of-fit and smoothness of the cubic spline in (2.4)

and $K(\cdot)$ is a fixed kernel function defined as

$$K(x) = \frac{1}{2} e^{-|x|/\sqrt{2}} \left[\sin(|x|/\sqrt{2} + \pi/4) \right].$$

For a general spatial variable x and fixed $n \in \{0, 1, \dots, N-1\}$, we denote

$$f^*(x) = u(x, t_n),$$

which is the ground truth of the underlying dynamic function $u(x, t_n)$ with t_n fixed. Besides,

we denote $\widehat{f}(x) = u(\widehat{x, t_n})$, which is an estimation of the ground truth of $f^*(x) = u(x, t_n)$ with

t_n fixed. Accordingly to the above discussion, this estimation of $\widehat{f}(x)$ can be written as

$$\widehat{f}(x) = \frac{1}{M\widetilde{\lambda}^{1/4}} \sum_{j=0}^{M-1} K\left(\frac{x-x_j}{\widetilde{\lambda}^{1/4}}\right) u_j^n,$$

where $\widehat{f}_i = \widehat{f}(x_i)$ for $i \in \{0, 1, \dots, M-1\}$

In order to bound $P\left(\sup |\widehat{f}(x) - f^*(x)| > \epsilon\right)$ for a general x , we decompose it as follows:

$$\begin{aligned} & P\left(\sup |\widehat{f}(x) - f^*(x)| > \epsilon\right) \\ = & P\left(\sup |\widehat{f}(x) - \widehat{f}^B(x) + \widehat{f}^B(x) - \widehat{f}^*(x)| > \epsilon\right) \\ = & P\left(\sup |\widehat{f}(x) - \widehat{f}^B(x) - E(\widehat{f}(x) - \widehat{f}^B(x)) + E(\widehat{f}(x) - \widehat{f}^B(x)) + \widehat{f}^B(x) - \widehat{f}^*(x)| > \epsilon\right) \\ = & P\left(\sup \underbrace{|\widehat{f}(x) - \widehat{f}^B(x) - E(\widehat{f}(x) - \widehat{f}^B(x))|}_{\mathcal{A}} + \underbrace{E(\widehat{f}(x) - \widehat{f}^B(x)) + \widehat{f}^B(x) - \widehat{f}^*(x)}_{\mathcal{B}} > \epsilon\right), \\ & \underbrace{E(\widehat{f}(x) - \widehat{f}^B(x))}_{\mathcal{C}} + \underbrace{\widehat{f}^B(x) - E(\widehat{f}^B(x))}_{\mathcal{D}} > \epsilon \\ \leq & P\left(\sup |\mathcal{A}| > \frac{\epsilon}{4}\right) + P\left(\sup |\mathcal{B}| > \frac{\epsilon}{4}\right) + P\left(\sup |\mathcal{C}| > \frac{\epsilon}{4}\right) + P\left(\sup |\mathcal{D}| > \frac{\epsilon}{4}\right) \end{aligned} \tag{G.29}$$

where the $\widehat{f^B}(x)$ in (G.29) the truncated estimator defined as

$$\widehat{f^B}(x) = \frac{1}{M\widetilde{\lambda}^{1/4}} \sum_{j=0}^{M-1} K\left(\frac{x-x_j}{\widetilde{\lambda}^{1/4}}\right) u_j^n \mathbb{1}\{u_j^n < B_M\}.$$

Here $\{B_M\}$ is an increasing sequence and $B_M \rightarrow +\infty$ as $M \rightarrow +\infty$, i.e., $B_M = M^b$ with constant $b > 0$, and we will discuss the value of b at the end of this proof.

In the remaining of the proof, we work on the upper bound of the four decomposed terms,

$$\text{i.e., } P\left(\sup |\mathcal{A}| > \frac{\epsilon}{4}\right), P\left(\sup |\mathcal{B}| > \frac{\epsilon}{4}\right), P\left(\sup |\mathcal{C}| > \frac{\epsilon}{4}\right), P\left(\sup |\mathcal{D}| > \frac{\epsilon}{4}\right).$$

First, let us discuss the upper bound of $P\left(\sup |\mathcal{A}| > \frac{\epsilon}{4}\right)$.

Because

$$\begin{aligned} P\left(\sup |\mathcal{A}| > \frac{\epsilon}{4}\right) &= P\left(\sup \left|\widehat{f}(x) - \widehat{f^B}(x)\right| > \frac{\epsilon}{4}\right) \\ &= P\left(\sup \left|\frac{1}{M\widetilde{\lambda}^{1/4}} \sum_{j=0}^{M-1} K\left(\frac{x-x_j}{\widetilde{\lambda}^{1/4}}\right) u_j^n \mathbb{1}\{u_j^n \geq B_M\}\right| > \frac{\epsilon}{4}\right) \\ &\leq P\left(\sup \left|\frac{K_{\max}}{M\widetilde{\lambda}^{1/4}} \sum_{j=0}^{M-1} u_j^n \mathbb{1}\{u_j^n \geq B_M\}\right| > \frac{\epsilon}{4}\right), \end{aligned}$$

where $K_{\max} = \max_{x \in [0, X_{\max}] \cup [0, T_{\max}]} K(x)$. If we let $\frac{\epsilon}{4} > \frac{K_{\max}}{M\widetilde{\lambda}^{1/4}} B_M$, then we have

$$\begin{aligned} P\left(\sup |\mathcal{A}| > \frac{\epsilon}{4}\right) &\leq P\left(\exists i = 0, \dots, M-1, \text{ s.t. } |u_i^n| \geq B_M\right) \\ &= P\left(\max_{i=0, \dots, M-1} |u_i^n| \geq B_M\right) \end{aligned}$$

Let $C_M = B_M - \|U\|_{L^\infty(\Omega)}$, where U is the random variable generated from the unknown

dynamic system, i.e., $U = u(x, t) + \epsilon$ with $\epsilon \sim N(0, \sigma^2)$. Then we have

$$\begin{aligned}
P\left(\sup |\mathcal{A}| > \frac{\epsilon}{4}\right) &= P\left(\sup \left|\widehat{f}(x) - \widehat{f}^B(x)\right| > \frac{\epsilon}{4}\right) \\
&\leq P\left(\max_{i=0, \dots, M-1} |U_i^n - u_i^n| \geq C_M\right) \\
&\leq 2Me^{-C_M^2/(2\sigma^2)}
\end{aligned}$$

Next, let us discuss the upper bound of $P\left(\sup |\mathcal{B}| > \frac{\epsilon}{4}\right)$.

$$\begin{aligned}
\mathcal{B} &= E\left(|\widehat{f}(x) - \widehat{f}^B(x)|\right) \\
&= E\left(\left|\frac{1}{M\widetilde{\lambda}^{1/4}} \sum_{j=0}^{M-1} K\left(\frac{x-x_j}{\widetilde{\lambda}^{1/4}}\right) u_j^n \mathbb{1}\{u_j^n \geq B_M\}\right|\right) \\
&\leq E\left(\frac{1}{M\widetilde{\lambda}^{1/4}} \sum_{j=0}^{M-1} \left|K\left(\frac{x-x_j}{\widetilde{\lambda}^{1/4}}\right)\right| |u_j^n| \mathbb{1}\{u_j^n \geq B_M\}\right) \\
&= \frac{1}{\widetilde{\lambda}^{1/4}} \int \int_{|u| \geq B_M} \left|K\left(\frac{x-a}{\widetilde{\lambda}^{1/4}}\right)\right| |u| dF_M(a, u) \tag{G.30}
\end{aligned}$$

$$\leq \int |K(\xi)| d\xi \times \underbrace{\sup_{\alpha} \int_{|u| \geq B_M} |u| f_M(\alpha, u) du}_{\mathcal{V}} \tag{G.31}$$

Here in (G.30), $F_M(\cdot, \cdot)$ is the empirical c.d.f. of (x, u) 's, and in (G.31), $f_M(\cdot, \cdot)$ is the empirical p.d.f. of (x, u) 's.

Now let us take a look at the upper bound of \mathcal{V} . For any $s > 0$, we have

$$\begin{aligned}
\sup_{\alpha} \int_{|u| \geq B_M} \frac{|u|}{B_M} f_M(\alpha, u) du &\leq \sup_{\alpha} \int_{|u| \geq B_M} \left(\frac{|u|}{B_M}\right)^s f_M(\alpha, u) du \\
&\leq \sup_{\alpha} \int \left(\frac{|u|}{B_M}\right)^s f_M(\alpha, u) du,
\end{aligned}$$

which gives

$$\mathcal{V} := \sup_{\alpha} \int_{|u| \geq B_M} |u| f_M(\alpha, u) du \leq B_M^{1-s} \underbrace{\sup_{\alpha} \int |u|^s f_M(\alpha, u) du}_{\pi_s}.$$

G.3 Proof of Lemma D.1

From the lemma statement we know that when $s = 2$, we have $\pi_s := \sup_\alpha \int |u|^s f_M(\alpha, u) du < +\infty$. If we set $A = \pi_s \int |K(\xi)| d\xi$, then we have

$$\mathcal{B} \leq AB_M^{1-s}$$

So when $\frac{\epsilon}{4} > AB_M^{1-s}$, we have

$$P\left(\sup |\mathcal{B}| > \frac{\epsilon}{4}\right) = P\left(E\left(|\widehat{f}(x) - \widehat{f}^B(x)|\right) \geq \frac{\epsilon}{4}\right) = 0.$$

Then, let us discuss the upper bound of $P\left(\sup |\mathcal{C}| > \frac{\epsilon}{4}\right)$. According to Lemma 5 in

Rice and Rosenblatt (1983), when

$$f^*(x) \in C^4, \quad \frac{d^2}{dx^2} f^*(x_0) = \frac{d^2}{dx^2} f^*(x_{M-1}) = 0 \text{ and } \frac{d^3}{dx^3} f^*(x_0) \neq 0, \frac{d^3}{dx^3} f^*(x_{M-1}) = 0, \text{ we}$$

have

$$\begin{aligned} & E(\widehat{f}(x)) - f^*(x) \\ &= \sqrt{2} \frac{d^3}{dx^3} f^*(0) \widetilde{\lambda}^{3/4} \exp\left(\frac{-x}{\sqrt{2}} \widetilde{\lambda}^{-1/4}\right) \cos\left(\frac{x}{\sqrt{2}} \widetilde{\lambda}^{-1/4}\right) + \ell(x), \end{aligned}$$

where the error term $\ell(x)$ satisfies

$$\int [\ell(x)]^2 dx = o\left(\int \left[E(\widehat{f}(x)) - f^*(x)\right]^2 dx\right).$$

So when $\frac{\epsilon}{4} > \sqrt{2} \frac{d^3}{dx^3} f^*(0) \widetilde{\lambda}^{3/4}$ and M is sufficiently large then we have

$$P\left(\sup |\mathcal{C}| > \frac{\epsilon}{4}\right) = 0$$

Finally, let us discuss the upper bound of $P(\sup |\mathcal{D}| > \frac{\varepsilon}{4})$.

In order to bound $P(\sup |D| > \frac{\varepsilon}{4})$, we further decompose \mathcal{D} into two components, i.e.,

$$\mathcal{D} := \hat{f}^B(x) - E(\hat{f}^B(x)) = e_M(x, t_n) + \frac{1}{\sqrt{M}} \rho_M(x, t_n).$$

The decomposition procedure and the definition of $e_M(x, t_n), \rho_M(x, t_n)$ are described in the following system of equations (see Mack and Silverman, 1982, Proposition 2):

$$\begin{aligned} \mathcal{D} &= \hat{f}^B(x) - E(\hat{f}^B(x)) \\ &= \frac{1}{M\tilde{\lambda}^{1/4}} \sum_{j=0}^{M-1} K\left(\frac{x-x_j}{\tilde{\lambda}^{1/4}}\right) u_j^n \mathbb{1}\{u_j^n < B_M\} - \\ &\quad E\left(\frac{1}{M\tilde{\lambda}^{1/4}} \sum_{j=0}^{M-1} K\left(\frac{x-x_j}{\tilde{\lambda}^{1/4}}\right) u_j^n \mathbb{1}\{u_j^n < B_M\}\right) \\ &= \frac{1}{\sqrt{M}\tilde{\lambda}^{1/4}} \int_{a \in \mathbb{R}} \int_{|u| < B_M} K\left(\frac{x-a}{\tilde{\lambda}^{1/4}}\right) u \, d\left(\underbrace{\sqrt{M}(F_M(a, u) - F(a, u))}_{Z_M(a, u)}\right) \quad (\text{G.32}) \\ &= \frac{1}{\sqrt{M}\tilde{\lambda}^{1/4}} \int_{a \in \mathbb{R}} K\left(\frac{x-a}{\tilde{\lambda}^{1/4}}\right) \int_{|u| < B_M} u \, d(Z_M(a, u)) \\ &= \frac{1}{\sqrt{M}\tilde{\lambda}^{1/4}} \int_{a \in \mathbb{R}} K\left(\frac{x-a}{\tilde{\lambda}^{1/4}}\right) \left[\int_{|u| < B_M} u \, d(Z_M(a, u) - B_0(T(a, u))) + \right. \\ &\quad \left. \int_{|u| < B_M} u \, dB_0(T(a, u)) \right] \quad (\text{G.33}) \\ &= \underbrace{\frac{1}{\sqrt{M}\tilde{\lambda}^{1/4}} \int_{a \in \mathbb{R}} \int_{|u| < B_M} K\left(\frac{x-a}{\tilde{\lambda}^{1/4}}\right) u \, d(Z_M(a, u) - B_0(T(a, u)))}_{e_M(x, t_n)} \\ &\quad + \underbrace{\frac{1}{\sqrt{M}} \frac{1}{\tilde{\lambda}^{1/4}} \int_{a \in \mathbb{R}} \int_{|u| < B_M} K\left(\frac{x-a}{\tilde{\lambda}^{1/4}}\right) u \, dB_0(T(a, u))}_{\rho_M(x, t_n)}. \end{aligned}$$

In (G.32), $F_M(\cdot, \cdot) := F_M(\cdot, \cdot | t_n)$ is the empirical c.d.f of (x, u) with a fixed t_n , and $Z_M(a, u) =$

$\sqrt{M}(F_M(a, u) - F(a, u))$ is a two-dimensional empirical process (Tusnády, 1977; Mack and Silverman,

1982). In (G.33), $B_0(T(a, u))$ is a sample path of two-dimensional Brownian bride. And

G.3 Proof of Lemma D.1

$T(a, u) : \mathbb{R}^2 \rightarrow [0, 1]^2$ is the transformation defined by Rosenblatt (1952), i.e., $T(a, u) = (F_A(x), F_{U|A}(u|a))$, where F_A is the marginal c.d.f of A and $F_{U|A}$ is the conditional c.d.f of U given A (see Mack and Silverman, 1982, Proposition 2).

Through the above decomposition of \mathcal{D} , we have

$$P\left(\sup |D| > \frac{\epsilon}{4}\right) \leq P\left(\sup |e_M(x, t_n)| > \frac{\epsilon}{8}\right) + P\left(\sup \frac{1}{\sqrt{M}} |\rho_M(x, t_n)| > \frac{\epsilon}{8}\right).$$

For $e_M(x, t_n)$, we have

$$\begin{aligned} & P\left(\sup |e_M(x, t_n)| > \frac{\epsilon}{8}\right) \\ = & P\left(\sup \left| \frac{1}{\sqrt{M}\tilde{\lambda}^{1/4}} \int_{a \in \mathbb{R}} \int_{|u| < B_M} K\left(\frac{x-a}{\tilde{\lambda}^{1/4}}\right) u d(Z_M(a, u) - B_0(T(a, u))) \right| > \frac{\epsilon}{8}\right) \\ \leq & P\left(\frac{2B_M K_{\max}}{\sqrt{M}\tilde{\lambda}^{1/4}} \sup_{a, u} |Z_M(a, u) - B_0(T(a, u))| > \frac{\epsilon}{8}\right). \end{aligned}$$

Proved by Theorem 1 in Tusnády (1977), we know that, for any γ , we have

$$P\left(\sup_{a, u} |Z_M(a, u) - B_0(T(a, u))| > \frac{(C \log M + \gamma) \log M}{\sqrt{M}}\right) \leq Q e^{-L\gamma},$$

where C, Q, L are absolute positive constants which is independent of temporal resolution N

and spatial resolution M . Thus, when $\frac{\epsilon}{8} \geq \frac{2B_M K_{\max}}{\sqrt{M}\tilde{\lambda}^{1/4}} \frac{(C \log M + \gamma) \log M}{\sqrt{M}}$, we have

$$P\left(\sup |e_M(x, t_n)| > \frac{\epsilon}{8}\right) < Q e^{-L\gamma}.$$

G.3 Proof of Lemma D.1

For $\rho_M(x, t_n)$, by equation (7) in Mack and Silverman (1982), we have

$$\begin{aligned} \frac{\tilde{\lambda}^{1/8} \sup |\rho_M(x, t_n)|}{\sqrt{\log(1/\tilde{\lambda}^{1/4})}} &\leq \underbrace{16(\log V)^{1/2} S^{1/2} \left(\log \left(\frac{1}{\tilde{\lambda}^{1/4}} \right) \right)^{-1/2} \int |\xi|^{1/2} |dK(\xi)|}_{\mathcal{W}_{1,M}} + \\ &\quad \underbrace{16\sqrt{2}\tilde{\lambda}^{-1/8} \left(\log \left(\frac{1}{\tilde{\lambda}^{1/4}} \right) \right)^{-1/2} \int q(S\tilde{\lambda}^{1/4}|\tau|) |d(K(\tau))|}_{\mathcal{W}_{2,M}}, \end{aligned}$$

where V is a random variable satisfying $E(V) \leq 4\sqrt{2}\eta^4$ for $\eta^2 = \max_{i=0, \dots, M-1, n=0, \dots, N-1} E(U_i^n)^2$,

$S = \sup_x \int u^2 f(x, u) du$ with $f(\cdot, \cdot)$ as the distribution function of (x_i, u_i^n) , and $q(z) = \int_0^z \frac{1}{2} \sqrt{\frac{1}{y} \log \left(\frac{1}{y} \right)} dy$.

So we have the following system of equations:

$$\begin{aligned} &P \left(\sup \frac{1}{\sqrt{M}} |\rho_M(x, t_n)| > \frac{\epsilon}{8} \right) \\ &= P \left(\frac{\tilde{\lambda}^{1/8} \sup |\rho_M(x, t_n)|}{\sqrt{\log(1/\tilde{\lambda}^{1/4})}} > \frac{\sqrt{M}\tilde{\lambda}^{1/8}\epsilon}{8\sqrt{\log(1/\tilde{\lambda}^{1/4})}} \right) \\ &\leq P \left(\mathcal{W}_{1,M} + \mathcal{W}_{2,M} > \frac{\sqrt{M}\tilde{\lambda}^{1/8}\epsilon}{8\sqrt{\log(1/\tilde{\lambda}^{1/4})}} \right) \\ &\leq P \left(\mathcal{W}_{1,M} \geq \frac{\sqrt{M}\tilde{\lambda}^{1/8}\epsilon}{16\sqrt{\log(1/\tilde{\lambda}^{1/4})}} \right) + P \left(\mathcal{W}_{2,M} \geq \frac{\sqrt{M}\tilde{\lambda}^{1/8}\epsilon}{16\sqrt{\log(1/\tilde{\lambda}^{1/4})}} \right) \quad (\text{G.34}) \end{aligned}$$

Now let us bound $P \left(\mathcal{W}_{1,M} \geq \frac{\sqrt{M}\tilde{\lambda}^{1/8}\epsilon}{16\sqrt{\log(1/\tilde{\lambda}^{1/4})}} \right), P \left(\mathcal{W}_{2,M} \geq \frac{\sqrt{M}\tilde{\lambda}^{1/8}\epsilon}{16\sqrt{\log(1/\tilde{\lambda}^{1/4})}} \right)$ in (G.34) sep-

arately.

1. For the first term in (G.34), we have

$$\begin{aligned}
 & P \left(\mathcal{W}_{1,M} \geq \frac{\sqrt{M\tilde{\lambda}^{1/8}\epsilon}}{16\sqrt{\log(1/\tilde{\lambda}^{1/4})}} \right) \\
 &= P \left(16(\log V)^{1/2} S^{1/2} \left(\log \left(\frac{1}{\tilde{\lambda}^{1/4}} \right) \right)^{-1/2} \int |\xi|^{1/2} |dK(\xi)| \geq \frac{\sqrt{M\tilde{\lambda}^{1/8}\epsilon}}{16\sqrt{\log(1/\tilde{\lambda}^{1/4})}} \right) \\
 &= P \left((\log V)^{1/2} \geq \frac{\sqrt{M\tilde{\lambda}^{1/8}\epsilon}}{16^2 S^{1/2} \int |\xi|^{1/2} |dK(\xi)|} \right) \\
 &= P \left(\log V \geq \left(\frac{\sqrt{M\tilde{\lambda}^{1/8}\epsilon}}{16^2 S^{1/2} \int |\xi|^{1/2} |dK(\xi)|} \right)^2 \right) \\
 &= P \left(V \geq \exp \left[\left(\frac{\sqrt{M\tilde{\lambda}^{1/8}\epsilon}}{16^2 S^{1/2} \int |\xi|^{1/2} |dK(\xi)|} \right)^2 \right] \right) \\
 &\leq \frac{E(V)}{\exp \left[\left(\frac{\sqrt{M\tilde{\lambda}^{1/8}\epsilon}}{16^2 S^{1/2} \int |\xi|^{1/2} |dK(\xi)|} \right)^2 \right]} \tag{G.35}
 \end{aligned}$$

$$\leq \frac{4\sqrt{2}\eta^4}{\exp \left[\left(\frac{\sqrt{M\tilde{\lambda}^{1/8}\epsilon}}{16^2 S^{1/2} \int |\xi|^{1/2} |dK(\xi)|} \right)^2 \right]} \tag{G.36}$$

$$= 4\sqrt{2}\eta^4 \tilde{\lambda}^{\omega/4} \tag{G.37}$$

Here inequality (G.35) is due to Markov's inequality, and inequality (G.36) is due to

the fact that $E(V) \leq 4\sqrt{2}\eta^4$. Equality (G.37) is because we set $\frac{\sqrt{M\tilde{\lambda}^{1/8}\epsilon}}{16\sqrt{\log(1/\tilde{\lambda}^{1/4})}} =$

$\sqrt{\omega}\tilde{C}(t_n, \sigma, \|u\|_{L^\infty(\Omega)})$, where

$$\tilde{C}(t_n, \sigma, \|u\|_{L^\infty(\Omega)}) := 16\sqrt{S} \int |\xi|^{1/2} |dK(\xi)|$$

and $\omega > 1$ is an arbitrary scaler.

2. For the second term of (G.34), it converges to $\tilde{C}(t_n, \sigma, \|u\|_{L^\infty(\Omega)})$ by using arguments

similar to Silverman (1978) (page. 180-181) under the condition in Lemma D.1 that

$\int \sqrt{|x \log(|x|)|} |dK(x)| < +\infty$. Here we add $(t_n, \sigma, \|u\|_{L^\infty(\Omega)})$ after \tilde{C} to emphasize that

G.3 Proof of Lemma D.1

the constant $\tilde{C}(t_n, \sigma, \|u\|_{L^\infty(\Omega)})$ is dependent on $t_n, \sigma, \|u\|_{L^\infty(\Omega)}$.

It should be noted that

$$\tilde{C}(t_n, \sigma, \|u\|_{L^\infty(\Omega)}) < +\infty, \quad (\text{G.38})$$

given the reasons listed as follows. First, it can be easily verified that the term $\int |\xi|^{1/2} |dK(\xi)|$

in $\tilde{C}(t_n, \sigma, \|u\|_{L^\infty(\Omega)})$ is bounded. Second, for $S = \sup_x \int u^2 f(x, u) du$, it is also bounded.

The reasons are described as follows. For a general $\varrho > 0$, we have

$$\begin{aligned} & \sup_{x \in [0, X_{\max}]} \int |u|^\varrho f(x, u) du \\ &= \sup_{x \in [0, X_{\max}]} \int |u|^\varrho \frac{1}{\sqrt{2\pi\sigma^2}} \exp\left(-\frac{(u - u(x, t_n))^2}{2\sigma^2}\right) du \\ &= \sup_{x \in [0, X_{\max}]} \frac{1}{\sqrt{2}} \sigma^2 2^{\varrho/2} \Gamma\left(\frac{1+\varrho}{2}\right) G\left(-\frac{\varrho}{2}, \frac{1}{2}, -\frac{1}{2} \left(\frac{u(x, t_n)}{\sigma}\right)^2\right), \end{aligned}$$

where $G(a, b, z)$ is Kummer's confluent hypergeometric function of $z \in \mathbb{C}$ with parameters $a, b \in \mathbb{C}$ (Winkelbauer, 2012). Because $G(-\frac{\varrho}{2}, \frac{1}{2}, \cdot)$ is an entire function for fixed parameters, we have

$$\begin{aligned} & \sup_{x \in [0, X_{\max}]} \int |u|^\varrho f(x, u) du \\ &\leq \sup_{x \in [0, X_{\max}]} \frac{1}{\sqrt{2}} \sigma^2 2^{\varrho/2} \Gamma\left(\frac{1+\varrho}{2}\right) \sup_{z \in \left[-\frac{\max_{t \in \Omega} u^2(x, t)}{2\sigma^2}, -\frac{\min_{t \in \Omega} u^2(x, t)}{2\sigma^2}\right]} G\left(-\frac{\varrho}{2}, \frac{1}{2}, z\right) \\ &< +\infty. \end{aligned}$$

So we can bound $\sup_{x \in [0, X_{\max}]} \int |u|^\varrho f(x, u) du$ by a constant. If we take $\varrho = 2$, we can

obtain $S = \sup_x \int u^2 f(x, u) du$ bounded by a constant. So we can declare the statement

in (G.38).

G.3 Proof of Lemma D.1

We would also like to declare that there exist a constant $\tilde{C}(\sigma, \|u\|_{L^\infty(\Omega)}) > 0$ such that

for any $N \geq 1$, we have

$$\max_{n=0, \dots, N-1} \tilde{C}(t_n, \sigma, \|u\|_{L^\infty(\Omega)}) \leq \tilde{C}(\sigma, \|u\|_{L^\infty(\Omega)}),$$

where $\tilde{C}(\sigma, \|u\|_{L^\infty(\Omega)})$ is independent of t_n, x_i, M, N , and only depends on the noisy data

\mathcal{D} itself.

From the above discussion, we learn that $\mathcal{W}_{2,M}$ converges to $\tilde{C}(t_n, \sigma, \|u\|_{L^\infty(\Omega)})$, which

can be bounded by $\tilde{C}(\sigma, \|u\|_{L^\infty(\Omega)})$. If we set $\frac{\sqrt{M\tilde{\lambda}}^{1/8}\epsilon}{16\sqrt{\log(1/\tilde{\lambda}^{1/4})}} > \sqrt{\omega}\tilde{C}(\sigma, \|u\|_{L^\infty(\Omega)})$ with

$\omega > 1$, then there exists a positive integer $\dot{M}(\omega)$ such that as long as $M > \dot{M}(\omega)$, we

have $P\left(\mathcal{W}_{2,M} \geq \frac{\sqrt{M\tilde{\lambda}}^{1/8}\epsilon}{16\sqrt{\log(1/\tilde{\lambda}^{1/4})}}\right) = 0$.

For the value of ω , we set it as $\omega = M^{2r}$ with $r > 0$. And we will discuss the value of r

later.

By combining $P\left(\mathcal{W}_{1,M} \geq \frac{\sqrt{M\tilde{\lambda}}^{1/8}\epsilon}{16\sqrt{\log(1/\tilde{\lambda}^{1/4})}}\right), P\left(\mathcal{W}_{2,M} \geq \frac{\sqrt{M\tilde{\lambda}}^{1/8}\epsilon}{16\sqrt{\log(1/\tilde{\lambda}^{1/4})}}\right)$ together, we have when

$\frac{\epsilon}{16} > \sqrt{\omega}\tilde{C}(\sigma, \|u\|_{L^\infty(\Omega)})\sqrt{\frac{\log(1/\tilde{\lambda}^{1/4})}{M\tilde{\lambda}^{1/4}}}$ and $M > \dot{M}(\omega)$, we have

$$P\left(\sup\left|\frac{1}{\sqrt{M}}\rho_M(x, t_n)\right| > \frac{\epsilon}{8}\right) < 4\sqrt{2}\eta^4\tilde{\lambda}^{\omega/4}.$$

By combining the discussion on $P(\sup|\mathcal{A}| > \frac{\epsilon}{4}), P(\sup|\mathcal{B}| > \frac{\epsilon}{4}), P(\sup|\mathcal{C}| > \frac{\epsilon}{4})$, and

$P(\sup|\mathcal{D}| > \frac{\epsilon}{4})$, we can conclude that when

- $\frac{\epsilon}{4} > \frac{K_{\max}}{M\tilde{\lambda}^{1/4}}B_M$
- $\frac{\epsilon}{4} > AB_M^{1-s} \ (s = 2)$

- $\frac{\epsilon}{4} > \sqrt{2} \frac{d^3}{dx^3} f^*(0) \tilde{\lambda}^{3/4}$
- $\frac{\epsilon}{8} > \frac{2B_M K_{\max}(C \log M + \gamma) \log M}{\tilde{\lambda}^{1/4} M}$
- $\frac{\epsilon}{16} > \sqrt{\omega} \tilde{C}(\sigma, \|u\|_{L^\infty(\Omega)}) \sqrt{\frac{\log(1/\tilde{\lambda}^{1/4})}{M \tilde{\lambda}^{1/4}}}$

we have

$$P(\sup |\mathcal{A} + \mathcal{B} + \mathcal{C} + \mathcal{D}| > \epsilon) < \underbrace{2Me^{-\frac{C_M^2}{2\sigma^2}}}_{\mathcal{Z}_1} + \underbrace{Qe^{-L\gamma}}_{\mathcal{Z}_2} + \underbrace{4\sqrt{2}\eta^4 \tilde{\lambda}^{\omega/4}}_{\mathcal{Z}_3}. \quad (\text{G.39})$$

Let

$$\left\{ \begin{array}{ll} E_1 &= \frac{4K_{\max}}{M \tilde{\lambda}^{1/4}} B_M \\ E_2 &= 4AB_M^{1-s} \\ E_3 &= 4\sqrt{2} \frac{d^3}{dx^3} f^*(0) \tilde{\lambda}^{3/4} \\ E_4 &= \frac{16B_M K_{\max}(C \log M + \gamma) \log M}{\tilde{\lambda}^{1/4} M} \\ E_5 &= 16\sqrt{\omega} \tilde{C}(\sigma, \|u\|_{L^\infty(\Omega)}) \sqrt{\frac{\log(1/\tilde{\lambda}^{1/4})}{M \tilde{\lambda}^{1/4}}} \end{array} \right. ,$$

by setting $\tilde{\lambda} = M^{-a}$, $B_M = M^b$ with $a, b > 0$, we have

$$\left\{ \begin{array}{ll} E_1 &= \frac{4K_{\max}}{M \tilde{\lambda}^{1/4}} B_M = \frac{4K_{\max}}{M^{1-a/4-b}} \\ E_2 &= 4AB_M^{1-s} = 4A \frac{1}{M^{b(s-1)}} \\ E_3 &= 4\sqrt{2} \frac{d}{dx} f^*(0) \tilde{\lambda}^{3/4} = 4\sqrt{2} \frac{d}{dx} f^*(0) M^{-3a/4} \\ E_4 &= \frac{16B_M K_{\max}(C \log M + \gamma) \log M}{\tilde{\lambda}^{1/4} M} = \frac{16K_{\max}(C \log M + \gamma) \log(M)}{M^{1-a/4-b}} \\ E_5 &= 16\sqrt{\omega} \tilde{C}(\sigma, \|u\|_{L^\infty(\Omega)}) \sqrt{\frac{\log(1/\tilde{\lambda}^{1/4})}{M \tilde{\lambda}^{1/4}}} = 8\sqrt{a\omega} \tilde{C}(\sigma, \|u\|_{L^\infty(\Omega)}) \sqrt{\frac{\log(M)}{M^{1-a/4}}}. \end{array} \right.$$

G.3 Proof of Lemma D.1

To guarantee that $E_1, E_2, E_3, E_4, E_5 \rightarrow 0$ as $M \rightarrow +\infty$, we can set

$$\left\{ \begin{array}{l} 1 - a/4 - b = 3a/4 \\ b(s-1) > 0 \\ \frac{1}{2}(1 - a/4) = 3a/4 \\ a, b > 0 \\ s = 2 \end{array} \right. .$$

then we have

$$\left\{ \begin{array}{l} a = 4/7 \\ b = 3/7 \\ s = 2 \end{array} \right. .$$

Accordingly, we have

$$\left\{ \begin{array}{l} E_1 = \frac{4K_{\max}}{M^{3/7}} \\ E_2 = 4AM^{-3/7} \\ E_3 = 4\sqrt{2}\frac{d^3}{dx^3}f^*(0)M^{-3/7} \\ E_4 = \frac{16K_{\max}(C\log M + \gamma)\log(M)}{M^{3/7}} \\ E_5 = 16\sqrt{\frac{\omega}{7}}\tilde{C}(\sigma, \|u\|_{L^\infty(\Omega)})\frac{\sqrt{\log(M)}}{M^{3/7}} \end{array} \right. ,$$

where

$$E_1, E_2, E_3, E_5 \lesssim E_4$$

as $M \rightarrow +\infty$. Here, the operator \lesssim means that when $M \rightarrow +\infty$, the order of the left side hand

of \lesssim will be much smaller than that on the right side hand. So we can declare that when M is

sufficiently large and

$$\begin{aligned} \epsilon > \max \left\{ \frac{4K_{\max}}{M^{3/7}}, 4AM^{-3/7}, 4\sqrt{2} \frac{d^3}{dx^3} f^*(0) M^{-3/7}, \frac{16K_{\max}(C \log M + \gamma) \log(M)}{M^{3/7}}, \right. \\ \left. 16\sqrt{\frac{\omega}{7}} \tilde{C}(\sigma, \|u\|_{L^\infty(\Omega)}) \frac{\sqrt{\log(M)}}{M^{3/7}} \right\} \end{aligned}$$

we have

$$\begin{aligned} P(\sup |\mathcal{A} + \mathcal{B} + \mathcal{C} + \mathcal{D}| > \epsilon) &\leq 2Me^{-\frac{C_M^2}{2\sigma^2}} + Qe^{-L\gamma} + 4\sqrt{2}\eta^4 \tilde{\lambda}^{\omega/4} \\ &= 2Me^{-\frac{(M^{3/7} - \|U\|_{L^\infty(\Omega)})^2}{2\sigma^2}} + Qe^{-L\gamma} + 4\sqrt{2}\eta^4 M^{-\omega/7} \end{aligned}$$

□

G.4 Proof of Lemma C.2

Proof. For the estimation error $\|\nabla_t \mathbf{u} - \mathbf{X}\boldsymbol{\beta}^*\|_\infty$, we have

$$\begin{aligned} \|\nabla_t \mathbf{u} - \mathbf{X}\boldsymbol{\beta}^*\|_\infty &= \|\nabla_t \mathbf{u} - \nabla_t \mathbf{u}^* + \nabla_t \mathbf{u}^* - \mathbf{X}\boldsymbol{\beta}^*\|_\infty \\ &= \|\nabla_t \mathbf{u} - \nabla_t \mathbf{u}^* + \mathbf{X}^* \boldsymbol{\beta}^* - \mathbf{X}\boldsymbol{\beta}^*\|_\infty \\ &\leq \|\nabla_t \mathbf{u} - \nabla_t \mathbf{u}^*\|_\infty + \|(\mathbf{X}^* - \mathbf{X})\boldsymbol{\beta}^*\|_\infty. \end{aligned} \tag{G.40}$$

So accordingly, we have

$$P(\|\nabla_t \mathbf{u} - \mathbf{X}\boldsymbol{\beta}^*\|_\infty > \epsilon) \leq P\left(\|\nabla_t \mathbf{u} - \nabla_t \mathbf{u}^*\|_\infty > \frac{\epsilon}{2}\right) + P(\|(\mathbf{X}^* - \mathbf{X})\boldsymbol{\beta}^*\|_\infty).$$

In the remaining of the proof, we will discuss the bound of $P(\|\nabla_t \mathbf{u} - \nabla_t \mathbf{u}^*\|_\infty > \frac{\epsilon}{2})$ and

$P(\|(\mathbf{X}^* - \mathbf{X})\boldsymbol{\beta}^*\|_\infty)$ separately.

- First let us discuss the bound of $P(\|\nabla_t \mathbf{u} - \nabla_t \mathbf{u}^*\|_\infty > \frac{\epsilon}{2})$. Because

$$\begin{aligned} P\left(\|\nabla_t \mathbf{u} - \nabla_t \mathbf{u}^*\|_\infty > \frac{\epsilon}{2}\right) &\leq P\left(\max_{i=0, \dots, M-1} \sup_{t \in [0, T_{\max}]} \left| \widehat{\frac{\partial}{\partial t} u(x_i, t)} - \frac{\partial}{\partial t} u(x_i, t) \right| > \frac{\epsilon}{2}\right) \\ &\leq \sum_{i=0}^{M-1} P\left(\sup_{t \in [0, T_{\max}]} \left| \widehat{\frac{\partial}{\partial t} u(x_i, t)} - \frac{\partial}{\partial t} u(x_i, t) \right| > \frac{\epsilon}{2}\right), \end{aligned}$$

if we set

$$\begin{aligned} \frac{\epsilon}{2} &> \mathcal{C}_{(\sigma, \|u\|_{L^\infty(\Omega)})} \max \left\{ 4K_{\max} N^{-3/7}, 4\bar{A} N^{-3/7}, 4\sqrt{2} \frac{d^3}{dx^3} \bar{f}^*(0) N^{-3/7}, \right. \\ &\quad \frac{16K_{\max} \left[C_{(\sigma, \|u\|_{L^\infty(\Omega)})} \log(N) + \gamma(N) \right] \log(N)}{N^{3/7}}, \\ &\quad \left. 16\sqrt{\frac{\omega(N)}{7}} \tilde{C}_{(\sigma, \|u\|_{L^\infty(\Omega)})} \frac{\sqrt{\log(N)}}{N^{3/7}} \right\}, \end{aligned} \quad (\text{G.41})$$

then we have

$$\begin{aligned} &P\left(\|\nabla_t \mathbf{u} - \nabla_t \mathbf{u}^*\|_\infty > \frac{\epsilon}{2}\right) \\ &\leq M \left[2Ne^{-\frac{(N^{3/7} - \|U\|_{L^\infty(\Omega)})^2}{2\sigma^2}} + Q_{(\sigma, \|u\|_{L^\infty(\Omega)})} e^{-L\gamma(N)} + 4\sqrt{2}\eta^4 N^{-\omega(N)/7} \right] \end{aligned} \quad (\text{G.42})$$

where inequity (G.42) is derived according to Corollary D.1.

- Second, let us discuss the bound of $P(\|(\mathbf{X}^* - \mathbf{X})\beta^*\|_\infty)$. Because

$$\begin{aligned} &P\left(\|(\mathbf{X}^* - \mathbf{X})\beta^*\|_\infty > \frac{\epsilon}{2}\right) \\ &\leq P\left(\|\beta^*\|_\infty \max_{n=0, \dots, N-1} \sup_{x \in [0, X_{\max}]} \sum_{k=1}^K \|(\mathbf{X}_k^*(x, t_n) - \mathbf{X}_k(x, t_n))\|_\infty > \frac{\epsilon}{2}\right) \\ &= P\left(\max_{n=0, \dots, N-1} \sup_{x \in [0, X_{\max}]} \sum_{k=1}^K \|(\mathbf{X}_k^*(x, t_n) - \mathbf{X}_k(x, t_n))\|_\infty > \frac{\epsilon}{2\|\beta^*\|_\infty}\right) \\ &\leq \sum_{n=0}^{N-1} \sum_{k=1}^K P\left(\sup_{x \in [0, X_{\max}]} \|(\mathbf{X}_k^*(x, t_n) - \mathbf{X}_k(x, t_n))\|_\infty > \frac{\epsilon}{2K\|\beta^*\|_\infty}\right), \end{aligned}$$

if we set

$$\begin{aligned} \frac{\epsilon}{2K\|\beta^*\|_\infty} &> \mathcal{C}_{(\sigma, \|u\|_{L^\infty(\Omega)})} \max \left\{ 4K_{\max}M^{-3/7}, 4AM^{-3/7}, 4\sqrt{2}\frac{d^3}{dx^3}f^*(0)M^{-3/7}, \right. \\ &\quad \frac{16\left[C_{(\sigma, \|u\|_{L^\infty(\Omega)})} \log M + \gamma_{(M)}\right] \log(M)}{M^{3/7}}, \\ &\quad \left. 16\sqrt{\frac{\omega(M)}{7}}\tilde{C}_{(\sigma, \|u\|_{L^\infty(\Omega_{(M)})})}\frac{\sqrt{\log(M)}}{M^{3/7}} \right\}, \end{aligned} \quad (\text{G.43})$$

then we have

$$\begin{aligned} &P\left(\|(\mathbf{X}^* - \mathbf{X})\beta^*\|_\infty > \frac{\epsilon}{2}\right) \\ &\leq NK \left[2Me^{-\frac{(M^{3/7} - \|U\|_{L^\infty(\Omega)})^2}{2\sigma^2}} + Q_{(\sigma, \|u\|_{L^\infty(\Omega)})}e^{-L\gamma_{(M)}} + 4\sqrt{2}\eta^4 M^{-\omega_{(M)}} \right] \end{aligned} \quad (\text{G.44})$$

Inequality (G.44) is derived by Lemma D.1.

By combining the results in (G.41), (G.42), (G.43), (G.44), we have that when

$$\begin{aligned} \frac{\epsilon}{2} &> \mathcal{C}_{(\sigma, \|u\|_{L^\infty(\Omega)})} \max \left\{ 4K_{\max}M^{-3/7}, 4KK_{\max}\|\beta^*\|_\infty N^{-3/7}, \right. \\ &\quad 4AM^{-3/7}, 4K\|\beta^*\|_\infty \bar{A}N^{-3/7}, \\ &\quad 4\sqrt{2}\frac{d^3}{dx^3}f^*(0)M^{-3/7}, 4\sqrt{2}K\|\beta^*\|_\infty \frac{d^3}{dx^3}\bar{f}^*(0)N^{-3/7}, \\ &\quad \frac{16KK_{\max}\|\beta^*\|_\infty \left[C_{(\sigma, \|u\|_{L^\infty(\Omega)})} \log(M) + \gamma_{(M)}\right] \log(M)}{M^{3/7}}, \\ &\quad \frac{16K_{\max} \left[C_{(\sigma, \|u\|_{L^\infty(\Omega)})} \log(N) + \gamma_{(N)}\right] \log(N)}{N^{3/7}}, \\ &\quad 16\sqrt{\frac{\omega(M)}{7}}\tilde{C}_{(\sigma, \|u\|_{L^\infty(\Omega)})}\frac{\sqrt{\log(M)}}{M^{3/7}}, \\ &\quad \left. 16K\|\beta^*\|_\infty \sqrt{\frac{\omega(N)}{7}}\tilde{C}_{(\sigma, \|u\|_{L^\infty(\Omega)})}\frac{\sqrt{\log(N)}}{N^{3/7}} \right\}, \end{aligned}$$

we have

$$\begin{aligned}
 & P(\|\nabla_t \mathbf{u} - \mathbf{X}\boldsymbol{\beta}^*\|_\infty > \epsilon) \\
 \leq & M \left[2Ne^{-\frac{(N^{3/7} - \|U\|_{L^\infty(\Omega)})^2}{2\sigma^2}} + Q_{(\sigma, \|u\|_{L^\infty(\Omega)})} e^{-L\gamma(N)} + 4\sqrt{2}\eta^4 N^{-\omega(N)/7} \right] + \\
 & NK \left[2Me^{-\frac{(M^{3/7} - \|U\|_{L^\infty(\Omega)})^2}{2\sigma^2}} + Q_{(\sigma, \|u\|_{L^\infty(\Omega)})} e^{-L\gamma(M)} + 4\sqrt{2}\eta^4 M^{-\omega(M)/7} \right]
 \end{aligned}$$

Now, let us do some simplification of the above results. Let $M = N^\kappa, \gamma(M) = \gamma(N) =$

$\frac{1}{L}N^r, \omega(M) = \omega(N) = N^{2r}$, and

$$\left\{ \begin{array}{ll} \mathcal{J}_1 &= 4KK_{\max}\|\boldsymbol{\beta}^*\|_\infty N^{-3\kappa/7} \\ \mathcal{J}'_1 &= 4K_{\max}N^{-3/7} \\ \mathcal{J}_2 &= 4AK\|\boldsymbol{\beta}^*\|_\infty N^{-3\kappa/7} \\ \mathcal{J}'_2 &= 4\bar{A}N^{-3/7} \\ \mathcal{J}_3 &= 4\sqrt{2}K\|\boldsymbol{\beta}^*\|_\infty \frac{d^3}{dx^3} f^*(0) N^{-3\kappa/7} \\ \mathcal{J}'_3 &= 4\sqrt{2} \frac{d^3}{dx^3} \bar{f}^*(0) N^{-3/7} \\ \mathcal{J}_4 &= \frac{16KK_{\max}\|\boldsymbol{\beta}^*\|_\infty \left[C_{(\sigma, \|u\|_{L^\infty(\Omega)})} (\log(\kappa) + \log(N)) + N^r/L \right] (\log(\kappa) + \log(N))}{N^{3\kappa/7}} \\ \mathcal{J}'_4 &= \frac{16K_{\max} \left[C_{(\sigma, \|u\|_{L^\infty(\Omega)})} \log(N) + N^r \right] \log(N)}{N^{3/7}} \\ \mathcal{J}_5 &= 16K\|\boldsymbol{\beta}^*\|_\infty \sqrt{\frac{N^{2r}}{7}} \tilde{C}_{(\sigma, \|u\|_{L^\infty(\Omega)})} \frac{\sqrt{\log(\kappa) + \log(N)}}{N^{3\kappa/7}} \\ \mathcal{J}'_5 &= 16\sqrt{\frac{N^{2r}}{7}} \tilde{C}_{(\sigma, \|u\|_{L^\infty(\Omega)})} \frac{\sqrt{\log(N)}}{N^{3/7}} \end{array} \right. .$$

To guarantee that $\mathcal{J}_1, \mathcal{J}'_1, \mathcal{J}_2, \mathcal{J}'_2, \mathcal{J}_3, \mathcal{J}'_3, \mathcal{J}_4, \mathcal{J}'_4, \mathcal{J}_5, \mathcal{J}'_5 \rightarrow 0$, as $N \rightarrow +\infty$, we need

$$\left\{ \begin{array}{l} 3\kappa/7 - r > 0 \\ 3/7 - r > 0 \end{array} \right. ,$$

where the optimal κ is $\kappa = 1$. Accordingly, we have

$$\mathcal{J}_1, \mathcal{J}'_1, \mathcal{J}_2, \mathcal{J}'_2, \mathcal{J}_3, \mathcal{J}'_3, \mathcal{J}_5, \mathcal{J}'_5 \lesssim \mathcal{J}_4, \mathcal{J}'_4.$$

Based on the above discussion, we can declare that when N is sufficiently large, with

$$\epsilon > \mathcal{C}_{(\sigma, \|u\|_{L^\infty(\Omega)})} \frac{\log(N)}{N^{3/7-r}}$$

for any $r \in (0, \frac{3}{7})$ and $M = O(N)$, we have

$$\begin{aligned} & P \|\nabla_t \mathbf{u} - \mathbf{X}\boldsymbol{\beta}^*\|_\infty > \epsilon) \\ & \leq M \left[2Ne^{-\frac{(N^{3/7} - \|U\|_{L^\infty(\Omega)})^2}{2\sigma^2}} + Q_{(\sigma, \|u\|_{L^\infty(\Omega)})} e^{-L\gamma(N)} + 4\sqrt{2}\eta^4 N^{-\omega(N)/7} \right] + \\ & \quad NK \left[2Me^{-\frac{(M^{3/7} - \|U\|_{L^\infty(\Omega)})^2}{2\sigma^2}} + Q_{(\sigma, \|u\|_{L^\infty(\Omega)})} e^{-L\gamma(M)} + 4\sqrt{2}\eta^4 M^{-\omega(M)/7} \right] \\ & = M \left[2Ne^{-\frac{(N^{3/7} - \|U\|_{L^\infty(\Omega)})^2}{2\sigma^2}} + Q_{(\sigma, \|u\|_{L^\infty(\Omega)})} e^{-N^r} + 4\sqrt{2}\eta^4 N^{-N^{2r}/7} \right] + \\ & \quad NK \left[2Me^{-\frac{(M^{3/7} - \|U\|_{L^\infty(\Omega)})^2}{2\sigma^2}} + Q_{(\sigma, \|u\|_{L^\infty(\Omega)})} e^{-N^r} + 4\sqrt{2}\eta^4 M^{-N^{2r}/7} \right] \\ & = O(Ne^{-N^r}) \end{aligned}$$

Thus, we finish the proof of the theorem. \square

G.5 Proof of Theorem 3.1

Proof. By KKT-condition, any minimizer $\boldsymbol{\beta}$ of (2.10) must satisfies:

$$-\frac{1}{MN} \mathbf{X}^\top (\nabla_t \mathbf{u} - \mathbf{X}\boldsymbol{\beta}) + \lambda \mathbf{z} = 0 \quad \text{for } \mathbf{z} \in \partial \|\boldsymbol{\beta}\|_1,$$

G.5 Proof of Theorem 3.1

where $\partial\|\boldsymbol{\beta}\|_1$ is the sub-differential of $\|\boldsymbol{\beta}\|_1$. The above equation can be equivalently transformed into

$$\mathbf{X}^\top \mathbf{X}(\boldsymbol{\beta} - \boldsymbol{\beta}^*) + \mathbf{X}^\top [(\mathbf{X} - \mathbf{X}^*)\boldsymbol{\beta}^* - (\nabla_t \mathbf{u} - \nabla_t \mathbf{u}^*)] + \lambda MN \mathbf{z} = 0. \quad (\text{G.45})$$

Here matrix $\mathbf{X} \in \mathbb{R}^{MN \times K}$ is defined in (2.9), and matrix $\mathbf{X}^* \in \mathbb{R}^{MN \times K}$ is defined as

$$\mathbf{X}^* = (\mathbf{x}_0^0 \quad \mathbf{x}_1^0 \quad \dots \quad \mathbf{x}_{M-1}^0 \quad \mathbf{x}_1^0 \quad \dots \quad \mathbf{x}_{M-1}^{N-1})^\top,$$

with

$$\mathbf{x}_i^n = \left(1, \quad u(x_i, t_n), \quad \frac{\partial u(x_i, t_n)}{\partial x}, \quad \frac{\partial^2 u(x_i, t_n)}{\partial x^2}, \quad \left(\widehat{u(x_i, t_n)} \right)^2, \quad \dots, \quad \left(\frac{\partial^2 u(x_i, t_n)}{\partial x^2} \right)^{p_{\max}} \right)^\top \in \mathbb{R}^K.$$

And vector $\boldsymbol{\beta}^* = (\beta_1, \dots, \beta_K) \in \mathbb{R}^K$ is the ground truth coefficients. Besides, vector $\nabla_t \mathbf{u} \in \mathbb{R}^{MN}$ is defined in (2.8), and vector $\nabla_t \mathbf{u}^* \in \mathbb{R}^K$ is the ground truth, i.e.,

$$\nabla_t \mathbf{u}^* = \left(\frac{\partial u(x_0, t_0)}{\partial t}, \quad \frac{\partial u(x_1, t_0)}{\partial t}, \quad \dots, \quad \frac{\partial u(x_{M-1}, t_0)}{\partial t}, \quad \frac{\partial u(x_0, t_1)}{\partial t}, \quad \dots, \quad \frac{\partial u(x_{M-1}, t_{N-1})}{\partial t} \right)^\top.$$

Let us denote $\mathcal{S} = \{i : \beta_i^* \neq 0 \ \forall i = 0, 1, \dots, K\}$, then we can decompose \mathbf{X} into $\mathbf{X}_{\mathcal{S}}$ and $\mathbf{X}_{\mathcal{S}^c}$, where $\mathbf{X}_{\mathcal{S}}$ is the columns of \mathbf{X} whose indices are in \mathcal{S} and $\mathbf{X}_{\mathcal{S}^c}$ is the complement of $\mathbf{X}_{\mathcal{S}}$. And we can also decompose $\boldsymbol{\beta}$ into $\boldsymbol{\beta}_{\mathcal{S}}$ and $\boldsymbol{\beta}_{\mathcal{S}^c}$, where $\boldsymbol{\beta}_{\mathcal{S}}$ is the subvector of $\boldsymbol{\beta}$ only contains elements whose indices are in \mathcal{S} and $\boldsymbol{\beta}_{\mathcal{S}^c}$ is the complement of $\boldsymbol{\beta}_{\mathcal{S}}$.

By using the decomposition, we can rewrite (G.45) as

$$\begin{pmatrix} \mathbf{0} \\ \mathbf{0} \end{pmatrix} = \begin{pmatrix} \mathbf{X}_S^\top \mathbf{X}_S & \mathbf{X}_S^\top \mathbf{X}_{S^c} \\ \mathbf{X}_{S^c}^\top \mathbf{X}_S & \mathbf{X}_{S^c}^\top \mathbf{X}_{S^c} \end{pmatrix} \begin{pmatrix} \boldsymbol{\beta}_S - \boldsymbol{\beta}_S^* \\ \boldsymbol{\beta}_{S^c} \end{pmatrix} + \begin{pmatrix} \mathbf{X}_S^\top \\ \mathbf{X}_{S^c}^\top \end{pmatrix} [(\mathbf{X} - \mathbf{X}^*)_S \boldsymbol{\beta}_S^* - (\nabla_t \mathbf{u} - \nabla_t \mathbf{u}^*)] + \lambda MN \begin{pmatrix} \mathbf{z}_S \\ \mathbf{z}_{S^c} \end{pmatrix} \quad (\text{G.46})$$

Suppose the primal-dual witness (PDW) construction gives us an solution $(\check{\boldsymbol{\beta}}, \check{\mathbf{z}}) \in \mathbb{R}^K \times \mathbb{R}^K$,

where $\check{\boldsymbol{\beta}}_{S^c} = \mathbf{0}$ and $\check{\mathbf{z}} \in \partial \|\check{\boldsymbol{\beta}}\|_1$. By plugging $(\check{\boldsymbol{\beta}}, \check{\mathbf{z}})$ into the above equation, we have

$$\begin{aligned} \check{\mathbf{z}}_{S^c} &= \mathbf{X}_{S^c}^\top \mathbf{X}_S (\mathbf{X}_S^\top \mathbf{X}_S)^{-1} \mathbf{z}_S - \underbrace{\mathbf{X}_{S^c}^\top (\mathbf{I} - \mathbf{X}_S (\mathbf{X}_S^\top \mathbf{X}_S)^{-1} \mathbf{X}_S^\top)}_{\mathbf{H}_{X_s}} \frac{[(\mathbf{X} - \mathbf{X}^*)_S \boldsymbol{\beta}_S^* - (\nabla_t \mathbf{u} - \nabla_t \mathbf{u}^*)]}{\lambda MN} \\ &= \mathbf{X}_{S^c}^\top \mathbf{X}_S (\mathbf{X}_S^\top \mathbf{X}_S)^{-1} \mathbf{z}_S - \frac{1}{\lambda MN} \mathbf{X}_{S^c}^\top \mathbf{H}_{X_s} \underbrace{(\mathbf{X}_S \boldsymbol{\beta}_S^* - \nabla_t \mathbf{u})}_{\boldsymbol{\tau}} \end{aligned} \quad (\text{G.47})$$

From (G.47), we have

$$\begin{aligned} P(\|\check{\mathbf{z}}_{S^c}\|_\infty \geq 1) &= P\left(\left\|\mathbf{X}_{S^c}^\top \mathbf{X}_S (\mathbf{X}_S^\top \mathbf{X}_S)^{-1} \mathbf{z}_S - \frac{1}{\lambda MN} \mathbf{X}_{S^c}^\top \mathbf{H}_{X_s} \boldsymbol{\tau}\right\|_\infty > 1\right) \\ &\leq P\left(\left\|\mathbf{X}_{S^c}^\top \mathbf{X}_S (\mathbf{X}_S^\top \mathbf{X}_S)^{-1} \mathbf{z}_S\right\|_\infty > 1 - \mu\right) + \\ &\quad P\left(\left\|\frac{1}{\lambda MN} \mathbf{X}_{S^c}^\top \mathbf{H}_{X_s} \boldsymbol{\tau}\right\|_\infty > \mu\right). \end{aligned}$$

If we denote $\widetilde{Z}_j = \frac{1}{\lambda MN} (\mathbf{X}_{S^c})_j^\top \mathbf{H}_{X_s} \boldsymbol{\tau}$, where $(\mathbf{X}_{S^c})_j$ is the j -th column of \mathbf{X}_{S^c} , then we have

$$P(\|\check{\mathbf{z}}_{S^c}\|_\infty \geq 1) \leq P\left(\left\|\mathbf{X}_{S^c}^\top \mathbf{X}_S (\mathbf{X}_S^\top \mathbf{X}_S)^{-1}\right\|_\infty > 1 - \mu\right) + P\left(\max_{j \in S^c} |\widetilde{Z}_j| > \mu\right). \quad (\text{G.48})$$

G.5 Proof of Theorem 3.1

Now let us discuss the upper bound of the second term, i.e., $P\left(\max_{j \in \mathcal{S}^c} |\widetilde{Z}_j| > \mu\right)$. Because

$$\begin{aligned}
P\left(\max_{j \in \mathcal{S}^c} |\widetilde{Z}_j| > \mu\right) &= P\left(\left\|\frac{1}{\lambda MN} \mathbf{X}_{\mathcal{S}^c}^\top \mathbf{H}_{X_s} \boldsymbol{\tau}\right\|_\infty > \mu\right) \\
&\leq P\left(\left\|\frac{1}{\lambda MN} \mathbf{X}_{\mathcal{S}^c}^\top \mathbf{H}_{X_s} \boldsymbol{\tau}\right\|_2 > \mu\right) \\
&\leq P\left(\left\|\frac{1}{\lambda MN} \mathbf{X}^\top \mathbf{H}_{X_s} \boldsymbol{\tau}\right\|_2 > \mu\right) \\
&\leq P\left(\frac{1}{\lambda MN} \|\mathbf{X}\|_2 \|\boldsymbol{\tau}\|_2 > \mu\right) \\
&\leq P\left(\|\boldsymbol{\tau}\|_2 > \lambda \mu \sqrt{\frac{MN}{K}}\right) \\
&\leq P\left(\|\boldsymbol{\tau}\|_\infty > \lambda \mu \frac{1}{\sqrt{K}}\right) \tag{G.49}
\end{aligned}$$

By Lemma D.2, we know when

$$\lambda \mu \frac{1}{\sqrt{K}} > \mathcal{C}(\sigma, \|u\|_{L^\infty(\Omega)}) \frac{\log(N)}{N^{3/7-r}},$$

we have

$$P(\|\nabla_t \mathbf{u} - \mathbf{X} \boldsymbol{\beta}^*\|_\infty > \epsilon) < N e^{-N^r}.$$

So we know that

$$\begin{aligned}
P\left(\|\boldsymbol{\tau}\|_\infty > \lambda \mu \frac{1}{\sqrt{K}}\right) &= P\left(\|\nabla_t \mathbf{u} - \mathbf{X}_S \boldsymbol{\beta}_S^*\|_\infty > \lambda \mu \frac{1}{\sqrt{K}}\right) \\
&\leq P\left(\|\nabla_t \mathbf{u} - \mathbf{X} \boldsymbol{\beta}^*\|_\infty > \lambda \mu \frac{1}{\sqrt{K}}\right) \\
&< N e^{-N^r} \tag{G.50}
\end{aligned}$$

By plugging the results in (G.49) and (G.50) into (G.48), we have

$$\begin{aligned}
 P(\|\tilde{\mathbf{z}}_{S^c}\|_\infty \geq 1) &\leq P\left(\left\|\mathbf{X}_{S^c}^\top \mathbf{X}_S (\mathbf{X}_S^\top \mathbf{X}_S)^{-1}\right\|_\infty > 1 - \mu\right) + P\left(\max_{j \in S^c} |\widetilde{Z}_j| > \mu\right) \\
 &\leq P\left(\left\|\mathbf{X}_{S^c}^\top \mathbf{X}_S (\mathbf{X}_S^\top \mathbf{X}_S)^{-1}\right\|_\infty > 1 - \mu\right) + P\left(\|\boldsymbol{\tau}\|_\infty > \lambda\mu \frac{1}{\sqrt{K}}\right) \\
 &\leq P\left(\left\|\mathbf{X}_{S^c}^\top \mathbf{X}_S (\mathbf{X}_S^\top \mathbf{X}_S)^{-1}\right\|_\infty > 1 - \mu\right) + Ne^{-Nr}
 \end{aligned}$$

The probability for proper support set recovery is

$$\begin{aligned}
 P(\|\tilde{\mathbf{z}}_{S^c}\|_\infty < 1) &= 1 - P(\|\tilde{\mathbf{z}}_{S^c}\|_\infty \geq 1) \\
 &\geq 1 - \left[P\left(\left\|\mathbf{X}_{S^c}^\top \mathbf{X}_S (\mathbf{X}_S^\top \mathbf{X}_S)^{-1}\right\|_\infty > 1 - \mu\right) + Ne^{-Nr}\right] \\
 &= P\left(\left\|\mathbf{X}_{S^c}^\top \mathbf{X}_S (\mathbf{X}_S^\top \mathbf{X}_S)^{-1}\right\|_\infty \leq 1 - \mu\right) - Ne^{-Nr} \\
 &\leq P_\mu - Ne^{-Nr}.
 \end{aligned}$$

Thus, we finish the proof. \square

G.6 Proof of Theorem 3.2

Proof. By equation (G.46), we can solve $\boldsymbol{\beta}_S - \boldsymbol{\beta}_S^*$ as

$$\boldsymbol{\beta}_S - \boldsymbol{\beta}_S^* = (\mathbf{X}_S^\top \mathbf{X}_S)^{-1} \left[-\mathbf{X}_S^\top (\mathbf{X}_S - \mathbf{X}_S^*) \boldsymbol{\beta}_S^* + \mathbf{X}_S^\top (\nabla_t \mathbf{u} - \nabla_t \mathbf{u}^*) - \lambda M N \mathbf{z}_S \right].$$

Thus, we have the following series of equations:

$$\begin{aligned}
 & \max_{k \in \mathcal{S}} |\beta_k - \beta_k^*| \\
 & \leq \left\| (\mathbf{X}_S^\top \mathbf{X}_S)^{-1} \right\|_\infty \left\| \mathbf{X}_S^\top [\nabla_t \mathbf{u} - \nabla_t \mathbf{u}^* - (\mathbf{X}_S - \mathbf{X}_S^*) \beta_S^*] - \lambda MN \mathbf{z}_S \right\|_\infty \\
 & \leq \left\| (\mathbf{X}_S^\top \mathbf{X}_S)^{-1} \right\|_\infty \left[\left\| \mathbf{X}_S^\top [\nabla_t \mathbf{u} - \nabla_t \mathbf{u}^* - (\mathbf{X}_S - \mathbf{X}_S^*) \beta_S^*] \right\|_\infty + \lambda MN \|\mathbf{z}_S\|_\infty \right] \\
 & = \left\| (\mathbf{X}_S^\top \mathbf{X}_S)^{-1} \right\|_\infty \left[\left\| \mathbf{X}_S^\top (\nabla_t \mathbf{u} - \mathbf{X}_S \beta_S^*) \right\|_\infty + \lambda MN \|\mathbf{z}_S\|_\infty \right] \tag{G.51}
 \end{aligned}$$

$$\leq \left\| \left(\frac{\mathbf{X}_S^\top \mathbf{X}_S}{MN} \right)^{-1} \right\|_\infty \left(\frac{\left\| \mathbf{X}_S^\top (\nabla_t \mathbf{u} - \mathbf{X}_S \beta_S^*) \right\|_\infty}{MN} + \lambda \right) \tag{G.52}$$

$$\leq \sqrt{K} C_{\min} \left(\frac{\left\| \mathbf{X}_S^\top (\nabla_t \mathbf{u} - \mathbf{X}_S \beta_S^*) \right\|_\infty}{MN} + \lambda \right) \tag{G.53}$$

$$\leq \sqrt{K} C_{\min} \left(\frac{\|\mathbf{X}_S\|_{\infty, \infty} \|\nabla_t \mathbf{u} - \mathbf{X}_S \beta_S^*\|_\infty}{MN} + \lambda \right) \tag{G.54}$$

$$\begin{aligned}
 & \leq \sqrt{K} C_{\min} \left(\frac{\|\mathbf{X}_S\|_F \|\nabla_t \mathbf{u} - \mathbf{X}_S \beta_S^*\|_\infty}{\sqrt{MN}} + \lambda \right) \\
 & \leq \sqrt{K} C_{\min} \left(\frac{\sqrt{MNK} \|\nabla_t \mathbf{u} - \mathbf{X}_S \beta_S^*\|_\infty}{\sqrt{MN}} + \lambda \right) \tag{G.55}
 \end{aligned}$$

$$\begin{aligned}
 & = \sqrt{K} C_{\min} \left(\sqrt{K} \|\nabla_t \mathbf{u} - \mathbf{X}_S \beta_S^*\|_\infty + \lambda \right) \\
 & \leq \sqrt{K} C_{\min} \left(\sqrt{K} \mathcal{C}_{(\sigma, \|u\|_{L^\infty(\Omega)})} \frac{\log(N)}{N^{3/7-r}} + \lambda \right) \tag{G.56}
 \end{aligned}$$

Equation (G.51) is because $\nabla_t \mathbf{u}^* = \mathbf{X}_S \beta_S^*$. Inequality (G.52) is because $\|\mathbf{z}_S\|_\infty = 1$. In-

equality (G.53) is because of Condition 3.3. Inequality (G.54) is because for a matrix \mathbf{A} and

a vector \mathbf{x} , we have $\|\mathbf{A}\mathbf{x}\|_q \leq \|\mathbf{A}\|_{p,q} \|\mathbf{x}\|_p$. Here the matrix norm for matrix $\mathbf{A} \in \mathbb{R}^{m \times n}$

in $\|\mathbf{A}\|_{\infty, \infty} = \|\text{vector}(\mathbf{A})\|_\infty$. In inequality (G.55), the norm of matrix $\mathbf{A} \in \mathbb{R}^{m \times n}$ is that

$\|\mathbf{A}\|_F = \sqrt{\sum_{i=1}^m \sum_{j=1}^n |A_{ij}|^2}$, and the norm of vector $\mathbf{a} \in \mathbb{R}^d$ is $\|\mathbf{a}\|_\infty = \max_{1 \leq i \leq d} |a_i|$. Inequal-

ity (G.55) is because we normalized columns of \mathbf{X} . Inequality (G.56) is due to Lemma Lemma

D.2 under probability $1 - O(Ne^{-N^r}) \rightarrow 1$. \square

H. Checking Conditions of Example 1,2,3

In this section, we check Condition 3.1 - Condition 3.6 of the above three examples: (1) example 1 (the transport equation), (2) example 2 (the inviscid Burgers' equation) and (3) example 3 (the viscous Burgers' equation).

H.1 Verification of Condition 3.1, 3.2, 3.3

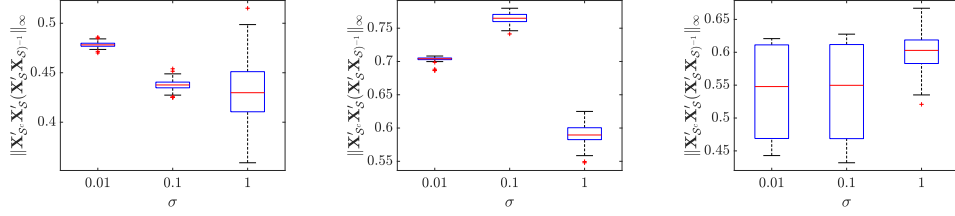
In this section, we check the Condition 3.1 - Condition 3.3 under example 1,2,3, though the applicability of the results is by no means restricted to these.

The verification results can be found in Fig. 11 and Fig. 12, where (a),(b),(c) are the box plot of $\|\mathbf{X}_{S^c}^\top \mathbf{X}_S (\mathbf{X}_S^\top \mathbf{X}_S)^{-1}\|_\infty$ and the minimal eigenvalue of matrix $\frac{1}{NM} \mathbf{X}_S^\top \mathbf{X}_S$ of these three examples under $\sigma = 0.01, 0.1, 1$, respectively. From Fig. 11, we find the value of $\|\mathbf{X}_{S^c}^\top \mathbf{X}_S (\mathbf{X}_S^\top \mathbf{X}_S)^{-1}\|_\infty$ is smaller than 1, so there exist a $\mu \in (0, 1]$ such that Condition 3.2 is met. From Fig. 12, we find the minimal eigenvalue of matrix $\frac{1}{MN} \mathbf{X}_S^\top \mathbf{X}_S$ are all strictly larger than 0, so we declare Condition 3.3 is satisfied, and thus its weak version – Condition 3.1 – is also satisfied.

H.2 Verification of Condition 3.4 and Condition 3.5

In example 1,2,3, the design points x_0, x_1, \dots, x_{M-1} and t_0, t_1, \dots, t_{N-1} are equally spaced, i.e., $x_0 = 1/M, x_1 = 2/M, \dots, x_{M-1} = 1$ and $t_0 = 0.1/N, t_1 = 0.2/N, \dots, t_{N-1} = 0.1$. Under this scenario, there exist an absolutely continuous distribution $F(x) = x$ for $x \in [1/M, 1]$ and $G(t) =$

H.2 Verification of Condition 3.4 and Condition 3.5

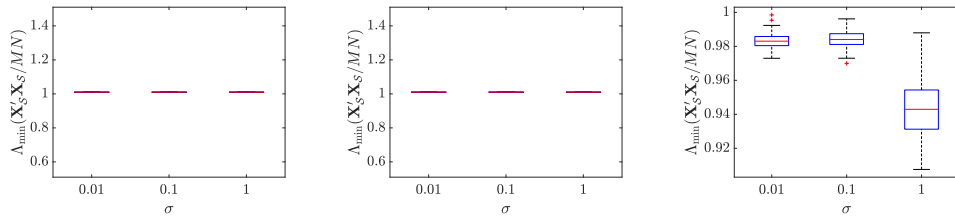


(a) example 1:

(b) example 2:

(c) example 3:

Figure 11: Box plots of $\|\mathbf{X}_{\mathcal{S}^c}^\top \mathbf{X}_{\mathcal{S}} (\mathbf{X}_{\mathcal{S}}^\top \mathbf{X}_{\mathcal{S}})^{-1}\|_\infty$ under $\sigma = 0.01, 0.1, 1$ when $M = N = 100$.



(a) example 1:

(b) example 2:

(c) example 3:

Figure 12: Box plots of the minimal eigenvalue of matrix $\frac{1}{NM} \mathbf{X}_{\mathcal{S}}^\top \mathbf{X}_{\mathcal{S}}$ under $\sigma = 0.01, 0.1, 1$ when $M = N = 100$.

H.3 Verification of Condition 3.6.

$0.1t$ for $t \in [0.1/N, 0.1]$, where the empirical c.d.f. of the design points x_0, x_1, \dots, x_{M-1} and t_0, t_1, \dots, t_{N-1} will converge to $F(x), G(t)$, respectively, as $M, N \rightarrow +\infty$. For the $F(x), G(t)$, we know their first derivatives is bounded for $x \in [1/M, 1]$ and $t \in [0.1/N, 0.1]$, respectively. In the simulation of this paper, we take the equally spaced design points as an illustration example, and its applicability is by no means restricted to this case.

H.3 Verification of Condition 3.6.

The Condition 3.6 ensures that the smoothing parameter does not tend to zero too rapidly. Silverman (1984) shows that for the equally spaced design points, this condition meets. For other types of design points, for instance, randomly and independently distributed design points, it can also be verified that Condition 3.6 is satisfied (see Silverman, 1984, Section 2).

I. Details of the Case Study

The header of the CALIPSP dataset and its visualization can be found in Table 4 and Fig. 9(a), respectively. Fig. 9(a) shows presents the curves of the dynamic in the CALIPSP dataset, where the x-axis is the longitude and the y-axis is the value of the observed temperature. Here the black curve plots the observed temperature in January 2017, and the lighter color presents the later month. As seen from Fig. 9, we find overall there is an increasing trend of the temperature in the first half-year and then the temperature decreases.

Table 4: The header of the CALIPSP dataset

	longitude						
	-177.5	-172.5	-167.5	...	167.5	172.5	177.5
Jan 2017	-46.5103	-48.4720	-44.6581	...	-44.2778	-47.3354	-44.0146
Feb 2017	-46.2618	-43.1994	-47.6370	...	-46.8409	-46.2727	-40.5556
⋮	⋮	⋮	⋮	⋮	⋮	⋮	⋮
Dec 2017	-47.3145	-47.6505	-50.8332	...	-43.9705	-43.0475	-46.0618

¹ The data is downloaded from https://asdc.larc.nasa.gov/data/CALIPSO/LID_L3_Tropospheric_APro_CloudFree-Standard-V (registration is required).

² The negative and positive longitude refer to the west and east longitude, respectively.